Material, Fabrication, and Repair Considerations for Austenitic Alloys Subject to Embrittlement and Cracking in High Temperature 565 °C to 760 °C (1050 °F to 1400 °F) Refinery Services

API TECHNICAL REPORT 942-B
FIRST EDITION, MAY 2017

EFFECTIVE DATE: NOVEMBER 1, 2017

AMERICAN PETROLEUM INSTITUTE

Special Notes

API publications necessarily address problems of a general nature. With respect to particular circumstances, local, state, and federal laws and regulations should be reviewed.

Neither API nor any of API's employees, subcontractors, consultants, committees, or other assignees make any warranty or representation, either express or implied, with respect to the accuracy, completeness, or usefulness of the information contained herein, or assume any liability or responsibility for any use, or the results of such use, of any information or process disclosed in this publication. Neither API nor any of API's employees, subcontractors, consultants, or other assignees represent that use of this publication would not infringe upon privately owned rights.

API publications may be used by anyone desiring to do so. Every effort has been made by the Institute to assure the accuracy and reliability of the data contained in them; however, the Institute makes no representation, warranty, or guarantee in connection with this publication and hereby expressly disclaims any liability or responsibility for loss or damage resulting from its use or for the violation of any authorities having jurisdiction with which this publication may conflict.

Users of this Technical Report should not rely exclusively on the information contained in this document. Sound business, scientific, engineering, and safety judgment should be used in employing the information contained herein.

Foreword

Nothing contained in any API publication is to be construed as granting any right, by implication or otherwise, for the manufacture, sale, or use of any method, apparatus, or product covered by letters patent. Neither should anything contained in the publication be construed as insuring anyone against liability for infringement of letters patent.

The verbal forms used to express the provisions in this document are as follows.

Shall: As used in a standard, “shall” denotes a minimum requirement in order to conform to the standard.

Should: As used in a standard, “should” denotes a recommendation or that which is advised but not required in order to conform to the standard.

May: As used in a standard, “may” denotes a course of action permissible within the limits of a standard.

Can: As used in a standard, “can” denotes a statement of possibility or capability.

This document was produced under API standardization procedures that ensure appropriate notification and participation in the developmental process and is designated as an API standard. Questions concerning the interpretation of the content of this publication or comments and questions concerning the procedures under which this publication was developed should be directed in writing to the Director of Standards, American Petroleum Institute, 1220 L Street, NW, Washington, DC 20005. Requests for permission to reproduce or translate all or any part of the material published herein should also be addressed to the director.

Generally, API standards are reviewed and revised, reaffirmed, or withdrawn at least every five years. A one-time extension of up to two years may be added to this review cycle. Status of the publication can be ascertained from the API Standards Department, telephone (202) 682-8000. A catalog of API publications and materials is published annually by API, 1220 L Street, NW, Washington, DC 20005.

Suggested revisions are invited and should be submitted to the Standards Department, API, 1220 L Street, NW, Washington, DC 20005, standards@api.org.

Contents

Tables

Introduction

The API Committee on Refinery Equipment, Subcommittee of Corrosion and Materials, identified a need to develop a technical report focusing on the materials, fabrication, and repair of austenitic stainless steels and nickel-iron-chromium alloys in high temperature 565 °C to 760 °C (1050 °F to 1400 °F) refinery services. Many of these alloys are subject to embrittlement and cracking after prolonged exposure to these temperatures. Susceptible equipment in the following processing units are addressed:

— fluid catalytic cracking units,

— hydrogen/syngas plants,

— catalytic reformers,

— cokers,

— hydroprocessing units.

This report summarizes industry experience and recommends methods to improve reliability and process safety, and increases industry awareness to high temperature embrittlement issues.

NOTE Embrittlement can be a serious personnel safety issue if plant personnel are not careful about hand-holds and foot-holds when inspecting embrittled piping and vessel components. There has been at least one case where an inspector was seriously injured when an embrittled support failed.

Material, Fabrication, and Repair Considerations for Austenitic Alloys Subject to Embrittlement and Cracking in High Temperature 565 °C to 760 °C (1050 °F to 1400 °F) Refinery Services

1 Technical Approach/Report Organization and Scope

As a basis of this report, technical literature, industry experience, and published case studies were reviewed. The review included materials of construction, damage mechanisms, and component-specific fabrication and repair issues.

The scope of this report includes the following wrought austenitic alloys: Alloys 800, 800H, 800HT®, and 300 series austenitic stainless steels, and corresponding welding consumables. Limits in chemical composition, microstructural requirements, and heat treating practices that mitigate susceptibility to embrittlement and cracking are identified. Potentially viable upgrades to commonly used alloys are identified where applicable.

The remainder of this report is organized as follows.

Section 3, Process Units, gives a brief process overview followed by an explanation of the various damage mechanisms found in that unit. Component specific considerations and examples of in-service damage are also included. Inspection recommendations and general repair method considerations are also included.

Section 4, Damage Mechanisms, contains detailed discussions of high-temperature damage mechanisms; including fundamental details of the solid state reactions, their rate of reaction, and recommended mitigation measures. Section 4 also incorporates fabrication and repair practices that can be used for cracked or embrittled equipment.

NOTE Excluded from the scope of this document are Hydrogen Reformer catalyst tubes, outlet pigtails and outlet headers. With the exception of catalyst tubes, these are covered in TR 942-A, *Materials, Fabrication, and Repair Considerations for Hydrogen Reformer Furnace Outlet Pigtails and Manifolds*. Also excluded are expansion bellows in elevated temperature service.

2 Acronyms and Abbreviations

For the purposes of this document, the following acronyms and abbreviations apply.

CCC	complete carbon monoxide combustion
CO	carbon monoxide
CRCR	continuously regenerated catalytic reformer
CVN	Charpy V-notch
FCCU	fluid catalytic cracking unit
FN	ferrite number
GTAW	gas tungsten arc welding
ID	inside diameter
MTR	material test report
NDE	non-destructive examination
NDT	non-destructive testing

PASCC	polythionic acid stress corrosion cracking
PCC	partial CO combustion
PFZ	precipitation free zone
PT	penetrant testing
PWHT	post weld heat treatment
SAGBO	stress assisted grain boundary oxidation
SRC	stress relaxation cracking
SS	stainless steel
T/C	thermocouple
TTT	time temperature transformation
UT	ultrasonic testing
UTSW	ultrasonic testing shear wave
WRC	Welding Research Council

3 Process Units

3.1 General

Table 1 summarizes common embrittlement mechanisms in each of the listed refinery process units. Implications for specific equipment are discussed in more detail in the section for each respective process unit. Information on damage mechanisms can be found in API 571 and in Section 4 of this document.

3.2 Fluid Catalytic Cracking Units (FCCUs)

3.2.1 Process Description

FCCUs are used to process heavy feedstocks, converting them to gasoline, diesel, and furnace oils. A simplified process flow diagram for the FCCU is shown in Figure 1 [1]. The catalytic reaction occurs mostly inside the riser prior to reaching the reactor at temperatures ranging from approximately 480 °C to 565 °C (900 °F to 1050 °F). In modern FCCUs, the "reactor" functions as a hydrocarbon/catalyst separator. During the process, the catalyst becomes deactivated as it becomes coated with carbon (coke). The catalyst is sent to the regenerator where it is exposed to air, promoting the burn off of coke at approximately 650 °C to 780 °C (1200 °F to 1475 °F).

Inside FCCU reactors and regenerators are cyclones which are used to separate the catalyst from the overhead vapor streams. Most regenerators have multiple sets of primary and secondary cyclones. Primary cyclones direct the vapor flow from inside the reactor or regenerator in a centrifugal pattern, forcing the heavier catalyst particles outward against the inside wall, and allowing the catalyst particles to then fall down into the catalyst bed. The lighter vapor stream exits out the top of the primary and into the secondary cyclone to remove residual catalyst from the vapor stream. Primary and secondary cyclones can be seen in Figure 2 [2].

Units that process heavier feeds are called resid fluid catalytic cracking units (resid FCCUs) and these feeds typically have higher sulfur contents. In addition, resid FCCU feeds typically develop higher carbon residues on the catalyst particles. Carbon residues, as indicated by the Conradson Carbon Residue test of Resid FCCU feeds, are significantly higher with up to 5 to 10 wt.%, compared to <1 wt.% for a typical FCCU feed. These heavier feeds also

Table 1—Process Units, Conditions, and Typical Austenitic Stainless Steel Damage Mechanisms*

Process Unit/ Affected Equipment	Operating Temperature Range	Sigma Phase Embrittlement	Stress Relaxation Cracking	Carburization	Creep
FCCU (regenerator)	650 °C to 800 °C 1200 °F to 1475 °F	Yes	Possible	Yes	Yes
H_2 Plants (steam superheater tubes)	370 °C to 540 °C 700 °F to 1300 °F	Yes	Yes	Yes	Yes
Catalytic reformers (regeneration vessels)	515 °C to 565 °C 960 °F to 1050 °F	No	Possible	Yes	No
Coker (heater tubes)	574 °C to 760 °C 1065 °F to 1400 °F	Yes	Possible	Yes	Yes
Hydro processing plants recycle H_2 heaters	545 °C to 675 °C 1010 °F to 1250 °F	Yes	Yes	Yes	Yes

*This table only lists mechanisms covered in this document.

usually contain more metals, and require higher temperatures to crack. This can lead to increased carburization and sigma embrittlement of regenerator cyclones if higher burn temperatures are used.

There are two modes of regenerator operation: Complete Carbon-monoxide (CO) Combustion (CCC) or Partial CO Combustion (PCC). Both types of operation are subject to upsets (including “afterburns”) that can cause rapid localized temperature excursions.

Afterburn (CO combustion) in a regenerator can lead to localized high temperatures, up of 900 °C (1650 °F) or hotter, which can cause major damage to regenerator internals.

Causes of afterburn in a PCC Regenerator include the following.

— Lack of promoter activity that causes oxygen slip to the dilute phase. (Promoters are catalyst additives that enhance control of CO, SO_x, and NO_x.)

— Excessive air/coke ratio (too close to the stoichiometric ratio). Regenerators are intended to operate either with clearly less than stoichiometric air (PCC) or with excess air (greater than 1:1) where there is CCC operation.

Afterburns tend to be more of a problem with CCC operation. Reasons for afterburn in a CCC regenerator include: slow CO combustion in the dense bed, due to lack of promotion activity and localized deficit in the air supply to the bed, either from asymmetric design or air grid damage.

3.2.2 FCCU Damage Mechanisms

3.2.2.1 General

The rate of damage mechanism development depends on a complex set of factors that include: exposure time, temperature, thermal cycles, process upsets, the number of start-ups and shut-downs, peak temperatures, mode of operation (e.g. partial or full combustion), and operating upsets (such as afterburns). In particular, process upsets and rapid start-ups and shut-downs all generate abnormal stresses that can both initiate and propagate cracking.

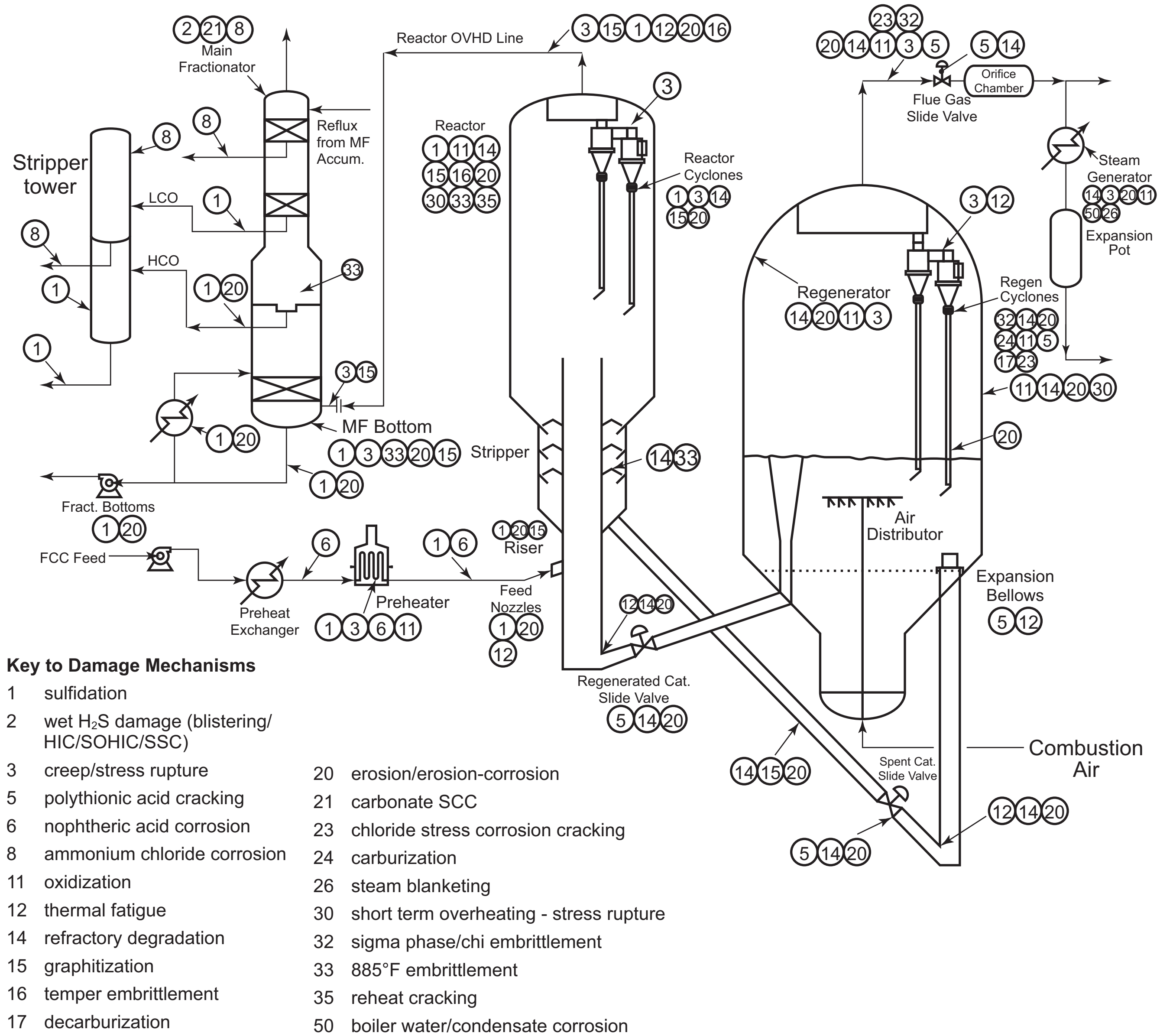

Figure 1—FCCU Simplified Process Flow Diagram

3.2.2.2 Sigma Phase Embrittlement

Sigma phase embrittlement is a common high temperature problem for austenitic alloys used in FCCU regenerators. Over time, high-temperature service promotes the formation of this hard, brittle, nonmagnetic phase. Sigma phase is an intermetallic compound of iron and chromium (FeCr) and is discussed further in 4.2. Sigma forms most readily from the ferrite phase in stainless steel welds in one year of service or less. However, sigma can also form from austenite given enough time at elevated temperatures.

Figure 2—Replacement of Primary (Outer Ring) and Secondary (Inner Ring) Cyclones

Weld solidification relies on ferrite contents of 3 % to 10 % to increase hot ductility and minimize the potential for solidification cracking. Therefore, in general, when exposed to typical regenerator operating temperatures, the weld metal exhibits higher percentage of sigma phase than the corresponding base metal, and will have more tendency to embrittle sooner.

3.2.2.3 Carburization

Typical operating conditions in FCCU regenerators cause low rates of carburization of the stainless steel cyclones and other internal components. Resid FCCUs regenerator internals, with their corresponding higher temperatures, have an increased susceptibility to carburization, as well as faster sigma formation. One resid FCCU using Type 304H stainless steel at 730 °C to 760 °C (1350 °F to 1400 °F) reported a cyclone life of only 5 to 6 years due to the development of deep carburized layers [3].

Afterburn in regenerators not only raises combustion temperatures, but because it involves the combustion of CO, can cause severely carburizing atmospheres.

FCCU internal components can also suffer sensitization [4]. Sensitization can be aggravated by excess dissolved carbon due to carburization and can make the material susceptible to polythionic acid stress corrosion cracking (PASCC). A polythionic acid can be formed when sulfide scales formed at high temperatures on the surface of a stainless steel are cooled and exposed to moisture. The polythionic acid can cause intergranular SCC on sensitized stainless steel which is referred to as “PASCC”. This mechanism is covered more fully in NACE SP0170-2012 [78]. Some refiners reduce the potential for PASCC by minimizing moisture when the vessel is opened during shutdowns, while others use a neutralizing soda ash washing.

3.2.2.4 Creep

Long-term creep cracking can occur in the regenerator internal support structures. The shortening of creep life can be impacted by sigma formation, particularly in the welds.

Short-term creep/stress rupture is usually caused by afterburning episodes that result in local hot spots. Localized heating promotes high thermal stresses and weakens the material, increasing the potential for cracking. During afterburning, stresses can be high due to non-uniform temperature gradients inside the regenerator, resulting in distortion of cyclones, cyclone support structure, and regenerator plenums, and particularly at gas outlets.

Detection of creep cracks is usually performed by visual inspection or by liquid penetrant testing. To determine the extent of creep damaged material, field metallography and replication techniques can be used prior to deciding the amount of material to repair or replace.

3.2.2.5 Stress Relaxation Cracking

Stress relaxation cracking (SRC) is usually associated with fabrication heat treatments or short-term thermal in-service failures due to low creep ductility, but has not been widely reported in FCCUs. For Type 347 stainless steel and Alloy 800 series components with wall thicknesses greater than 12 mm ($^1/_2$ in.) or for fillet weld joints, fabrication, and in particular repair welding procedures, should consider measures such as stress relief to avoid or minimize this damage mechanism. Experience has shown that SRC is unlikely with 304H stainless steel. Refer to Table 3 and Table 4 for susceptibility to SRC for different materials.

3.2.3 Component Specific Considerations

3.2.3.1 Regenerator Cyclones

Regenerator cyclones are commonly fabricated from Type 304H stainless steel; however, other 300 series stainless steels have been used. Primary embrittlement is due to sigma phase formation, although carburization can also occur.

In-service cyclone cracking failures have not been reported, however, there have been cases of cyclones dropping while the regenerator was being shut down. Failures during shut down are often due to the fact that sigma phase is reasonably tough at high temperature, but typically loses toughness when cooled below about 260 °C (500 °F) (more details are given in Section 4).

Based on comments captured in the minutes of meetings of NACE Committee TEG 205X (formerly T-8) on Refining Industry Corrosion, regenerator cyclones are seldom replaced due to sigma phase content alone, but occasionally are replaced when they become too brittle to repair efficiently. It is more common to see cyclones replaced in order to increase capacity or improve efficiency. Decisions to repair or replace them should be judged case-by-case. If repairs are very difficult during a given shutdown, it may be more cost effective to build new cyclones to be installed during the subsequent shutdown.

Measures to predict cyclone repairability can include weldability testing, Charpy V-notch (CVN) toughness testing, or bend testing. Some predictive methods include removal and testing of coupons from aged components such as from the barrel of a cyclone.

Mechanical testing of cyclones replaced due to poor repairability often show low toughness, typically with CVN test values of less than 20 J (15 ft-lb) at ambient test temperature.

Bend tests on butt welds can also be used to gauge repairability. Test welds can be deposited using a small coupon removed from a cyclone. The ability to perform repair welding would be suspect if the test welds fail to pass a 90-degree bend test at ambient temperature [or with a 150 °C (300 °F) preheat temperature if desired].

Another weldability test is a simple gas tungsten arc welding (GTAW) autogenous weld (no filler metal) on an actual cyclone, which can be done without removing a coupon. If penetrant testing shows crack indications, there is a high potential for cracking during weld repairs.

If carburization is suspected, the carburized layer needs to be removed by grinding or by other methods prior to welding. Carburized stainless steel can be magnetic; therefore, a simple magnet test can be used to detect carburization. More details can be found in Section 4.

Inspection of cyclones typically includes visual examination looking for distortion, cracking and loss of protective refractory. Penetrant Testing (PT) and Ultrasonic Testing Shear Wave (UTSW) of support clips and other high stress locations are also typically performed.

3.2.3.2 Regenerator Refractory Anchors and Hexagonal Mesh

Many regenerator components have erosion resistant refractory which is typically held in place using hexagonal mesh or shaped wire anchors made of austenitic grades of stainless steels such as Types 304 or 304H. Examples of hexagonal mesh are shown in Figure 3, Figure 4, and Figure 5 [5].

Hexagonal mesh is typically made from thin materials that can be deformed and shaped to fit the curvature of regenerator cyclones. There are other designs, such as “Flexmetals,” that use a secured rod to provide a pivot point that allows freeform rolling to very small diameters, down to 150 mm (6 in.).

Sigma phase formation (sigmatization) of hexagonal mesh is expected for all regenerating operating conditions. In addition, hexagonal mesh can be prone to embrittlement and corrosion from carburization, oxidation, and sulfidation near the base metal.

For steels and other iron-based alloys, oxide scales formed from high temperature exposure are dense and black. High-temperature oxidation resistance of alloys is improved primarily by increasing chromium content, and secondarily, by increasing silicon. For most hexagonal mesh applications, the minimum alloy for oxidation resistance is an austenitic stainless steel with 18 % Cr.

As metals are heated in an air or steam environment, the rate of oxide scale formation increases logarithmically, until spalling occurs. When the temperature threshold for spalling is reached, metal loss rates can increase rapidly. For austenitic stainless steels containing 18 % to 20 % chromium, the spalling threshold temperature is about 900 °C (1650 °F). Higher chromium stainless steels, such as Types 310 or 330, have higher spalling threshold temperatures,

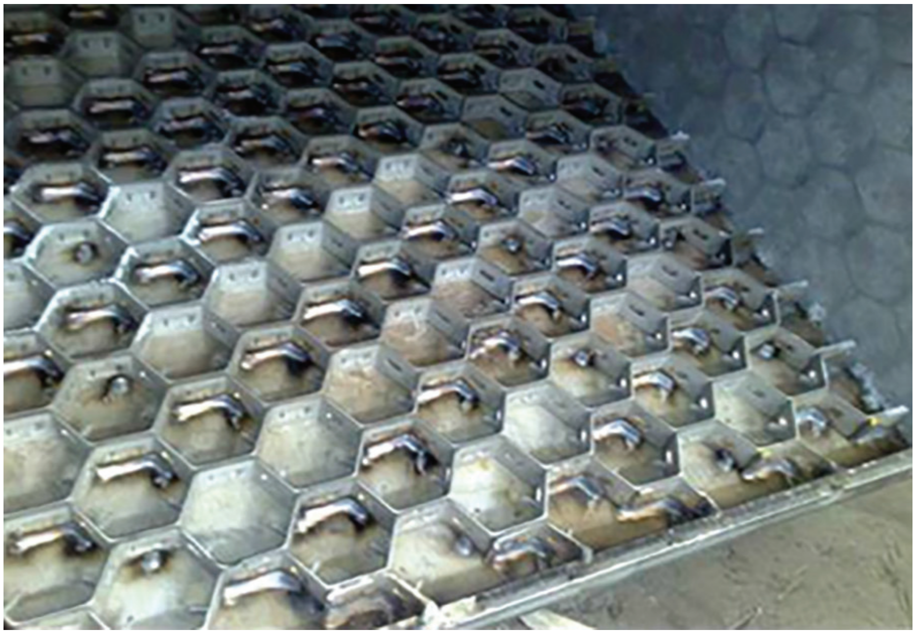

Figure 3—Example of New Hexagonal Mesh Welded Inside a Regenerator Cyclone

Figure 4—Large Areas of Internal Hexagonal Mesh and Refractory that Failed in a Brittle Manner

on the order of 1095 °C (2000 °F). Spalling damage, if it occurs, indicates that operating temperature excursions have occurred that exceeded 900 °C (1650 °F).

Figure 5—Example of External Refractory that Failed After a Short Time in Service

There have been a significant number of recent (2008 through 2011) Type 304/304L and Type 321 stainless steel hexagonal mesh failures that have caused loss of internal refractory resulting in plugged cyclones. This has forced shut downs of the units and caused significant reliability issues.

Factors contributing to premature hexagonal mesh failures are still under investigation at this time, although based on available information, some certain commonalities have been observed.

- When it occurs, the damage mechanisms generally cause refractory systems to fail in approximately 4 to 6 years, though there has been a case where failure occurred after only two years [4].

- Since embrittlement and corrosion occurs behind the refractory, damage is often not obvious from visual inspection.

- Cases have been reported in both complete and partial combustion units.

In the example shown in Figure 5, the regenerator cyclones were made of Type 304H stainless steel, and the hexagonal mesh and anchors were replaced with Type 321 stainless steel (previously Type 304 stainless steel). The refractory was in good condition, with the hexagonal mesh to cyclone welds being intact. Failures were within the Type 304 stainless steel hexagonal mesh, which was found to be very brittle and easily broken by hand pressure. Metallurgical examination revealed extensive carburization through the full thickness of the hexagonal mesh, including hexagonal mesh surfaces covered by the refractory. There was minimal wall loss at the exposed ends of the anchor system.

Iron sulfide and iron oxide scales were observed on the hexagonal mesh surface. Since sulfides can cause the chromium oxide layer to become porous, the presence of sulfides in the scale may be significant. Sulfidation and oxidation were most prevalent where the metal was carburized. Replacement hexagonal mesh was made of

Type 310 stainless steel. Although Types 304 and 321 stainless steel are reported to resist SO_2 to 800 °C (1470 °F), Type 310 stainless steel is resistant up to 1050 °C (1922 °F). However, Type 310 stainless steel is more prone to sigma phase formation than Types 304, 321, or 330 stainless steel. Since the hexagonal mesh flexes during start-ups and shut-downs, there is a concern that hexagonal mesh could fail due to embrittlement due to the high volume of sigma phase in the Type 310 stainless steel. Due to its overall good track record and performance or cost concerns with alternatives, Type 304H remains the industry workhorse for regenerator internals.

Another example involved refractory failure due to carburization of Type 321 stainless steel hexagonal mesh. In this case, examination of failed hexagonal mesh indicated that extensive carburization had occurred through the total thickness of the thin material. The carburization was homogenous, with carbide precipitation throughout the material. A denser layer of carburization was also visible on the outer extremities of the hexagonal mesh sample.

3.2.3.3 Internal Support Rods and Bars

Depending on the design, cyclones can be suspended from the dome of the regenerator by bars and rods or by the cyclone outlet tubes and hanger straps. Support components are usually made of Type 304H stainless steel. Creep failures have been reported in these components [6].

Creep voids were found at the failed end of the cyclone support rods and are shown in the referenced paper. Various stages of creep damage can be seen, including isolated voids, elongated voids, linked voids and macro cracking. Therefore, it is likely that this bar failed due to long-term creep damage.

There have been a number of support failures where it was suspected that afterburning events produced local hot spots and corresponding high thermal stresses resulting in support rod failures due to short-term stress rupture.

PT inspection of these components can be used to detect advanced stages of creep damage. Depending on the configuration, straight beam ultrasonic testing techniques of rod type supports can be used to detect advanced stages of concealed damage.

Sigma phase embrittlement of the support bars is also a concern. There have been cases where failure occurred during a shut-down as a result of transient thermal stresses on embrittled support structures.[ibid.]

3.2.3.4 Regenerator Plenum

The plenum acts as a header that channels flue gas from the cyclone gas outlet tubes to the overhead outlet nozzle.

Failures have been reported in plenums as a result of short-term stress rupture or long-term creep. The high temperatures and localized stresses needed to cause short-term stress rupture damage are often attributed to after-burning episodes. Long-term creep is more likely an issue at known high stress locations such as gas outlet tube-to-plenum welds. These can be inspected by PT if accessible or ultrasonic testing (UT) shear wave from the outside of the plenum to gas tube connection.

Some regenerator plenums have internal water sprays to reduce overhead flue gas temperatures due to downstream equipment temperature limitations. Several cases of thermal fatigue cracking were reported where injected water impinged on the plenum wall. Often, the refractory has spalled and thermal fatigue damage can appear as a fine network of cracks on the plenum floors or walls, distorted floors, and cracked fillet welds at gas outlet tube reinforcement pads.

With transgranular thermal fatigue cracking due to water injection, multiple cracks will be visible and indicate variations in stress orientation. Variations in crack width indicate that the cracking occurred over a period of time, not as a one-time event. Tight cracks will appear to be newer and indicate that the cracking is still active.

Thermal fatigue cracks can also occur when thermal growth of the plenum that combines with a stress concentration at a fillet weld that attaches the plenum skirt to the head. Cracks can form at the toe and root of the fillet weld [7].

These cracks can grow during startups and shutdowns, particularly during abrupt temperature fluctuations. Newer designs use a reinforced stub with a full penetration fillet weld [8].

Repairs of these components are often made using 16Cr-8Ni-2Mo (“16-8-2”) stainless steel weld metal. This is a variant of 308 series stainless filler metal, with lower chromium to produce less ferrite to reduce sigma phase. The addition of 2 % Mo improves creep strength in this ductile filler metal. More details on this filler metal are in Section 4 repair sections.

3.2.3.5 Flue Gas Overhead Duct Piping

Flue gas outlet piping from the regenerator is generally made from Type 304H stainless steel for hot wall designs. While sulfidation, oxidation, and carburization are generally not problems in overhead ducts, thermal stresses and low ductility due to sigma phase embrittlement of welds and base metal has resulted in online leaks.

Some sections are refractory lined to reduce skin temperature, thereby reducing thermal growth and the accompanying mechanical problems. When refractory is used, the refractory lining is terminated far enough upstream of any power recovery system (expander) to prevent spalled refractory from entering into the rotating equipment.

Piping and equipment designers should consider applied and induced loads from low-cycle thermal expansion during shut-down and start-up conditions. Significant damage can occur during rapid shutdowns due to upset conditions such as a loss of power.

Large diameter piping often utilizes mitered joints for elbows. These welds are subject to high stresses since thermal expansion and contraction is significant at the welds which are located at stress concentration points. As such, many users perform dye penetrant inspection of these joints during turnarounds.

Piping flexibility analysis of flue gas piping should include spring hanger and pipe support audits. These audits should include visual inspections of all piping supports to ensure that both spring cans are properly operating in both the hot and cold conditions and that piping shoes did not fall off of pedestals, restricting thermal movement, causing corresponding high localized stresses. Low-cycle thermal fatigue and creep/stress rupture can occur as a result.

Repair of equipment in FCCU regenerator overhead piping is complicated by its large diameter which is often inherently stiff and inflexible piping. The high ductility and strength of the 16-8-2 or similar filler metal, along with its resistance to sigma phase embrittlement, improves the reliability of repairs (see Section 4).

3.2.3.6 Metallurgical Embrittlement Considerations

Sigma phase embrittlement of high-ferrite weld deposits result in low ductility when cooled below about 260 °C (500 °F) and also in an inability to tolerate large thermal transients during process upsets. For this reason, cracks or leaks are often found during shut-downs or on-line following a rapid uncontrolled temperature swing.

Figure 6 [9] shows an example of a large diameter Type 304H stainless steel flue gas mitered elbow joint that was replaced after 11 years of service due to severe distortion and cracking. It operated at an average temperature of 715 °C (1320 °F) and suffered chronic cracking at the welds on the intrados that seemed to occur each time the unit was shut down and the piping was cooled to ambient temperature. The cracking was attributed to sigma phase embrittlement and required lengthy repairs involving crack removal and re-welding. On occasions, the old weld had to be removed as a window which encompassed both sides of the weld and replaced with inserts and a new weld. In another refinery with similar problems, the mitered elbows were replaced by formed elbows.

In a case [10] of creep cracking shown in Figure 7, Figure 8, and Figure 9, a crack 2.4 m (8 ft) long developed in a longitudinal weld seam in a 180 cm (72 in.) diameter Type 304H stainless steel duct that was flux-cored arc welding (FCAW) with Type 308H stainless steel consumable.

Figure 6—An Example of a Mitered Joint After Removal From Service

Interdendritic creep cracking was found in the large welds at the outside diameter (OD) of the piping. The pipe longitudinal seam welds appeared to have been welded with a two pass submerged arc weld procedure. Test of material removed from the weld showed high levels of sigma phase and that the weld had half the remaining creep life of the base metal.

Figure 7—Creep Failure on a FCCU Regenerator Overhead Line

In a fourth reported case, inspection noted a 1 m (3 ft) crack in a circumferential duct weld. Cracking was attributed to the presence of bismuth in the FCAW welding consumable. Bismuth limits of 0.002 wt% (as given in API 582) should be observed when service temperatures are above 538 °C (1000 °F).

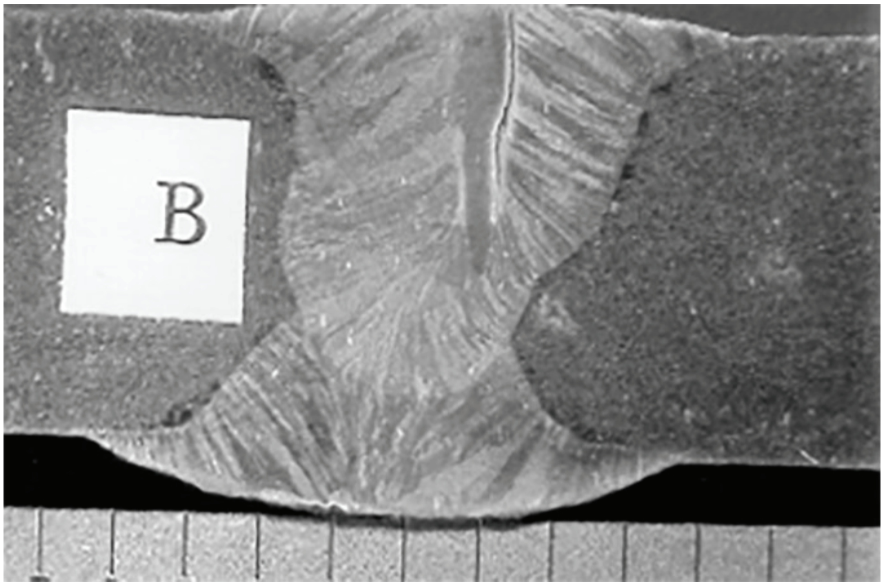

Figure 8—A Two Pass SAW Weld Was Found with Creep Cracking in the Outside Weld Bead

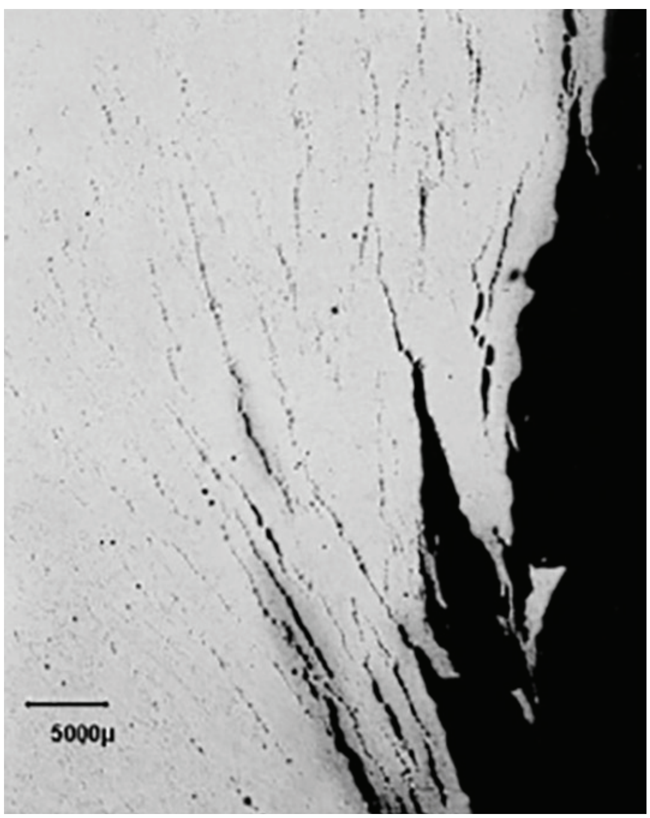

Figure 9—Interdendritic Creep Voids and Cracking in a Weld Cross Section

Another case involved a hot wall piping design that was 25 years old with operating temperatures at about 640 °C (1184 °F). Approximately 10 years prior, portions were replaced using Type 321H stainless steel welded with Type 347 stainless steel filler metal without post weld heat treatment (PWHT). After a failure, samples of weld metal were cut out for laboratory analysis. The Type 347 stainless steel weldments were found to be extremely brittle and the delta ferrite had transformed to sigma. Weld samples exhibited very low ductility when bent. Metallographically, the area fraction of sigma phase was 5 % to 8 %. When heated to 1037 °C (1900 °F), the sigma phase transformed back to ferrite. After heat treatment, the ferrite number was measured to be 5 FN to 8 FN. Results of hardness testing found the welds were 240 to 320 Vickers. Chemical analysis revealed high Nb concentrations, approximately 1%.

3.3 Hydrogen/Syngas Plants

3.3.1 Process Description

3.3.1.1 General

Hydrogen and syngas plants use heat and steam to reform hydrocarbons (primarily methane) into hydrogen, carbon monoxide and carbon dioxide. A simplified process flow diagram is show in Figure 10 [1]. Depending on the design, the mixed feed (steam and hydrocarbon) typically enters the radiant section via inlet headers and inlet pigtails. The inlet piping systems of older vintage reformers (generally built prior to 2000) typically operate at temperatures between 370 °C to 593 °C (700 °F to 1100 °F) and are usually fabricated from low-alloy steels (Cr-Mo steels), which are outside the scope of this report.

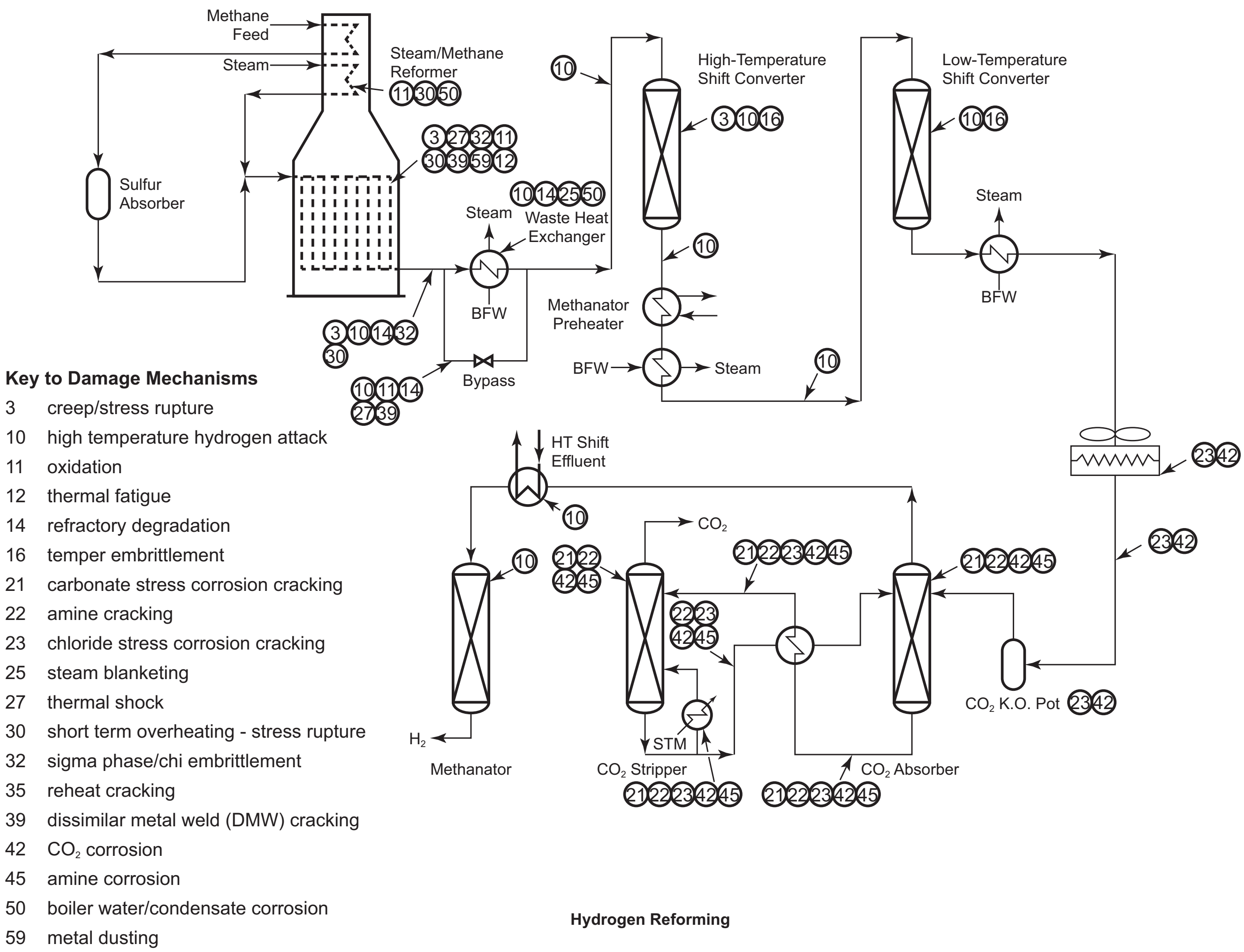

Figure 10—Hydrogen Reforming Process Flow Diagram

Reformer product gases leave the furnace at temperatures ranging from 790 °C to 860 °C (1450 °F to 1580 °F). Reformer effluent is typically cooled in waste heat recovery boilers that operate at conditions which can promote embrittlement and cracking. Waste heat boilers equipped with a bypass tend to suffer sigma phase embrittlement and metal dusting of their austenitic stainless steel liners and bypass valve components. An alternate design employs a secondary reformer in place of a waste heat boiler. In this design, the hot syngas from the primary reformer outlet is used to heat incoming feed and generate additional syngas. The secondary reformer vessel, internals, and associated piping are typically fabricated from austenitic stainless steels and are exposed to temperatures covered by this document. These components can be susceptible to stress relaxation cracking, sigma phase embrittlement and metal dusting, which is a significant concern; however, metal dusting is outside the scope of this document.

3.3.1.2 Preheater Feed Coil Inlet Header and Coil in the Reforming Furnace

In unit designs which have a preconverter, such as shown in Figure 11 [11], there is typically a feed/steam preheat coil in the convection section of the reforming heater which has inlet and outlet temperatures of approximately 510 °C (950 °F) and 640 °C (1184 °F). A typical design temperature for this coil is 825 °C (1517 °F). The materials for the tubes and headers are typically grades of stainless steel such as Type 321 stainless steel and Alloy 800H/800HT®. The inlet piping and vessel are Cr-Mo steels, but the outlet piping can be either Cr-Mo steels or austenitic stainless steels.

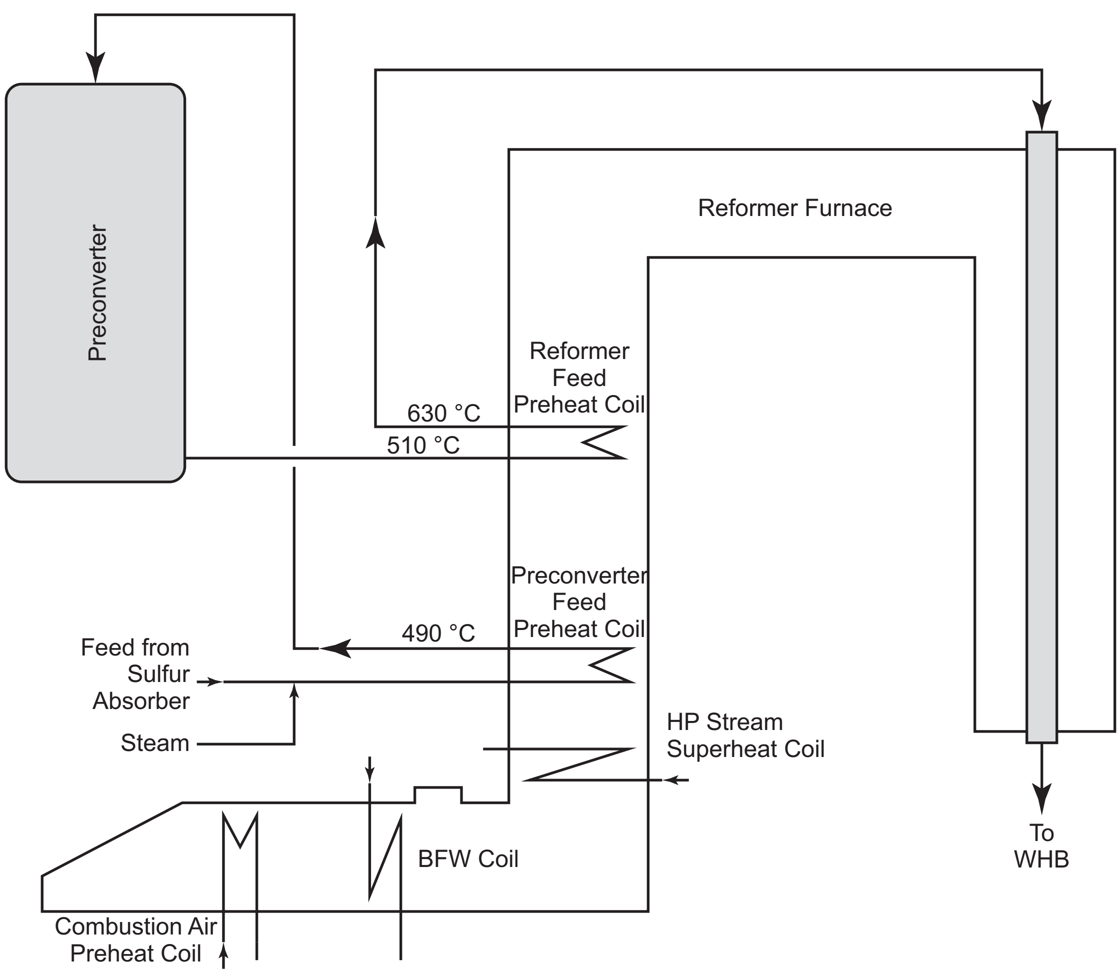

Figure 11—Reformer Feed Preheat Coil Arrangement in Units with a Preconverter

Stress relaxation cracking has occurred at stainless steel tube and outlet header welds on the Reformer Feed Preheat Coil. In one unit, leaks were detected after seven and nine years of service. The coil was then replaced with the same materials, but with the addition of PWHT to relieve residual stresses. The replacement coil has operated successfully up to the time of the report, but had only been in service for a few years.

Stress relaxation cracking failures have been reported in the inlet header piping. There are no reported failures attributed to sigma phase, perhaps due to operating temperatures being at the very low end of sigma phase precipitation temperature range. SRC failures have also been associated with heavy (thick) pads fillet welded to the OD of the inlet headers.

Reformers that have Preconverters utilize higher reformer inlet temperatures between 566 °C to 630 °C (1050 °F to 1166 °F) and the inlet piping to the reformer section are normally fabricated with Type 304H or Type 347H stainless steel.

3.3.1.3 Superheater Tubes

Wrought 300 series stainless steels and Alloys S800H and 800HT® are commonly used for the hottest convection section tubes and headers. Stress relaxation cracking, a mechanism associated with fabrication stresses and heat treatments, and short term stress rupture in-service failures have been reported in these alloys.

Steam superheater coil failures from various refinery processes have been included in this section (hydrogen reformers and hydrotreaters). One reported failure [12] occurred in Alloy 800H tubes in the convection section of a reformer heater operating at approximately 675 °C (1250 °F). Tube metal temperatures were monitored using skin thermocouples (T/Cs) that were protected by T/C shields. T/C shields, shown in Figure 12 [ibid.], are used to reduce temperature measurement errors due to radiation from burner flames and other furnace components. While the original shields did not crack, thermocouple replacements required new shields that cracked at the attachment welds when placed back into service.

Failures were attributed to stress relaxation cracking. Cracks, shown in Figure 13 [ibid.], were slightly branched intergranular cracks and had a Ni-rich filament which is typical of this damage mechanism. The original welds made without PWHT did not crack; however, the post-fabrication welds that were made on aged material without PWHT cracked. It was concluded that the aged material suffered a loss of creep ductility and cracked due to high residual stresses from welds which relaxed during high-temperature service. Cracks were removed by grinding. The affected tubes were then solution heat treated at 1150 °C to 1177 °C (2100 °F to 2150 °F) for one hour to restore ductility. Welds were deposited, and afterward were stress relieved at 900 ±14 °C (1650 ±25 °F) for 1½ hours. In this way, the residual stresses were relaxed before aging could occur (with the subsequent loss of creep ductility).

In another steam-methane reformer convection section feed preheat coil, stress relaxation cracking and sigma phase embrittlement were observed in pipe welds and in forged fitting-to-outlet header welds operating between 517 °C (963 °F) and 630 °C (1166 °F). Damage was observed after about nine years of service. The tubes were Alloy 800H and the header was Type 321 stainless steel.

In another case, circumferential cracking was observed after three months of service in Alloy 800HT® steam superheater coil welds in a hydrocracker heater. Subsequent investigation revealed intergranular fissuring and oxidation with intergranular and transgranular penetration on both the tube ID and OD. The average operating temperature was 616 °C (1140 °F), with occasional excursions to 766 °C (1412 °F).

Details for avoiding SRC and repair procedures are given in Section 4. Typically, repairs include the use of a solution annealing procedure to improve ductility while welding followed by a stress relief procedure to reduce the potential for future cracking.

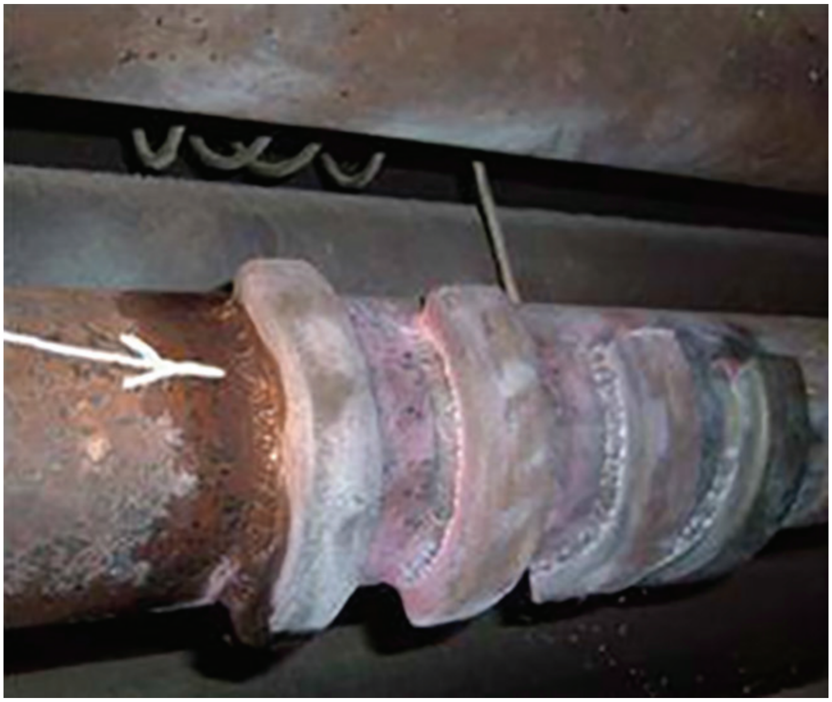

Figure 12—Multiple T/C Shields Welded to an Alloy 800H Superheater Tube

Figure 13—Cross Section of a Crack at the Toe of One of the TC Shields Showing Intergranular SRC

3.3.2 Reformer Effluent Heat Exchanger

Figure 14 [13] shows the inlet channel of a reformer effluent heat exchanger with syngas on the tube side and superheated steam [2.7 MPa (400 psig)] on the shell side that cracked during service. The inlet channel and tubesheet that were fabricated from Alloy 625 while the tubes were 2$^1/_4$Cr-1Mo with Alloy 601 ferrules installed at the inlet. The tubes were strength welded to the tubesheet with Inconel 52 filler metal, AWS A5.14, and ERNiCrFe-7. The shell was fabricated from A516-70 carbon steel in 1999.

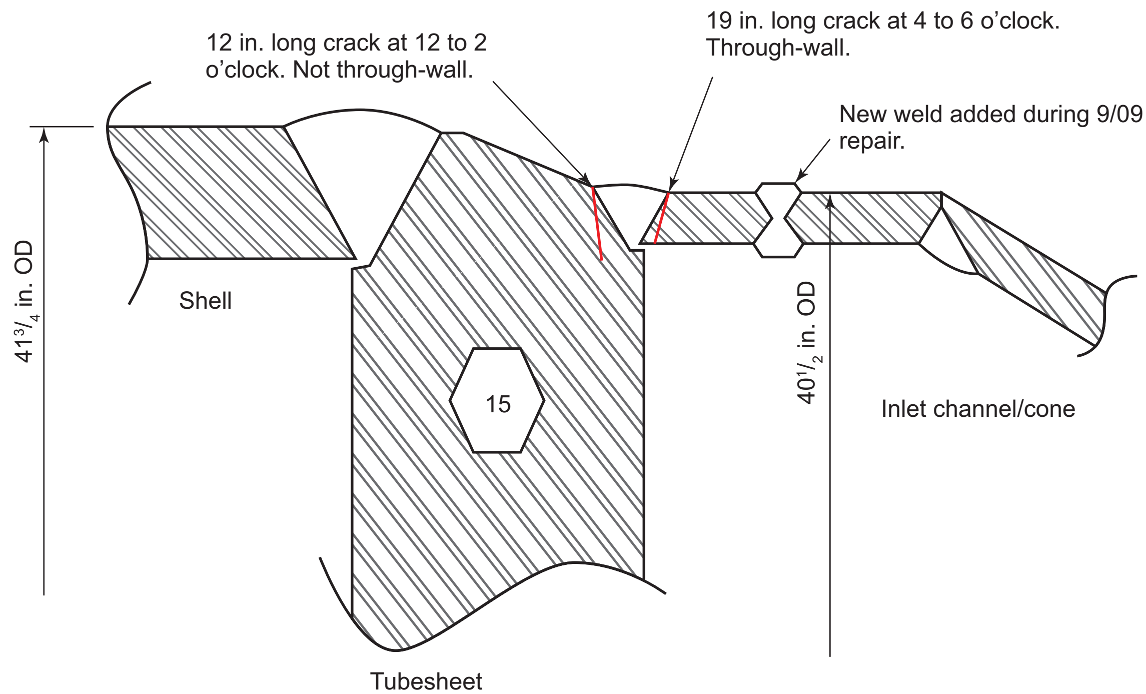

Figure 14—Tubesheet-to-Inlet Channel Cone that Cracked in Service

After 10 years of operation, the channel was cut off to repair ferrules at which time it was also discovered the tubes had suffered metal dusting. A new weld was added to re-install the channel and the exchanger was placed back in service. Approximately two months later, the inlet channel leaked, causing a fire.

The leak was from a 48 cm (19 in.) long crack on the stub side of the new channel-to-tubesheet weld. A second 30 cm (12 in.) long crack was found on the tubesheet side of this weld. Figure 15.[ibid.] shows one of the cracks, all of which originated from the OD. Hardness values of the Alloy 625 were found to range from 42 to 45 HRC. Cracking was intergranular and displayed creep voids ahead of the crack. The failure was attributed to SRC.

The existing channel and stub were removed and the existing tubesheet was heated to 482 °C (900 °F) for 7 hours to bake out any residual hydrogen. Alloy 625 full penetration tubes to tubesheet strength welds were made. A new annealed Alloy 625 channel was installed, and the unit was brought online.

To reduce the hot inlet channel outer diameter skin temperature by approximately 110 °C (200 °F), a band of insulation on the inlet channel was removed and a steam ring was added at the tubesheet.

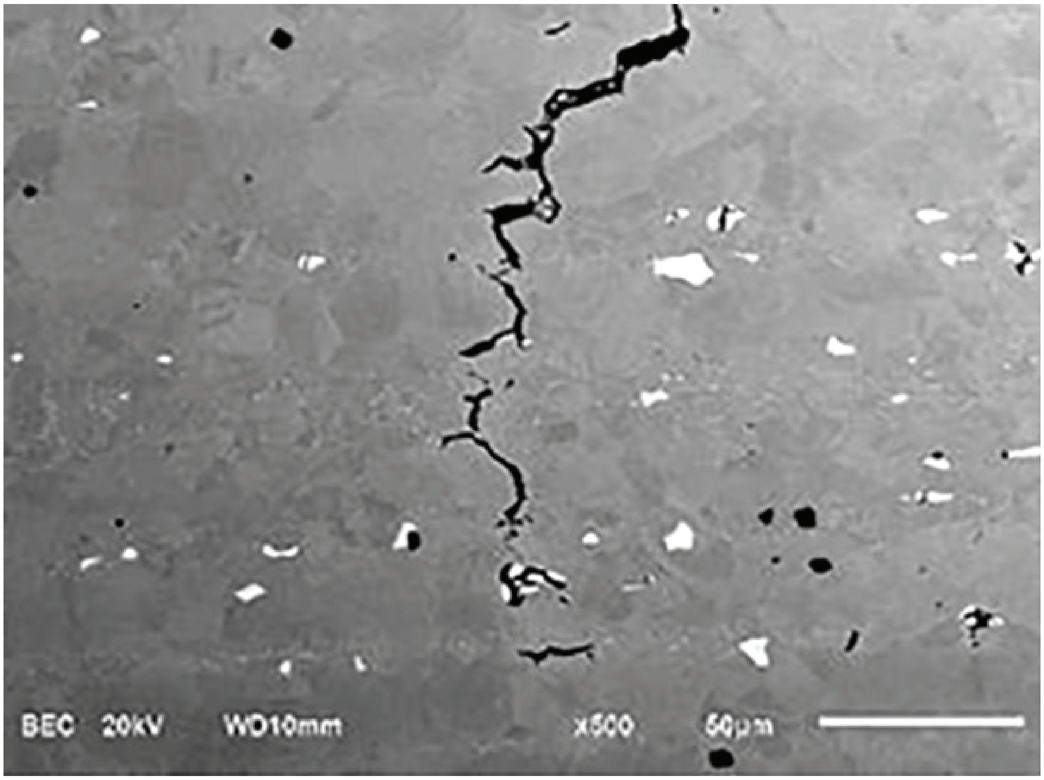

Figure 15—Cracking From the OD Was Intergranular and Was Attributed to SRC

3.4 Catalytic Reformers

3.4.1 Process Description

Catalytic reformers convert low octane refinery feeds into a high-octane product called “reformate”. A simplified process flow diagram of a catalytic reformer is shown in Figure 16 [1]. Reformate is added to gasoline stocks to increase the octane number.

Currently, catalytic reformer units are classified into two generic types; fixed bed (cyclic and semi-regenerative) and moving bed which are referred to as “continuously regenerated catalytic reformers” (CRCRs), and one is shown in Figure 17 [14].

Fixed bed units generally operate below 524 °C (975 °F). Metallurgy of the reactors in this style unit is generally either low-alloy Cr-Mo steels or carbon steel lined with insulating refractory. Heater tubes are typically $2^1/_4$Cr-1Mo steel or 9Cr-1Mo steel. Fixed bed units are not included in this report since they generally do not utilize austenitic stainless steels or alloys.

CRCRs utilize stacked Cr-Mo reactors that operate at 516 °C to 565 °C (960 °F to 1050 °F). Catalyst flows downward from the top reactor to the bottom reactor. CRCRs have two high-temperature sections, the reactor section which includes reactors and heaters, and the regenerator section where catalyst is cycled through a series of vessels to remove coke and prepare it for reuse.

3.4.2 Reactor Section

In a CRCR unit, the process stream is heated before entering each reactor in fired heaters that usually use Cr-Mo alloys, but sometimes use Type 321H or Type 347H stainless steel or Alloy 800H type materials. Problems have been

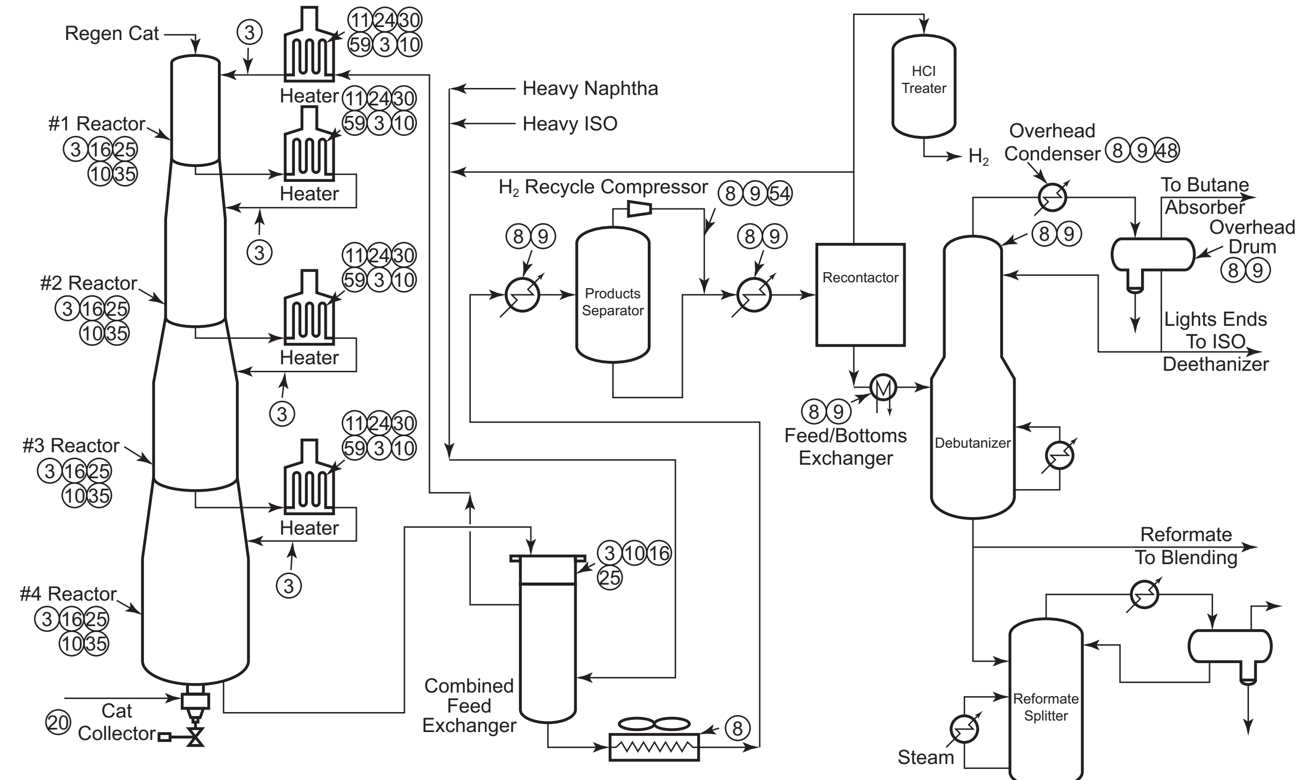

Key to Damage Mechanisms

3 creep/stress rupture
8 ammonium chloride corrosion
9 hci corrosion
10 high temperature hydrogen attack
11 oxidation
16 temper embrittlement
20 erosion/erosion-corrosion
21 carbonate stress corrosion cracking
24 carburization
25 hydrogen embrittlement
30 short term overheating—stress rupture
35 reheat cracking
48 ammonia stress corrosion cracking
49 cooling water corrosion
54 mechanical fatigue
59 metal dusting

Figure 16—Catalytic Reformer Simplified Process Flow Diagram

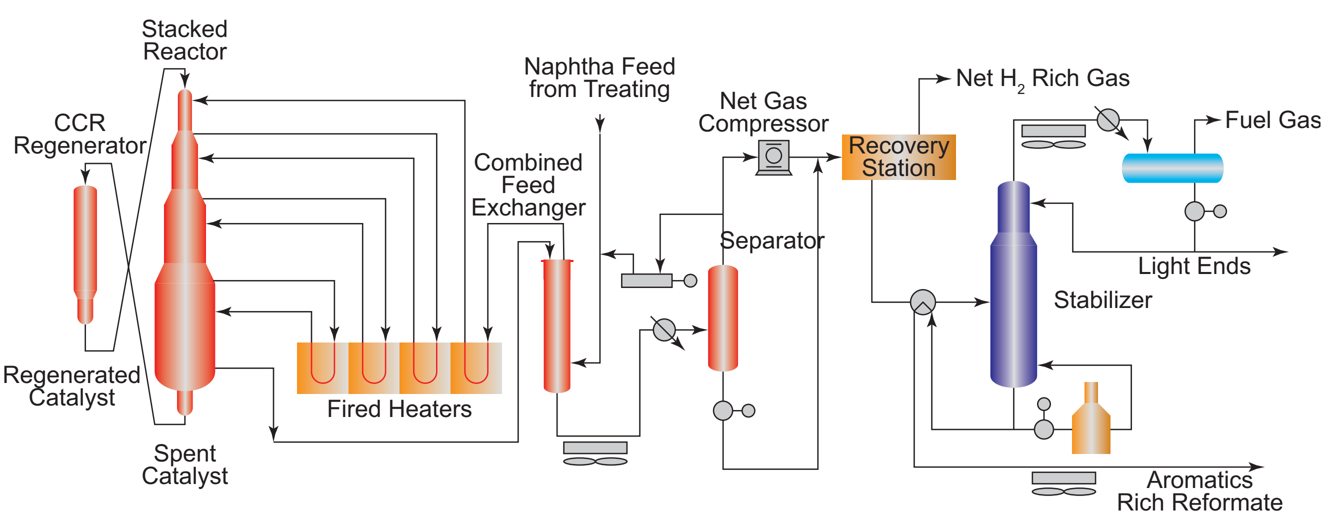

Figure 17—Continuous Regenerating Catalytic Reformer

experienced with thermal fatigue due to rain water contacting hot stainless steel heater headers at suspension type pipe support locations. Since these types of pipe supports require an insulation penetration above the pipe, designs that minimize the potential for rain ingress are preferred.

One type of insulation design that has experienced thermal fatigue cracking used a bolted rectangular box to cover the heaters' stainless steel inlet and outlet convection section headers. These rectangular box systems should be designed to prevent water from pooling on top and avoid dumping a stream of water onto the hot header. Thermal fatigue damage to the header can appear like a bulge that rises upward. Craze cracking (sometimes referred to as mud cracking) can also be present on the metal surface, which is typical of thermal fatigue.

Consideration can be given to using full encirclement bolt-on piping supports instead of fillet welded lugs. Stainless steel piping with fillet welded lugs can suffer stress relaxation cracking or creep cracking, depending on the stresses and temperatures.

There were no reported cases of stress relaxation cracking issues with 300 series or 800H/HT alloys in CRCRs, but operating temperatures are in the range where it is a concern. Refer to 4.4 for minimizing stress relaxation cracking risk of austenitic materials.

3.4.3 Regenerator Section

As the catalyst in these units becomes deactivated by carbon build-up; regeneration is required to burn off the coke. Regenerations are typically done at 428 °C to 570 °C (800 °F to 1060 °F) at low pressure in an oxygen controlled environment.

High-alloy nickel-based piping and equipment are used in CRCRs for catalyst extraction and regeneration. Equipment and piping are designed to inject the catalyst back into the reactor stack while on-line. The metallurgy from the point of catalyst extraction to re-injection uses high alloys to withstand the high temperatures, oxidizing and reducing atmospheres during the burn cycle, and hot chlorides during the chloriding cycle.

Inconel 600 is most commonly specified for hotter regenerator sections of CCRs and Inconel 625 is sometimes used in condensing areas. While Alloy 600 is not susceptible to high temperature embrittlement, long-term thermal exposure of Alloy 625 above 595 °C (1100 °F) may result in significant embrittlement [15]. However, cracking or embrittlement problems with these high nickel alloys have not been reported as an issue in regeneration vessels.

3.5 Delayed Cokers

3.5.1 Process Description

Delayed Cokers convert heavy, low-value hydrocarbons (such as vacuum resid) into coke and valuable lighter hydrocarbons. There are two primary coking processes, delayed coking and fluid coking. The most common coker technology is delayed coking, shown in Figure 18.

In delayed cokers, the heavy feedstock is heated in a coker heater and transferred to a coke drum where residence time promotes thermal cracking of the heavy hydrocarbons, producing coke and light hydrocarbons. This process is a semi-batch process, employing two or more drums in tandem.

Coker heater tubes are operated at inlet pressures of approximately 2086 kPa to 2413 kPa (300 psig to 350 psig). There is often a large pressure drop through the heater, typically down to 690 kPa (100 psig) at the outlet. Process outlet temperatures are typically 490 °C to 510 °C (915 °F to 950 °F) with tube metal temperatures sometimes in excess of 732 °C (1400 °F).

Coker heaters usually have a high heat load. Coking (coke layer formation) inside the tubes is a constant problem due to the heavy feeds and high temperatures. Steam is usually added to the feed to increase the stream velocity and minimize the amount of coke formed. The coke layer in the tube acts like an insulator and reduces the rate of heat

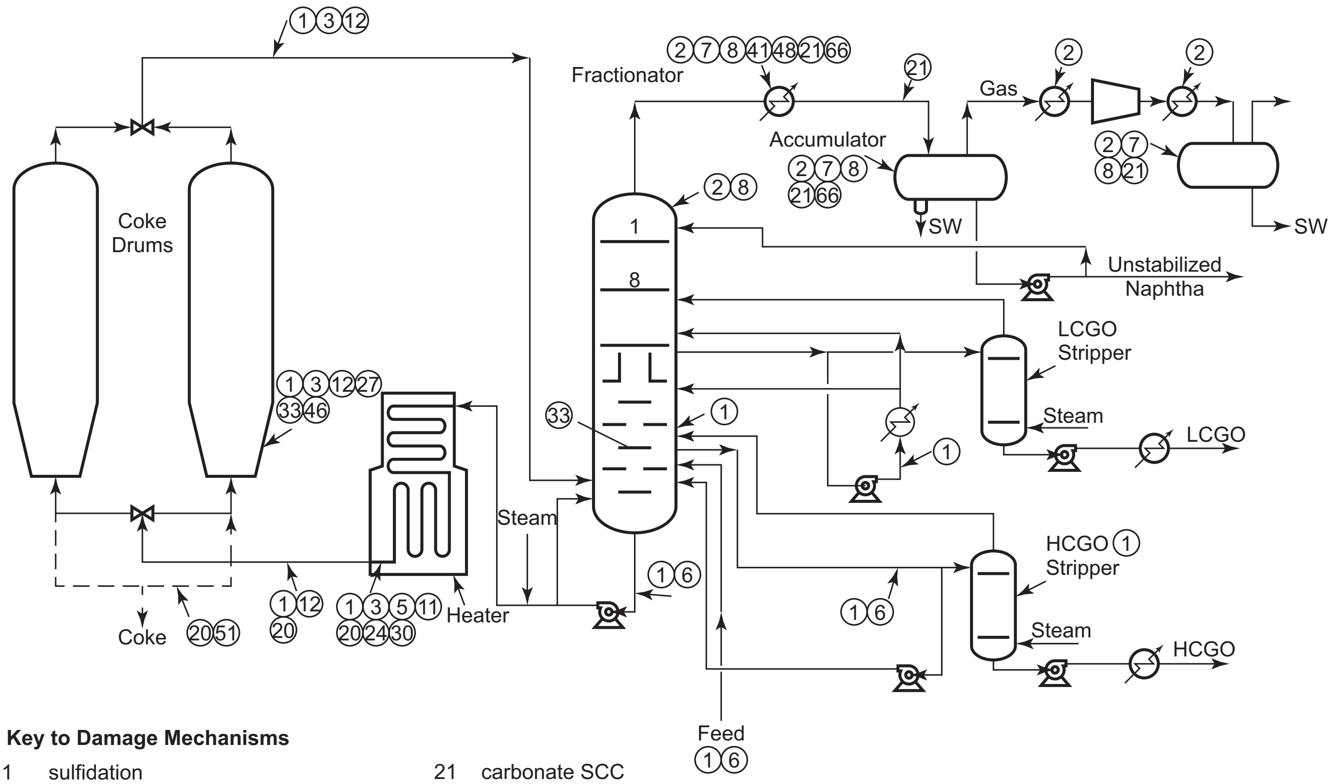

Key to Damage Mechanisms

1	sulfidation	21	carbonate SCC
2	wet H_2S damage (blistering/HC/SOHIC/SSC)	24	carburization
3	creep/stress rupture	27	thermal shock
6	naphthenic acid corrosion	30	short-term overheating—stress rupture
7	ammonium bisulfide	33	885 °F embrittlement
8	ammonium chloride corrosion	41	dealloying (dezincification/denicklification)
11	oxidation	46	corrosion under insulation (CUI)
12	thermal fatigue	48	ammonia stress corrosion cracking
20	erosion/erosion-corrosion	51	microbiologically induced corrosion (MIC)
		66	organic acid corrosion

Figure 18—Delayed Coker Simplified Process Flow Diagram

transfer into the hot oil. Therefore, as the furnace tubes coke, higher firing temperatures and corresponding higher tube metal temperatures are needed to heat the oil to the same temperature.

Coke build-up inside heater tubes also creates flow resistance, thus increasing the pressure drop across the heater. The combination of pressure drop and upper limits on tube metal temperatures dictate the need for periodic decoking. Decoking procedures include on-line spalling, steam/air decoking, or the use of specialized pigs to scrape the coke from the inside surfaces of the heater tubes.

On-line spalling involves replacing the oil in one pass with steam and/or boiler feed water to rapidly cool the coke layer. During the cooling, some of the coke deposit breaks free (i.e. spalls) as the coke layer shrinks in size. Excessive spall rates can cause plugging while excessive steam flow rates can cause erosion of the return bends.

Steam/air decoking is performed off-line. A steam spall is performed first, followed by a controlled burn of the coke deposits. This burn is achieved by using a mixture of steam and air inside the tubes at controlled temperatures. Coke on the inside of the tube ignites and burns. If not carefully monitored, tube damage (primarily distortions and creep) can occur due to excessive tube metal temperatures.

The pig decoking procedure is also done off-line; this method uses foam pigs with inserts (studs) to scrape the coke from the ID surface. There is a potential for incomplete removal of the coke due to tube swelling. Often, it is better to replace any tube sections with bulges, since these are probably close to creep failure. The scraping action of the pigs can remove the protective scale from the ID. The exposed base metal is more susceptible to carburization and corrosion due to the loss of the protective scale. The use of wider contoured carbide scrapers rather than sharp pointed carbide tips has reduced the grooving problems associated with this method.

3.5.2 Components

Coker heater tubes are commonly made of 9Cr-1Mo steel, but are sometimes fabricated from austenitic stainless steel or Alloy 800H type materials.

When 300 series austenitic radiant section tubes are used, they are usually made of thermally stabilized Type 321H or Type 347H stainless steel to minimize the risks of polythionic stress corrosion cracking during downtime.

3.5.3 Damage Mechanisms

3.5.3.1 Creep

Coker furnace tubes almost always operate in the creep regime. When evaluating tube condition, operating pressures and tube metal temperatures are important variables that can vary significantly during the run length due to internal coking.

Internal coke layers cause an increase in pressure drop across the furnace, requiring higher inlet pressures to achieve the same outlet pressure. This coke layer also necessitates higher tube wall temperatures for a given process outlet temperature.

In most furnaces, tubes near the outlet of the furnace are typically the most at risk of creep failure since the temperatures are highest. In coker heaters, creep can happen almost anywhere, usually associated with locations of heaviest coking. Since there is a large pressure drop across the furnace, the stresses at the inlet are higher, thus the inlet tubes cannot tolerate the same temperatures as the outlet tubes.

Some operators have suffered rapid short-term overheating, also called stress rupture, failures as seen in Figure 19 [16]. Burner flame patterns can result in local hot spots that reach temperatures well above the rapid creep threshold temperature which is 815 °C (1500 °F) for most austenitic stainless steels. Stress ruptures are characterized by open “fishmouth” failures and are usually accompanied by thinning at the fracture surface.

NOTE A triangle shaped sample was removed at the failure origin.

Figure 19—Stress Rupture of a Coker Heater Tube

3.5.3.2 Carburization

The conservative maximum tube metal temperature for carburization of austenitic alloys is approximately 593 °C (1100 °F). However, general experience is that the rate and extent of carburization becomes a significant problem above 730 °C (1350 °F).

Figure 20 [ibid.] shows an example of a Type 347H stainless steel tube that failed during pig decoking due to embrittlement from carburization and sigma phase formation. Carburization resulted in higher internal corrosion rates on the fire side of the tube. The tube cracked due to a lack of ductility at high hydrostatic pressure stresses during pigging operations.

The fire side of the tube was carburized up to 50 % of the wall thickness. It is possible that the localized carburization was accelerated by the internal scraping of the pig.

Cross sections of the tube wall (shown in Figure 21 [ibid.]) revealed variations in the depth of carburization. The scale at the bottom of this figure shows 0.1 in. divisions.

Subsequent creep testing revealed that the tube did not suffer a reduction of creep strength due to carburization. However, carburization and sigma phase tied up much of the chromium in the matrix, thereby reducing the sulfidic corrosion resistance to that of a lower grade alloy. One report found only 5 % Cr in the remaining matrix. Corrosion rates indicated that the tubes were corroding in a manner similar to 5Cr-Mo steel.

Figure 20—Carburized Tube that Cracked During Pig Decoking

Repair of carburized tubes is difficult since the carburized material melts at a lower temperature than the uncarburized base metal. If the furnace design is one where the tubes extend outside the firebox, repairs are generally easier in this zone since internal carburization is not present or is minimized.

3.5.3.3 Reheat Cracking/Stress Relaxation Cracking (SRC)

Although stress relaxation cracking is a possibility for Type 347H stainless steel coker heater tubes, it has not been reported as an issue in new fabrication probably because tube wall thickness is less than 12 mm ($^1/_2$ in.). Alloy 800H, and particularly Alloy 800HT®, are more susceptible to this issue than Type 347H stainless steel and coker heater operations are in the prime 593 °C to 704 °C (1100 °F to 1300 °F) metal temperatures for SRC. An operator reported having an issue with this in one coker heater with Alloy 800HT® tubes. The plant was trying to replace eroded bends during a shut down and could not make the new welds without HAZ cracks on the old tube side of the weld. The tubes

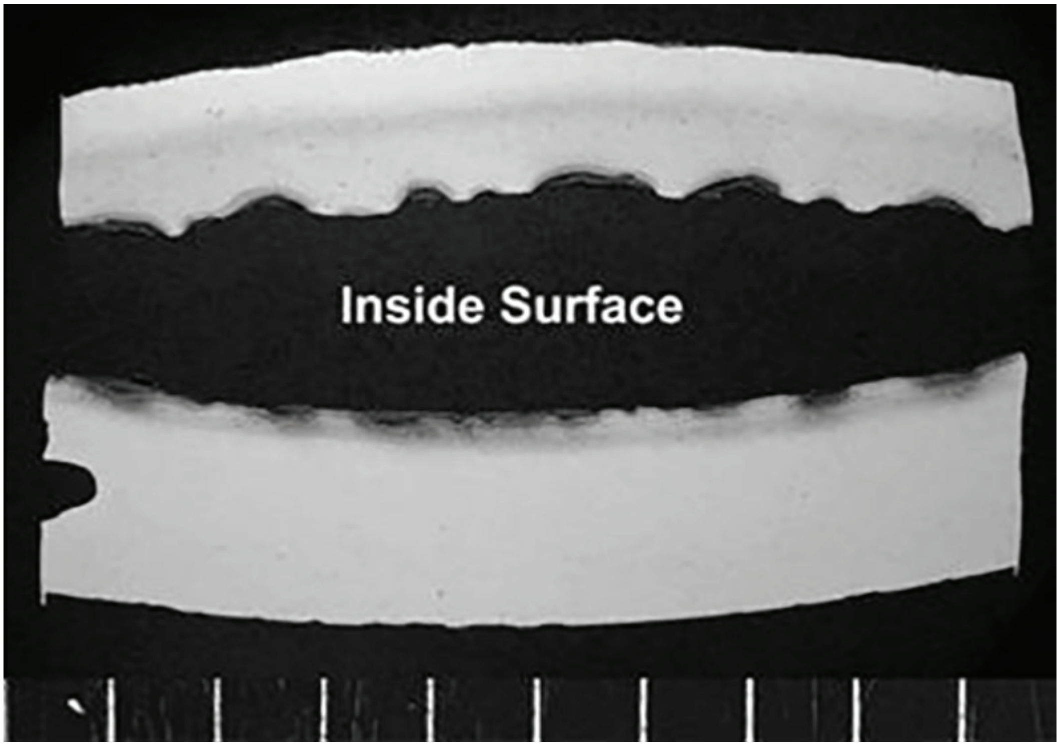

Figure 21—Carburized Tube Cross Section Showing Variations in Depth of Carburization

required a solution anneal of the old base metal to make a successful weld. For further discussions on repairs, please refer to 4.4 for minimizing stress relaxation cracking risk of Alloy 800H/HT® materials.

3.6 Hydroprocessing Units

3.6.1 Process Description

Hydroprocessing encompasses a family of high temperature processes that includes hydrotreating (for the removal of sulfur and nitrogen from feedstock), hydrocracking, hydrogenation and hydrofinishing. These reactions are conducted at varying temperatures depending on the feed composition and the desired products. Most reactors operate at temperatures less than 460 °C (860 °F), which is below the temperature threshold of concern in this report of 565 °C (1050 °F). However, some hydroprocessing units employ recycle hydrogen heaters that have elevated outlet temperatures above 565 °C (1050 °F) with tube metal temperatures that are higher in order to supply additional heat to mixed hydrogen-hydrocarbon feed streams. Hydroprocessing simplified process flow diagrams for Hydrotreating and Hydrocracking are shown in Figure 22 [1] and Figure 23 [17].

3.6.2 Materials of Construction

High-temperature damage to austenitic stainless steels and high Ni-Cr-Fe alloys are of concern for recycle hydrogen heaters and their outlet piping. Heavy wall reactors and stainless steel feed/effluent piping are also included in the scope of this document because they may experience stress relaxation cracking problems during fabrication. Steam super heater coils may be located in the convection section of the fired heaters in this unit. Steam super heater coils are discussed in the hydrogen/syngas plant section, 3.3.1.

Recycle hydrogen heater tubes are often made with austenitic stainless steel or Alloy 800H or Alloy 800HT®. Reactor feed and effluent piping and hot recycle hydrogen piping are commonly made of either Type 321 or Type 347 stainless steel.

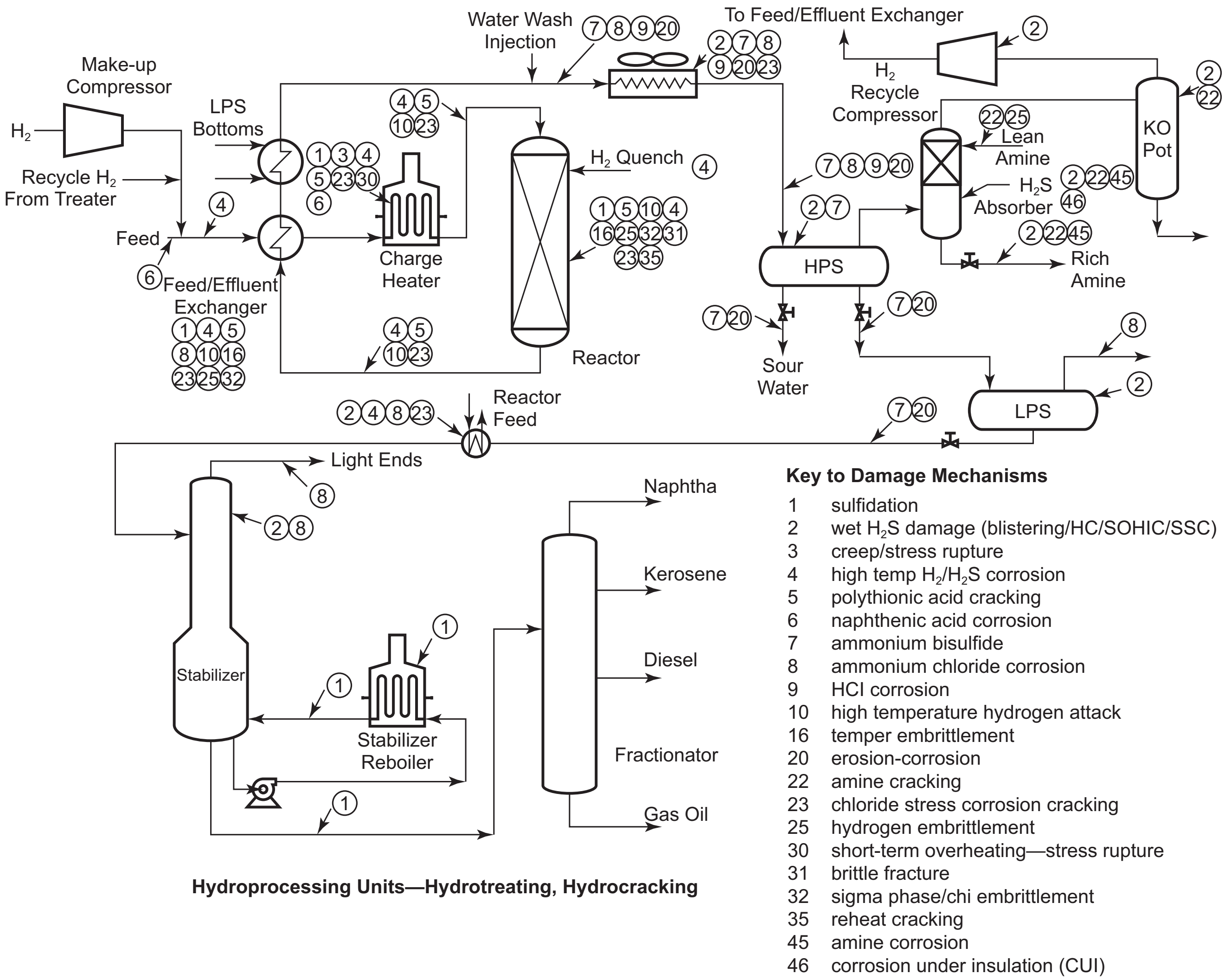

Figure 22—Hydroprocessing Simplified Process Flow Diagrams for Hydrotreating and Hydrocracking

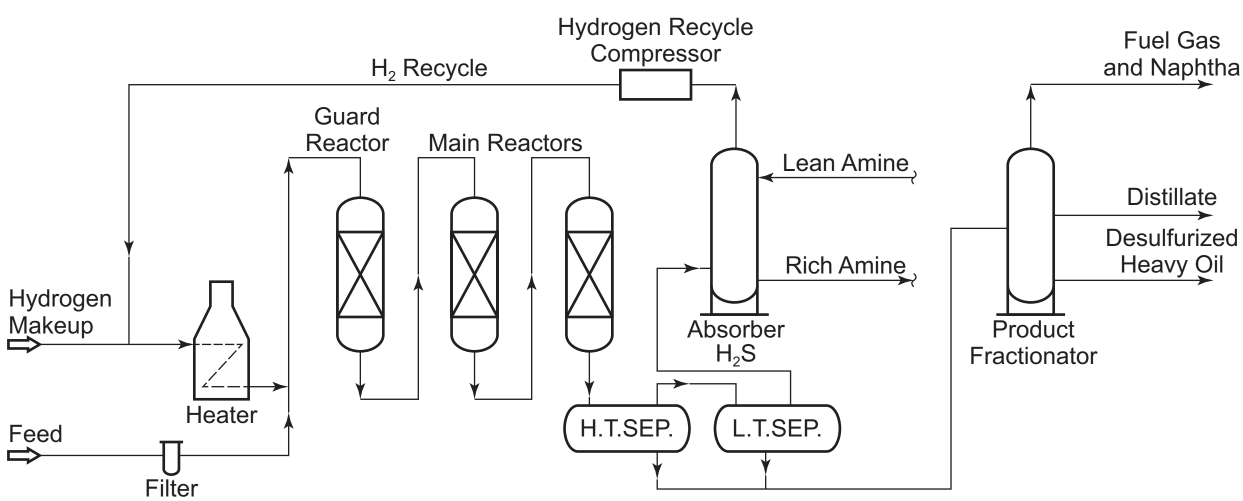

Figure 23—Hydroprocessing Simplified Process Flow Diagram of a Hydrotreater with a Recycle Hydrogen Heater

3.6.3 Damage Mechanisms

Recycle heater tube and outlet piping potential damage mechanisms include creep, sigma phase embrittlement, and SRC.

Heavy wall reactor feed and effluent piping can suffer SRC during fabrication. SRC during fabrication is usually not a problem with piping or tubing with roughly less than 19 mm ($^3/_4$ in.) wall thickness. Repairs to embrittled materials can suffer SRC at any wall thickness.

3.6.4 Hot Recycle Hydrogen Piping

A 254 mm (10 in.) diameter piping run from a hydrogen heater to a hydrocracker reactor suffered 12 on-line leaks within 16 years of operation [18]. The pipe was fabricated from Type 347H stainless steel with matching weld metal. Based on published information, the leaks reportedly caused 12 unplanned shutdowns for a total of 64 days lost production. The line operated at a pressure of 19.5 MPa (2825 psig) and a temperature of 554 °C (1030 °F). Pipe wall thickness was 25.8 mm (1.017 in.).

Cracking was attributed to stress relaxation cracking compounded by:

— ferrite transformation to sigma in the weld metal, causing embrittlement;

— piping support malfunctions that contributed to high stresses (spring cans that relied on sliding friction with pipe support shoes);

— residual stresses from repair welds to materials that were already embrittled, causing repeat cracking that occurred at an increasing frequency;

— stress intensification at weld discontinuities, such as peaking in long seam welded piping and internal root beads and external cap reinforcements on butt welds; and

— field welds at high stress locations.

To remedy these problems, a number of corrective actions were taken. Specifically:

— performed a piping stress and flexibility analysis to determine where to locate field welds in order to be in low stress locations—longer spool piping segments were required which made field installation more complicated;

— increased relative wall thickness to reduce the pipe operating stresses;

— reduced the ferrite content in welds by:

  — limiting the filler metal selection to those batches that produced welds with 3-8 FN and

  — using a GTAW welding process that produced fewer reheat cracking problems;

— reduced stresses at pipe supports:

  — changed fillet welded bottom sliding supports to overhead suspended supports to allow more freedom for thermal expansion—this required additional support structures to be installed—and

  — used full encirclement pipe hangers;

— reduced weld discontinuities to decrease localized stresses:

  — used seamless pipe when available to minimize any joint high/low mismatch of the ID or OD surfaces,

  - used long weld neck flanges to move the weld away from changes in section thickness,
  - used bent pipe long radius elbows when possible, and
  - removed external weld reinforcement and ID root bead profile when possible; and
- increased the amount of non-destructive testing (NDT) to detect fabrication cracks prior to placing equipment in service.

3.6.5 Reactor Feed and Effluent Piping

While reactor feed and effluent operating temperatures are not subject to embrittlement in service, stress relaxation cracking has been reported in pipe-to-fitting fabrication welds of Type 321 stainless steel pipe in a hydrocracker. The major cause of the problem was reported to be excessive restraint and thermal stresses during local PWHT. A piping stress and flexibility analysis was performed to identify key locations of restraint and high stresses during the PWHT cycle [19, 20].

For further details on repairs, please refer to 4.4 for minimizing stress relaxation cracking risk.

4 Damage Mechanisms

4.1 Metallurgical Embrittlement

With all forms of metallurgical embrittlement, formation of the various phases occurs as a function of time at high temperature. The presence of intermetallic compounds within the grains and at grain boundaries embrittles the material. While formation of these phases occurs at elevated temperatures, embrittlement is usually much more harmful once the material cools below 260 °C (500 °F). Also, while the compositions of the different phases within the alloy can be very different, the overall chemical composition of the alloy remains the same.

Different alloying elements help control the phase composition of an alloy. Table 2 lists the elements that promote the formation of either ferrite or austenite. This table is useful to help understand the general effects of alloy composition on the phases that can be present.

Table 2—Ferrite and Austenite Formers

Ferrite Formers	Austenite Formers
Iron	Nickel
Chromium	Nitrogen
Molybdenum	Carbon
Silicon	Manganese
Niobium (Columbium)	Copper
Aluminum	Cobalt
Titanium	—
Tungsten	—

Chemistry of the alloy, exposure temperature and time are the key factors in what secondary precipitated phases will form. Often, added elements will have multiple effects. For instance, while molybdenum is a ferrite former, it can create unstable oxides at high temperatures, reducing an alloy's oxidation resistance. It also promotes sigma and laves phase formation on long-term aging.

Nitrogen stabilizes and strengthens austenite and it slows down the formation of secondary phases, including sigma phase and carbides. Manganese stabilizes austenite and it increases nitrogen solubility. Niobium and titanium are very strong carbide formers that contribute to high-temperature strength and mitigate grain boundary chromium carbide formation that causes sensitization.

Sulfur and phosphorus are kept to their lowest practical limit since they do not contribute any benefits to high-temperature applications. They reduce hot ductility (including creep ductility) and increase the likelihood of solidification cracking during welding. Too little sulfur can lead to weld penetration problems [21].

Time temperature transformation (TTT) diagrams are used to understand the relationship of time at a given temperature that will result in various precipitated phases. An example TTT diagram that has a curve for carbide precipitation and a curve for sigma, Chi, and Laves phases appears in the referenced publication for Type 316 stainless steel [22]. The diagram indicates that carbide formation occurs much quicker than sigma and other phases. It takes approximately 100 hours to begin forming Laves and Chi phases and 1000 hours to form sigma phase. These are generally not a concern for welding, but embrittlement is a concern if operating above 500 °C (950 °F).

In order to solution anneal an alloy, the temperature must be higher than that of precipitation. The same referenced publication also has a TTT diagram for Alloy 800 material.

Table 3 [23] and Table 4 [ibid.] give the most common phases formed in the various alloys listed as well as a summary of the other embrittling damage mechanisms and temperatures at which they occur. These tables also give the solution annealing temperature required to dissolve embrittling secondary phases to put the alloy back into a more ductile condition, similar to original condition. Solution annealing will not remove creep, SRC, or any other cracking type of damage.

4.2 Sigma Phase Embrittlement

4.2.1 General

Sigma phase is a hard, brittle, nonmagnetic solid solution of a stoichiometry close to FeCr, which can precipitate in commercial iron-chromium, iron-chromium-nickel stainless steels, and heat resisting alloys at elevated temperatures. It was discovered by Griffiths and Bain in 1927, after eluding investigators for years. Prior to 1927, its existence was a highly debated subject, as sigma phase was difficult to detect due its very slow reaction rates.

In commercial alloys, sigma phase forms at temperatures ranging from 550 °C to 954 °C (1020 °F to 1750 °F), depending on composition, with the most favorable conditions ranging from 710 °C to 800 °C (1310 °F to 1470 °F). While corrosion resistance may be affected at these elevated temperatures, the greatest detriment of sigma phase is its tendency to significantly reduce room temperature fracture toughness from ambient up to around 260 °C (500 °F). However, severely sigma embrittled materials can have low toughness even at high temperatures.

While reduction of area and elongation are strongly influenced by the extent of sigma in the matrix, there appears to be no trend relating the tensile and yield properties of alloys that have undergone sigma formation. Charpy V-Notch (CVN) impact energy tests appear to be the mechanical property most affected by sigma formation [24].

Sigma can form from two mechanisms, transformation from ferrite to sigma or it can be formed by a transformation from austenite to sigma. Sigma phase forms much faster from ferrite. Deposited weld metal is typically designed to have ferrite contents of 3 % to 12 % in order to increase hot ductility and minimize the potential for solidification cracking. Austenitic stainless steel castings are typically designed with ferrite contents of 10 % to 25 % to minimize solidification cracking. The ferrite number (FN) is a calculated value indicating the ability of a particular chemical compound of steel to form ferrite upon solidification from the molten state. The higher the FN, the higher the percent of ferrite formed. Weld metal with significant ferrite (FN > 9) and castings exposed to high temperatures exhibit higher percentages of sigma phase than do the corresponding base or wrought metals. Because of this, the ferrite number/concentration is typically limited in high-temperature component welds and should be held as low as practicable for high-temperature cast stainless steel.

Table 3—Austenitic Stainless Steel Embrittlement Phases and Stress Relaxation Cracking Susceptibility

Alloy	High Temp. Embrittlement Temperature Range	Embrittlement Phase Laves -η Sigma -σ Chi -χ	Stress Relaxation Cracking Temperature Range	Applicable PWHT to Minimize Stress Relaxation Cracking	Sensitization Temperature Range	Carbide Formed	Comments
304/304H 316/316H, 317	550 °C to 900 °C (1020 °F to 1650 °F)	η	500 °C to 780 °C (1110 °F to 1740 °F)	N/A PWHT causes sensitization concerns.	370 °C to 815 °C (700 °F to 1500 °F)	MC	Low susceptibility of SRC for these grades.
	550 °C to 1050 °C (1020 °F to 1920 °F)	σ			600 °C to 950 °C (1110 °F to 1740 °F)	$M_{23}C_6$	H grades have higher elevated temperature strength, but increased susceptibility to sensitization.
	600 °C to 900 °C (1110 °F to 1650 °F)	χ			700 °C to 950 °C (1290 °F to 1740 °F)	M_6C	
304L, 316L, 317L	550 °C to 900 °C (1020 °F to 1650 °F)	η	500 °C to 780 °C (1110 °F to 1740 °F)	N/A Excessively long PWHT may cause sensitization concerns.	370 °C to 815 °C (700 °F to 1500 °F)	MC	Low susceptibility of SRC for these grades.
	550 °C to 1050 °C (1020 °F to 1920 °F)	σ			600 °C to 950 °C (1110 °F to1740 °F)	$M_{23}C_6$	Reduced sensitization due to low carbon.
	600 °C to 900 °C (1110 °F to 1650 °F)	χ			700 °C to 950 °C (1290 °F to 1740 °F)	M_6C	
321	550 °C to 900 °C (1020 °F to 1650 °F)	η	500 °C to 780 °C (1110 °F to 1740 °F)	PWHT: 900 °C (1650 °F) 1 hr/25 mm (1 in.), 3 hr minimum, followed by still air cool.	370 °C to 815 °C (700 °F to 1500 °F)	MC	Carbides stabilized with Ti; thus have a reduced risk of sensitization.
	550 °C to 1050 °C (1020 °F to 1920 °F)	σ			600 °C to 950 °C (1110 °F to1740 °F)	$M_{23}C_6$	PWHT also improves sensitization resistance.
	600 °C to 900 °C (1110 °F to1650 °F)	χ			700 °C to 950 °C (1290 °F to 1740 °F)	M_6C	
347	550 °C to 900 °C (1020 °F to 1650 °F)	η	500 °C to 780 °C (1110 °F to 1740 °F)	PWHT: 900 °C (1650 °F) 1 hr/25 mm (1 in.), 3 hr minimum, followed by still air cool.	370 °C to 815 °C (700 °F to 1500 °F)	MC	Carbides stabilized with Nb; thus have a reduced risk of sensitization.
	550 °C to 1050 °C (1020 °F to 1920 °F)	σ			600 °C to 950 °C (1110 °F to 1740 °F)	$M_{23}C_6$	PWHT also improves sensitization resistance.
	600 °C to 900 °C (1110 °F to 1650 °F)	χ			700 °C to 950 °C (1290 °F to 1740 °F)	M_6C	

Table 4—Nickel Based Alloy Embrittlement Phases and Stress Relaxation Cracking Susceptibility

Alloy	High Temperature Embrittlement Temperature Range	Embrittlement Phase Delta δ Gamma -γ Laves -η Sigma -σ Chi -χ	Subject to Stress Relaxation Cracking	Applicable Heat Treatments/ PWHT to Minimize Stress Relaxation Cracking	Sensitization Temperature Range	Carbide Formed	Comments
Inconel 600	427 °C to 593 °C (800 °F to 1100 °F)	TiN	N	Solution Anneal: 1010 °C (1850 °F) for 15 min PWHT: 900 ± 14 °C (1650 ± 25 °F) for 1.5 hours per 25 mm (1 in.) thick. Rapid cool through 760 °C to 538 °C (1400 °F to 1000 °F) range to prevent sensitization.	538 °C to 760 °C (1000 °F to 1400 °F)	Cr_7C_3	Not age hardenable, but can be strengthened by cold work. Does not harden/embrittle with exposure to high temperatures. Will sensitize similar to 300 series stainless steel.
					760 °C to 982 °C (1400 °F to 1800 °F)	$Cr_{23}C_6$	
Inconel 625	500 °C to 760 °C (930 °F to 1400 °F)	γ" - Ni_3Nb δ - $Ni_3(Nb, Mo)$	Y	Solution Anneal: 1177 °C (2150 °F) for 15 min PWHT: 900 ±14 °C (1650 ±25 °F) for 1.5 hours per 25 mm (1 in.) thick. Slow cooling should be avoided.	650 °C to 1038 °C (1200 °F to 1900 °F)	MC M_6C $M_{23}C_6$	Age hardenable.
Incoloy 800	500 °C to 760 °C (930 °F to 1400 °F)	η – Ni_3Ti δ – Ni_3Nb γ' - $Ni_3(Al, Ti)$ γ" - Ni_3Nb	Y	Solution Heat Treat: 982 °C (1800 °F) for 15 min PWHT: 900 ±14 °C (1650 ±25 °F) for 1.5 hours per 25 mm (1 in.) thick. Rapid cool through 760 °C to 538 °C (1400 °F to 1000 °F) range to prevent sensitization.	538 °C to 760 °C (1000 °F to 1400 °F)	Cr_7C_3	Lower risk of stress relaxation cracking than 800H, but lower creep strength if fine grained. Grain growth at temperatures above 982 °C (1800 °F).
					760 °C to 1093 °C (1400 °F to 2000 °F)	$Cr_{23}C_6$	
Incoloy 800H	500 °C to760 °C (930 °F to 1400 °F)	η – Ni_3Ti δ – Ni_3Nb γ' - $Ni_3(Al, Ti)$ γ" - Ni_3Nb	Y	Solution Heat Treat: 1177 °C (2150 °F) PWHT: 900 ±14 °C (1650 ±25 °F) for 1.5 hours per 25 mm (1 in.) thick. Rapid cool through 760 °C to 538 °C (1400 °F to 1000 °F) range to prevent sensitization.	538 °C to 760 °C (1000 °F to 1400 °F)	Cr_7C_3	Preferred over 800HT® due to lower Al+Ti contents to reduce risk for stress relaxation cracking. (Want chemistry to match 800H, but not 800HT®) Anneal at 1177 °C (2150 °F) will result in grain growth and grain size ~ ASTM #5.
					760 °C to 1093 °C (1400 °F to 2000 °F)	$Cr_{23}C_6$	
Incoloy 800HT®	500 °C to 760 °C (930 °F to 1400 °F)	η – Ni_3Ti δ – Ni_3Nb γ' - $Ni_3(Al, Ti)$ γ" - Ni_3Nb	Y	Solution Heat Treat: 1177 °C (2150 °F) PWHT: 900 ±14 °C (1650 ±25 °F) for 1.5 hours per 25 mm (1 in.) thick. Rapid cool through 760 °C to 538 °C (1400 °F to 1000 °F) range to prevent sensitization.	538 °C to 760 °C (1000 °F to 1400 °F)	Cr_7C_3	Higher risk of stress relaxation cracking than 800H, but higher creep strength.
					760 °C to 1093 °C (1400 °F to 2000 °F)	$Cr_{23}C_6$	
Incoloy 825	427 °C to 593 °C (800 °F to 1100 °F)	TiN	Y	Solution Heat Treat: 940 °C (1725 °F) for 1 hour with rapid air or water quench. PWHT: 900 ±14 °C (1650 ±25 °F) for 1.5 hours per 25 mm (1 in.) thick.	650 °C to 760 °C (1200 °F to 1400 °F)	MC, M_6C and $M_{23}C_6$	Age hardenable. Incoloy 825 is not typically used at high temperatures.

References:

Volume 13A, *ASM Handbook*, Pg. 270.

Special Metals Corporation online datasheets.

API 938C, *Use of Duplex Stainless Steels in the Oil Refinery Industry.*

Structure and Properties of Engineering Alloys, Smith, McGraw-Hill, 1981.

Other names for stress relaxation cracking include:	
During Fabrication:	During Service:
Reheat Cracking	Creep Embrittlement Cracking
Stress Relief Cracking	Stress Induced Cracking
	Stress Assisted Grain Boundary Oxidation Cracking

Carbide-forming alloy additions that are typical to commercial stainless steels (Mo, Ti, Si, and to a lesser extent Nb/Cb) have a tendency to enlarge the composition range in which sigma will form. Stabilizing elements (Ti and Nb/Cb), along with chromium and residual aluminum diffuse into the delta ferrite, resulting in a phase that is richer in these elements than the austenitic matrix. Additionally, the stabilizing elements promote sigma phase by excluding chromium from the carbides, thereby effectively increasing available chromium concentration in the matrix.

For the stainless steels with <17 % Chromium, sigma can form, but only after very long time periods. The lower limit of 16.5 % is sometimes seen as the threshold for an alloy to form sigma phase. This is one of the reasons that welding consumable 16-8-2 has good resistance to sigma formation.

Since ferrite is typically a grain boundary precipitate, it is not surprising that sigma is most observed at grain boundaries as well. Therefore, it is observed that for all other variables being constant, the matrix with smaller grains (more grain boundary area) promotes higher rates of sigma precipitation.

At lower temperatures within the sigma formation range, carbide concentration/dispersion also contributes to lowering room temperature CVN test results. The extent of embrittlement is not always constant for samples exhibiting the same amount of sigma formation. The extent of embrittlement is also strongly affected by the size, shape, and distribution of sigma particles, as well as carbide particles. Larger sigma phase particles segregated in the matrix reduce toughness more than smaller particles.

4.2.2 Chemistry of Sigma Phase

The Fe-Cr equilibrium phase diagram in Figure 24 [25] shows that sigma can form at temperatures between 500 °C to 830 °C (932 °F to 1526 °F) and will have a composition of 40 to 50 wt % Cr. The amount of sigma phase precipitation increases with increasing ferrite forming elements, specifically chromium, silicon, and molybdenum content. Increasing chromium content tends to favor the formation of body-centered cubic crystal structures (e.g. ferritic alloys). This encourages sigma formation. Accordingly, high chromium grades, such as Types 309 (23Cr) and 310 (25Cr) stainless steels, are more susceptible than is Type 304 stainless steel (18Cr).

An isothermal plot shows the phases present in an alloy at a particular temperature and is useful in predicting the phases and their amounts and compositions at that temperature. Figure 25 [26] shows a comparison of sigma formation of several types of stainless steel, including 304, 310, and 330. The compositions of these alloys are given in Table 5.

$$Cr_{eq} = Cr + 2\,[Si] + 1.5\,[Mo] + 5.5\,[Al] + 1.75\,[Nb] + 1.5\,[Ti] + 0.75\,[W]$$

$$Ni_{eq} = Ni + Co + 0.5\,[Mn] + 30\,[C] + 0.3\,[Cu] + 25\,[N]$$ [ibid.]

Sigma forming tendency in Fe-Cr-Ni alloys can be predicted from the chemical composition of the alloy, namely a ratio factor which is given by the formula [27]:

$$\text{Ratio Factor} = \frac{\%\,Cr - 16 \times \%\,C}{\text{fff}\,[\%\,Ni]}$$

If this factor is above 1.7, the alloy will likely form sigma phase. In order to incorporate the influence of other minor constituents in material, a % Cr equivalent can be substituted for the plain Cr weight percentage. The Cr_{eq}, proposed by Hull, is given by:

$$Cr_{eq} = Cr + 0.31\,Mn + 1.76\,Mo + 0.97\,W + 2.02\,V + 1.58\,Si + 2.44\,Ti + 1.7\,Nb + 1.22\,Ta - 0.266\,Ni - 0.177\,Co$$

A different method has been developed by Woodyatt et al [28] to estimate the sigma forming tendency of an alloy, based on the electron vacancy number, $\overline{N}_v$.

If $\overline{N}_v$ is higher than 2.52, the alloy would be expected to form sigma.

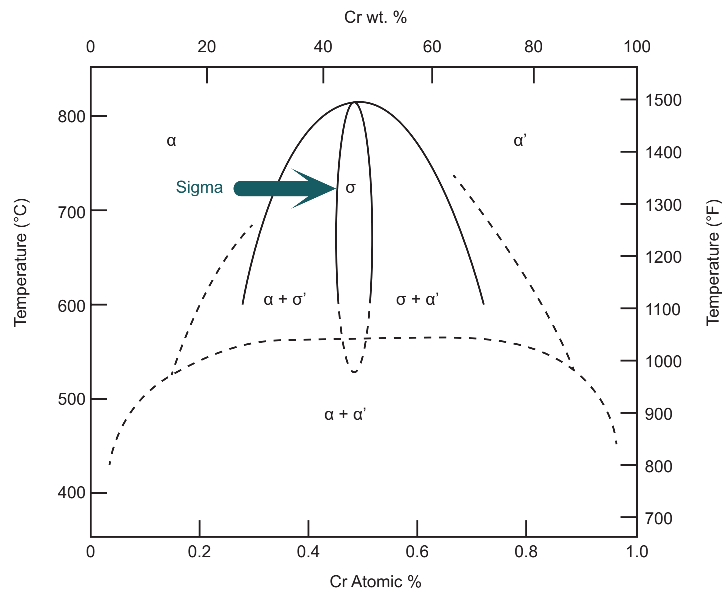

Figure 24—Fe-Cr Equilibrium Phase Diagram Showing Sigma at 40 % to 50 % Cr (Top Axis)

Table 5—Typical Compositions (wt %) of Select Alloys Shown in Figure 25

Element	304	310	330	16-8-2	"Lean" 16-8-2	308H	Alloy 800
Ni	8	20	34	9.5	7.5	9.85	32
Mn	2	2	2	2.5	0.5	1.65	1.5
C	0.08	0.25	0.08	0.10	0.06	0.005	0.10
Cu			1	0.75	—		
N							
Cr	18	25	17	16.5	14.5	20.45	21
Si	1	1.5		0.60	—	0.46	
Mo				1.3	1.0		
Al							0.4
Cb/Nb							
Ti							0.4
Fe_{eq}	69	43	45	66	74		44
Ni_{eq}	11	29	38	14	10		34
Cr_{eq}	20	28	17	20	16		22
Est. Sigma	3%	14%	0%	4%	0%		1%
As Welded FN*				6	1		

*Ferrite Number estimated using WRC-92 Diagram.

Other ferrite stabilizers (Si, Mo, Al, W, V, Ti, and Nb) tend to promote sigma formation, while austenite stabilizers (C, Ni, N, and Mn) tend to retard sigma formation. Most austenitic stainless steels typically exhibit a maximum of about 10 % to 20 % sigma phase, or less (with nickel contents of 8 to 15 wt %).

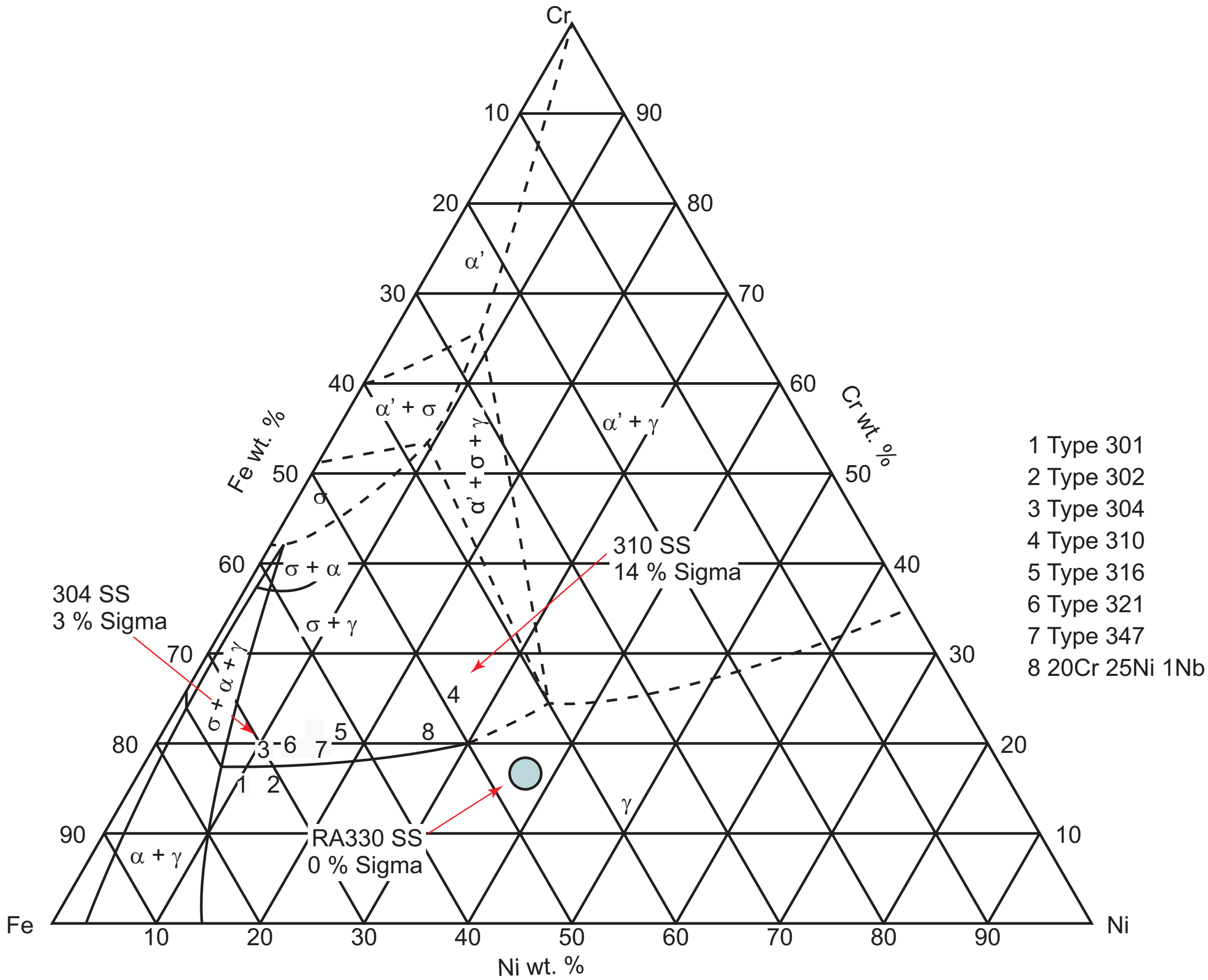

Figure 25—Isothermal Section of Fe-Cr-Ni Phase Diagram at 650 °C (1202 °F)

Fully sigmatized cast austenitic stainless steels typically have higher ferrite/sigma content (up to 40 %). Alloys with a nominal composition of 60 % Fe and 40 % Cr (about the composition of sigma) can be transformed to essentially 100 % sigma.

4.2.3 Transformation Rate of Sigma Phase

Conversion of ferrite to sigma in austenitic stainless steels can occur in a few hours, as evidenced by the known tendency for sigma to form if an austenitic stainless steel is subjected to a postweld heat treatment at 691 °C (1275 °F). While embrittlement can result by holding within the transformation range, sigma phase formation rates are usually insignificant when cooling through the range.

Generally, industry experience has shown that sigma phase development is far from being predictable. In addition to time in service, the amount of sigma phase formed strongly depends on the chemistry of the steel involved. Thus, for a given prolonged time in service, some austenitic stainless steels, such as Type 304H, can develop low levels (3 % to 7 %) of sigma phase, while others having exactly the same steel specification can develop 10 % or more. Such variations are thought to be related to variations in steel chemistry, the amount of cold work and thermal processing during fabrication [29, 30, 31].

Sigma phase formation happens more quickly and embrittles more severely when the alloy has been cold worked. Sigma may not seriously harm the performance of the alloy while it is operating at high temperature. Indeed, sigma phase may be beneficial, at low content levels, by providing precipitation strengthening at high temperatures. When sigma is located on the grain boundaries it can significantly reduce creep ductility, but has little effect when it precipitates within the grains.

At elevated temperatures, ferrite can turn into sigma phase in one year of service or less. It is for this reason that sigma phase is usually first detected in welds. Sigma phase can also form in 300 series stainless steel base metal (austenite phase), but reportedly 100 times more slowly than from ferrite [32].

In general, the weld metal exhibits a higher percentage of sigma phase than the corresponding base metal. This is expected because austenitic stainless steel welds contain ferrite contents of 3 % to 8 % to increase hot ductility and minimize the potential for solidification cracking.

Figure 26 [33] shows the varying amounts of precipitated sigma phase in different grades of austenitic stainless steel at 700 °C (1292 °F); percent sigma was based on area etched by KOH.

The rate that sigma phase forms is faster in stabilized grades than other grades of stainless steel. From Figure 26, sigma can form in just 1000 hours at 700 °C (1292 °F) in stabilized grades 321 and 347 stainless steel, as compared to more than 10,000 hours for Type 304 stainless steel. The amount of sigma formation is also greater in stabilized grades 347 and 321, as compared to Types 316 and 304 stainless steel.

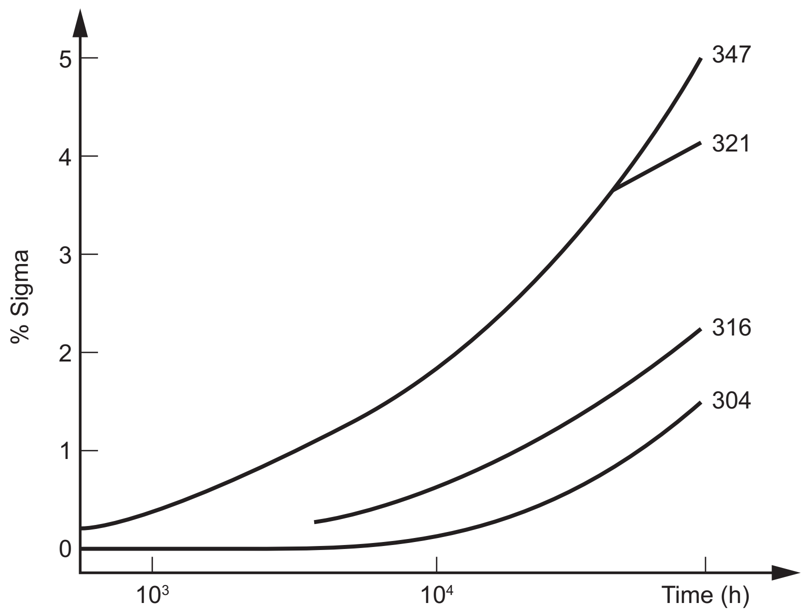

Figure 26—Precipitation of Sigma Phase in Different Grades of Austenitic Stainless Steel at 700 °C (1292 °F)

4.2.4 Visual Appearance of Sigma Phase

Sigma phase embrittlement cannot be confirmed by visual appearance; it can be confirmed only through metallographic examination and mechanical testing (customarily by impact testing). The embrittling effect of this mechanism is visible in the brittle appearance of crack surfaces. However, this appearance is not diagnostic; as there are other forms of high temperature brittle cracking (e.g. stress relaxation cracking).

Cracking due to sigma phase embrittlement tends to occur at welds or in areas of high restraint. An example is shown in Figure 27. [34] The photograph shows liquid penetrant crack indications in a Type 308H stainless steel butt weld that was partially ground out and was embrittled by sigma phase formation.

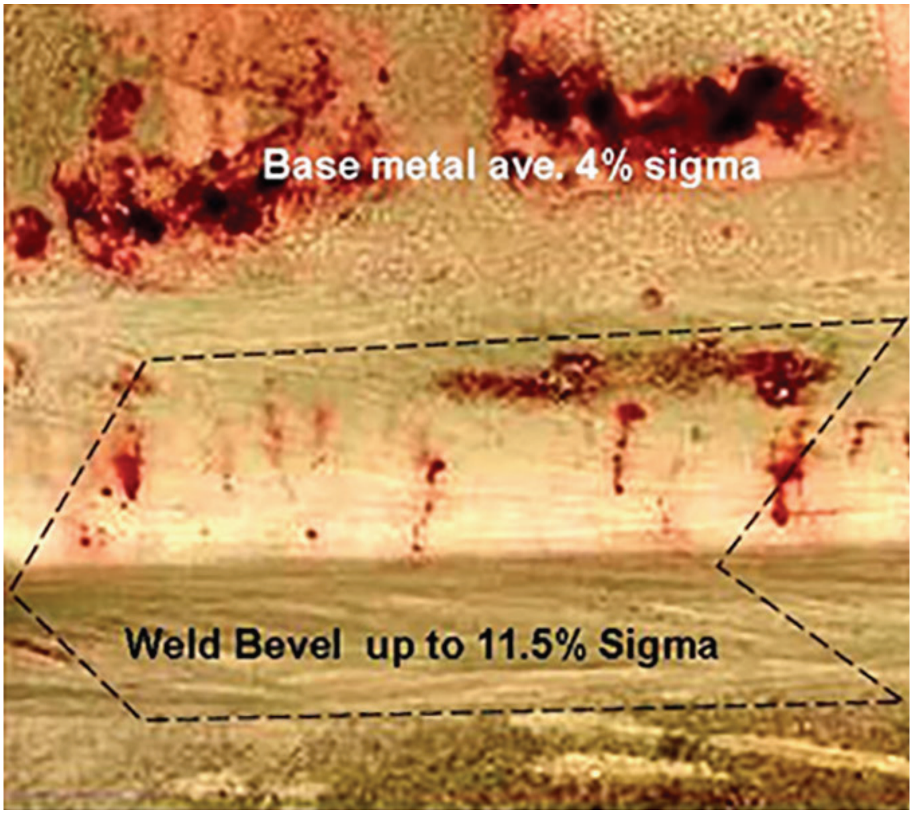

NOTE The bevel is shown by the dashed line.

Figure 27—Penetrant Test Showing Sigma Phase Embrittlement Cracking in Type 308H SS Butt Weld

4.2.5 Microscopic Appearance of Sigma Phase

Sigma phase precipitates are most prevalent at grain boundaries and triple points. The intergranular precipitation of sigma phase ties up chromium that would normally be in solid solution. One consequence is that the material becomes more susceptible to intergranular corrosion (similar consequence as chromium carbide formation). Sigma phase precipitates are not normally seen on twin boundaries.

Intergranular precipitates become blocky with increasing age. Intragranular precipitates appear to initiate and grow more slowly and have an acicular morphology. Acicular sigma embrittles the material significantly more than globular shaped sigma.

Figure 28, Figure 29, and Figure 30 [ibid.] show a cross section view near the outside surface of an FCC regenerator plenum chamber that had an increased content of sigma phase due to cold working. The multiple parallel lines within the grain boundaries are referred to as twinning.

The abnormal concentration and distribution of sigma phase particles near the outside surface due to cold work is particularly well illustrated in Figure 28 and Figure 29. More sigma is seen at the outer surface where the amount of cold working was highest. The same stainless steel sample is shown in Figure 30 with KOH electrolytic etch. The previous case was with electrolytic etching in 10 % oxalic acid to reveal the cold work. Cold work is not revealed by electrolytic etching in KOH.

These microstructures are from a typical regenerator cyclone with an operating temperature of 635 °C (1175 °F). The Type 304H stainless steel cyclones had been in service for 22 years and were found to have approximately 7 % sigma.

Figure 31 and Figure 32 [ibid.] show the microstructures from Type 304H stainless steel cyclones after 14 years of operating at a nominal temperature of 716 °C (1320 °F). The estimated amount of sigma phase is 5 %.

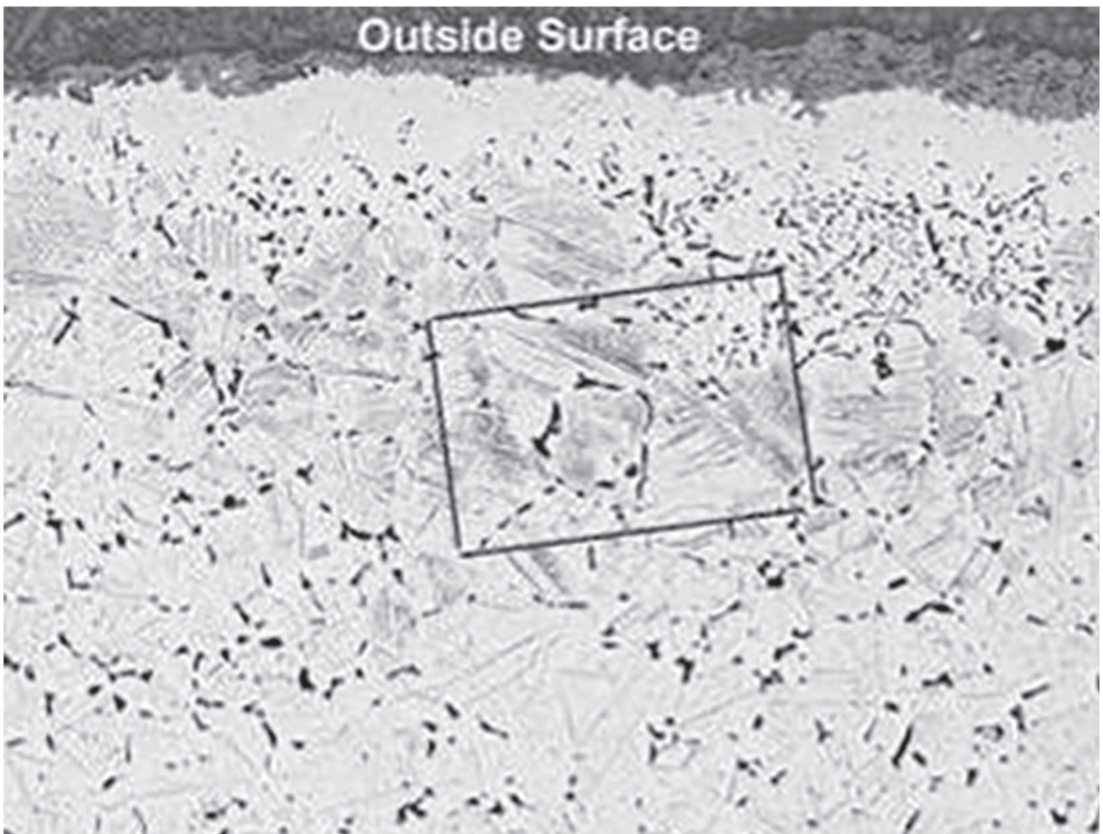

NOTE 10 % oxalic electrolytic etch at 100X.

Figure 28—Cross Section View of Sigma Phase in a Type 304H SS FCCU Regenerator Plenum

4.2.6 Mechanical Properties of Sigma Phase

As stated previously, sigma phase has little effect on the room temperature tensile and yield strengths, but significantly decreases room temperature ductility.

Figure 33 [ibid.] shows Type 304H stainless steel samples containing 12 % sigma that were removed from a FCCU flue gas duct. Bend testing showed that embrittlement affected the steel only at temperatures below 315 °C (600 °F). Above this temperature, the material was ductile. It has been shown that a 50 % loss in creep ductility occurs with aging in Type 304H stainless steel and the loss was primarily attributed to sigma-phase formation [35]. Figure 34 [36] shows the results of tensile tests that were performed at: a) 21 °C (70 °F), and b) 716 °C (1320 °F) on material with 12 % sigma. Results show an increase in ductility at operating temperatures as compared to room temperature (shut down) conditions.

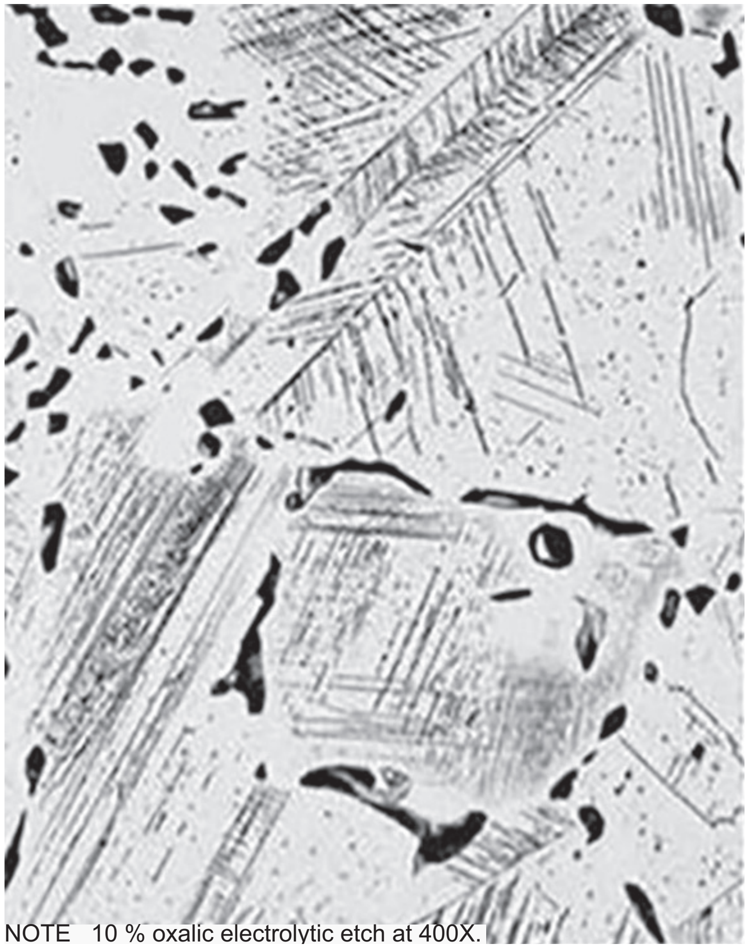

NOTE 10 % oxalic electrolytic etch at 400X.

Figure 29—Cold-worked Microstructure Containing Higher Amounts of Sigma Phase

Figure 35 [37] and Figure 36 [38] illustrate that brittle fracture primarily occurs at lower temperatures and not near-service temperatures. This is why there is a much greater chance of cracking during cooling, when the temperature reaches 260 °C (500 °F) or below.

The presence of sigma phase in austenitic stainless steel and nickel alloys greatly increases notch-sensitivity (i.e. reduces notch toughness). Impact strength is affected more than any other property. There is evidence that sigma content over about 10 % tends to promote high-temperature notch sensitivity. The degree of embrittlement can be somewhat quantified by percent shear measurements with ambient temperature CVN testing using full size specimens.

Percent shear indicates what percent of the Charpy impact fracture surface shows ductility. For the 10 % sigma, the shear values ranged from 0 % at room temperature to 60 % at 649 °C (1200 °F). The impact toughness of this material was less than 10 % of its original annealed toughness at room temperatures, but only increased to a maximum of 20 % when heated. Thus, although the impact toughness did not improve much, the tensile specimens broke in a 100 % ductile fashion, indicating that the material is still suitable. The lack of fracture ductility (0 % at room temperature) indicates that care should be taken to avoid application of high stresses to sigma embrittled materials during shutdowns; a brittle fracture could result.

Figure 35 summarizes impact property data found for two sigma levels of Type 304 stainless steel using service embrittled toughness as compared to annealed toughness. Figure 36 and its corresponding Table 6 [ibid.] give the results of weld metal impact testing for different levels of sigma embrittlement.

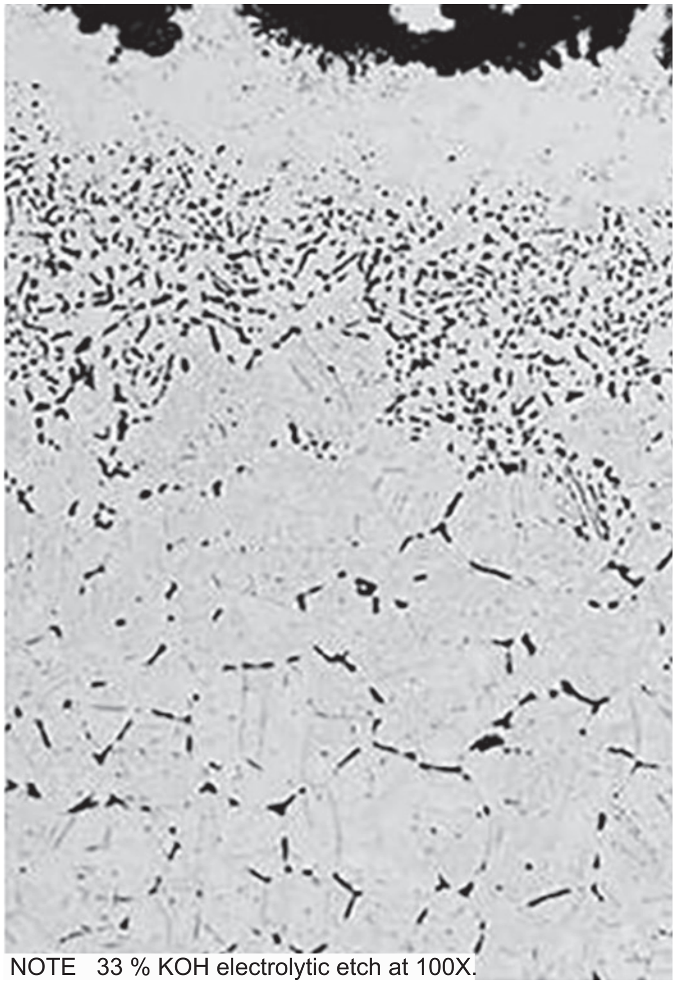

NOTE 33 % KOH electrolytic etch at 100X.

Figure 30—KOH Etch Revealing the Sigma Phase, but Not the Cold Working

In general, the reduction in toughness (i.e. decreased impact energy absorption and decreased percent shear) is most pronounced at temperatures below 260 °C (500 °F). This does not mean that all materials behave in a ductile manner at high temperatures. In one study [39], aged Type 310 stainless steel (with a sigma content of about 20 %) had Charpy V-notch impact values of 2.3 ft-lb at room temperature and only 3.3 ft-lb at 565 °C (1050 °F).

In another study, tests performed on sigmatized stainless steel samples from an FCC regenerator internal showed that even with 10 % sigma formation, the Charpy impact toughness was 39 ft-lb at 649 °C (1200 °F). This would be considered adequate for most steels even though it is much less than the 190 ft-lb obtained for solution annealed stainless steel. In this specimen, the impact toughness was reduced to 13 ft-lb at room temperature, a marginal figure but still acceptable for many applications.

A study conducted by E. L. Creamer et al [40] was performed on Type 347 stainless steel weld metal and plate. Data was reported on the amount of sigma formed after three months of exposure at various temperatures. This data was graphed and the graph appears in the referenced report. It shows that the most sigma was formed at 727 °C (1340 °F). The weld metal formed 18.9 % sigma, while the base metal only formed 5.3 %.

Figure 37 and Figure 38 [ibid.] show the toughness testing results of the weld and plate samples that contained the most sigma phase.

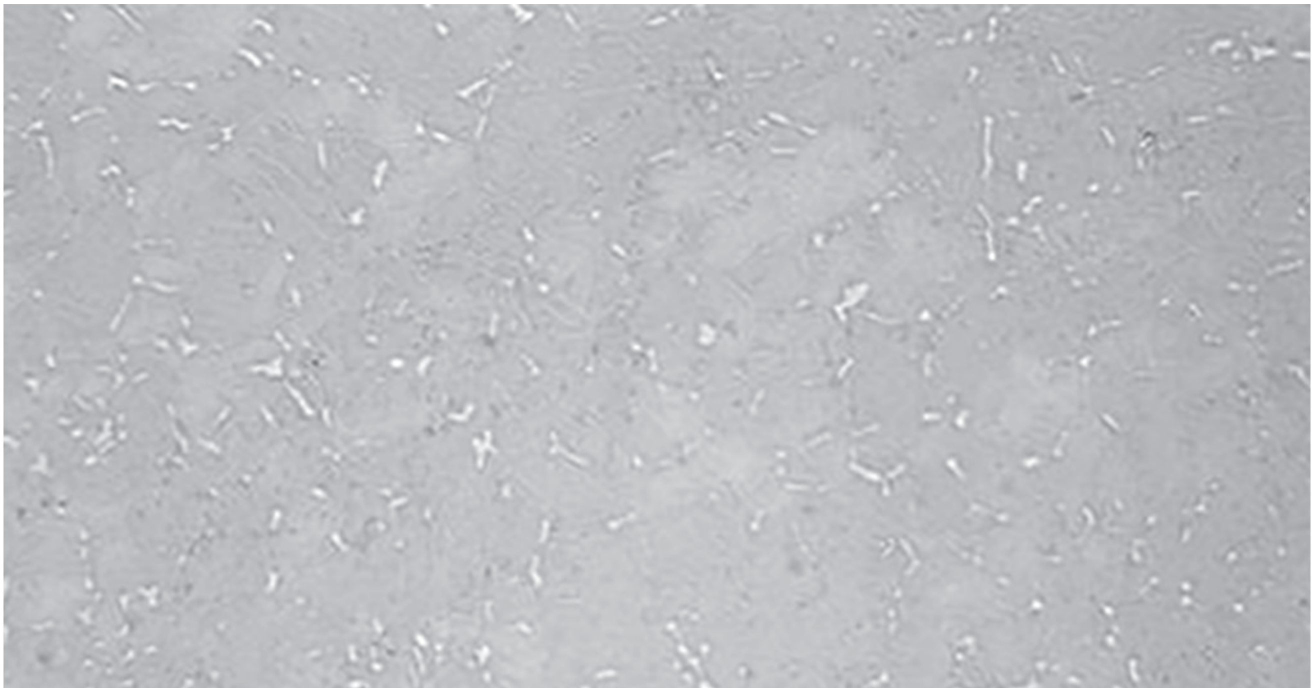

NOTE Vilella's Reagent etch at 100X.

Figure 31—SEM of a Type 304H SS Cyclone After 14 Years of Operation at 716 °C (1321 °F), 5 % Sigma Phase

NOTE KOH electrolytic etch at 200X.

Figure 32—Metallograph of Sigma Phase in a 304H SS Cyclone After 14 Years Operation at 716 °C (1321 °F), 5 % Sigma Phase

(a) 70 °F (b) 400 °F

(c) 600 °F (d) 1300 °F

Figure 33—Bend Test Results of Type 304H SS with 12 % Sigma

4.2.7 Prevention of Sigma Phase

The best ways to prevent sigma phase embrittlement are to either avoid exposing susceptible materials to their embrittling temperature range or use alloys that are resistant to sigma formation. For example, testing has shown that Type 330 stainless steel (Fe: 43, Cr: 19, Ni: 35, and Si: 1.25) that this alloy is not susceptible to sigma phase embrittlement. Previously, it was mentioned that silicon promotes sigma formation. However, the nickel content of Type 330 stainless steel, along with its moderate chromium content, inhibits the formation of sigma phase even with silicon as high as 2 %. This type of alloy could be useful for hexagonal mesh applications since they are thin, highly stressed, and subject to sigma, carburization, and corrosion.

The use of either Type 310S or Type 309S stainless steel at temperatures below about 760 °C (1400 °F) is not recommended; these two grades can form significant amounts of sigma and have only limited high-temperature benefits, as compared to Type 304H stainless steel at temperatures of 593 °C to 760 °C (1100 °F to 1400 °F).

In FCCU cyclone and overhead piping, selecting an alloy immune to sigma phase embrittlement is not likely feasible. Typically, Type 304 materials are selected to minimize sigma formation, yet anticipating that embrittlement will occur in the future, potentially causing problems with repairs. Some users have found that periodic upgrades to the cyclone system have been the primary reason for cyclone replacement, not due to embrittlement and weldability problems.

The 16-8-2 consumables have a controlled composition to operate at temperatures of up to about 800 °C (1472 °F). If a component could be exposed to temperatures above 650 °C (1650 °F) in stagnant air, there is a risk of catastrophic oxidation [41, 42] of the molybdenum in the weld metal. To minimize the potential for catastrophic oxidation,

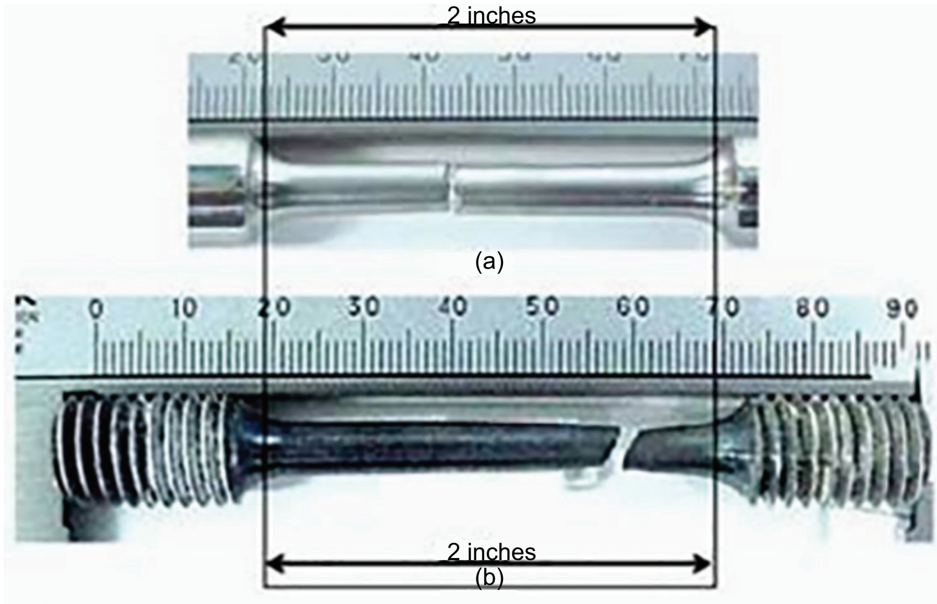

Figure 34—Tensile Test of 304H SS with (a) 12 % Sigma at 21 °C (70 °F) Depicting Brittle Fracture and (b) Ductile Fracture at 716 °C (1320 °F)

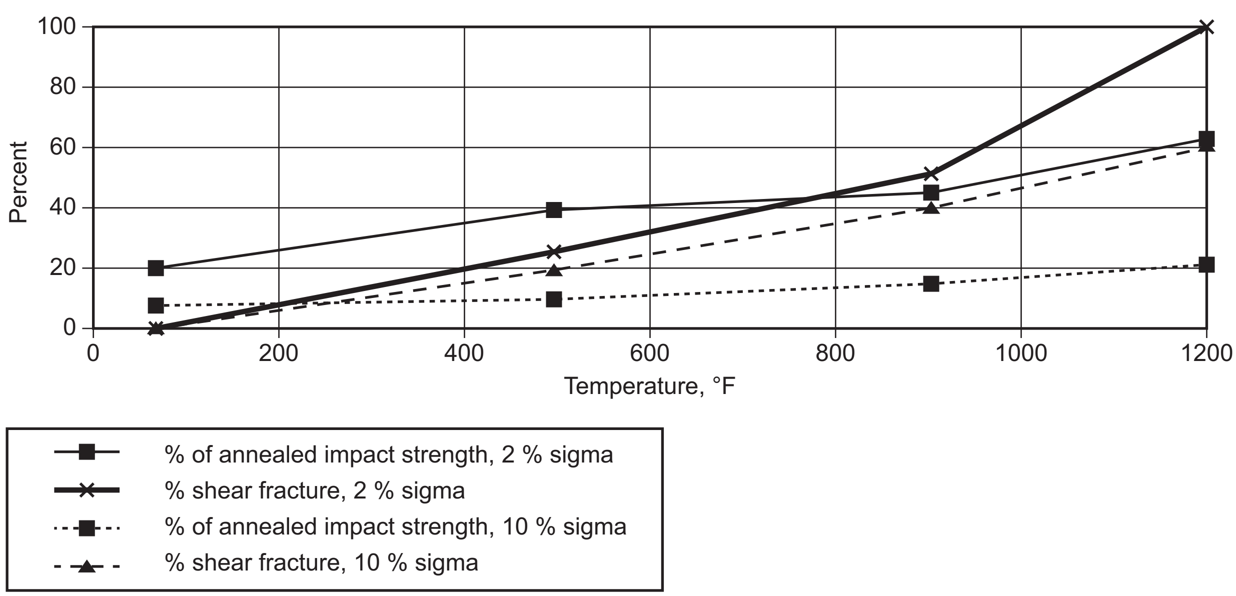

Figure 35—Impact Properties of 304 Type Stainless Steel with 2 % and 10 % Sigma

Table 6—Average Impact Test Results in Joules (ft-lb) Shown in Figure 36

Refinery	Location	Years of Service	Sigma Phase Content (%)	Impact Energy J (ft-lbs)	
				RT	Service
A	Base metal	17	4.0	85 (63)	145 (107)
A	Weld metal	17	8.7	37 (27)	100 (74)
B	Base metal	19	12.0	12 (9)	43 (32)
C	Base metal	13	1.5	35 (26)	75 (55)

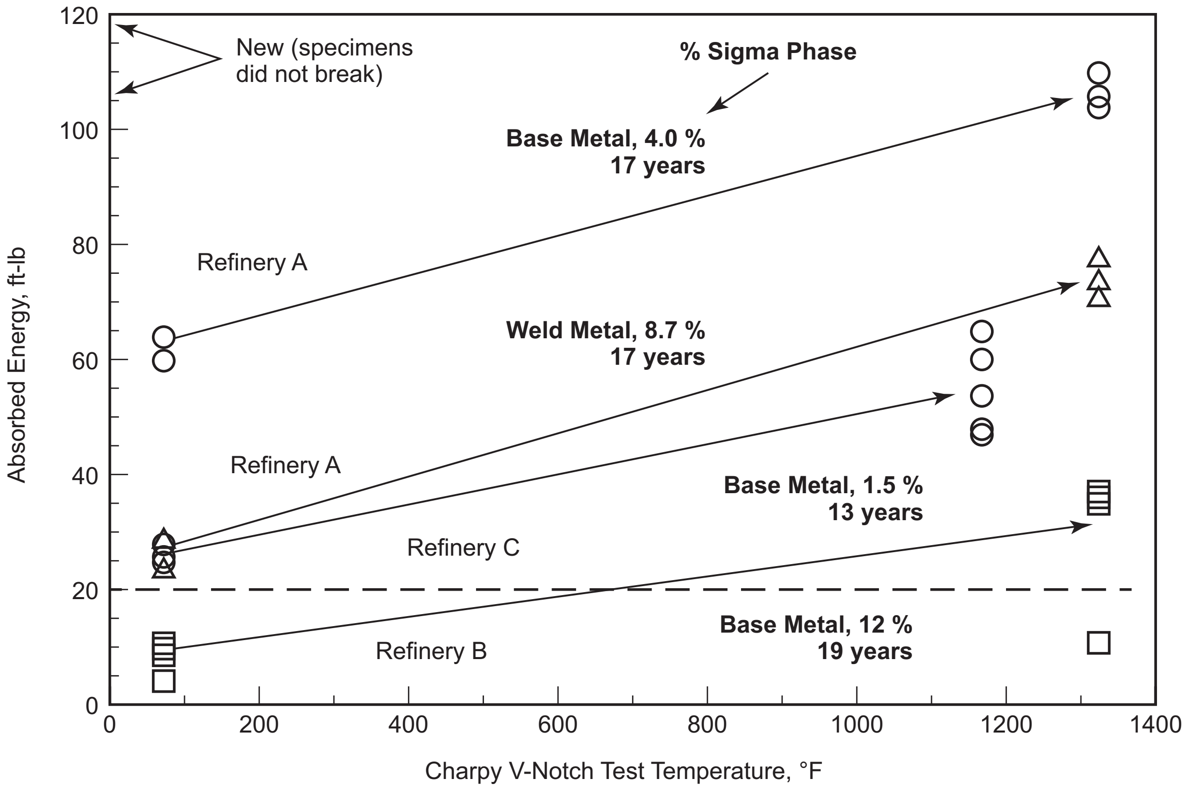

Figure 36—Charpy V-notch Impact Test Results at Room Temperature and Service Temperature

continuous movement of air is needed, otherwise, molybdenum should be kept near the lower limit for AWS 16-8-2 (1.0 Mo to 2.0 Mo). This weld filler metal is essentially a low alloy hybrid between E308H and E316H. It does not match any single parent material; industry experience has shown that it has good creep, oxidation and general corrosion resistance for welding all the ‘3XXH’ series of stainless steels with 0.04 % to 0.10 % carbon.

16-8-2 filler metal has a low total Cr+Mo with controlled carbon and ferrite content to achieve high resistance to sigma embrittlement. The level of Mo is controlled closely to provide creep ductility and thermal fatigue, balanced against control of oxidation under stagnant conditions above 650 °C and sigma or chi phase formation in service.

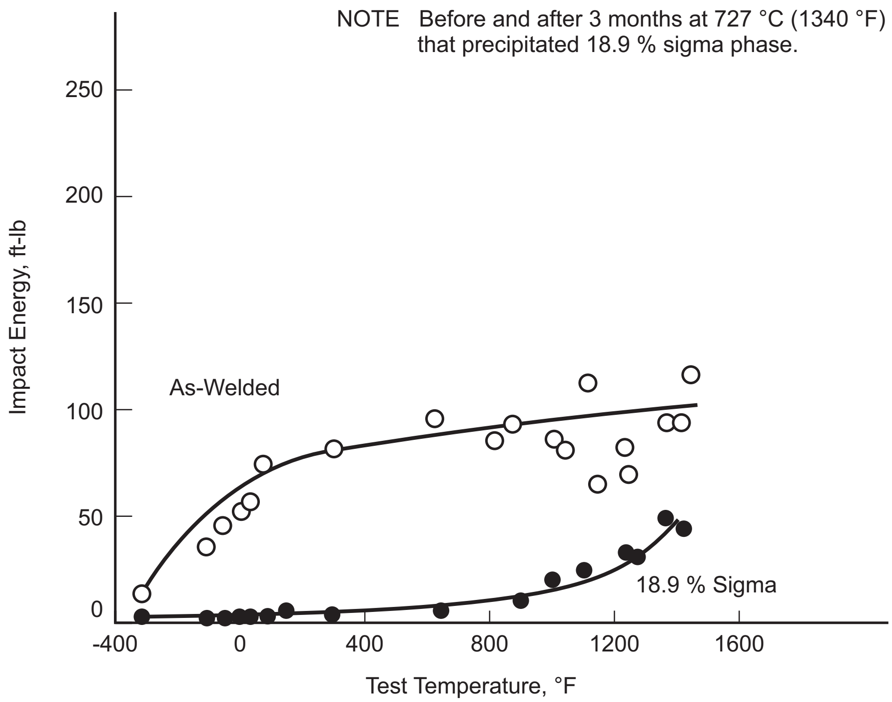

Figure 37—Temperature vs. Charpy V-notch Impact Energy of Type 347 SS Weld Metal

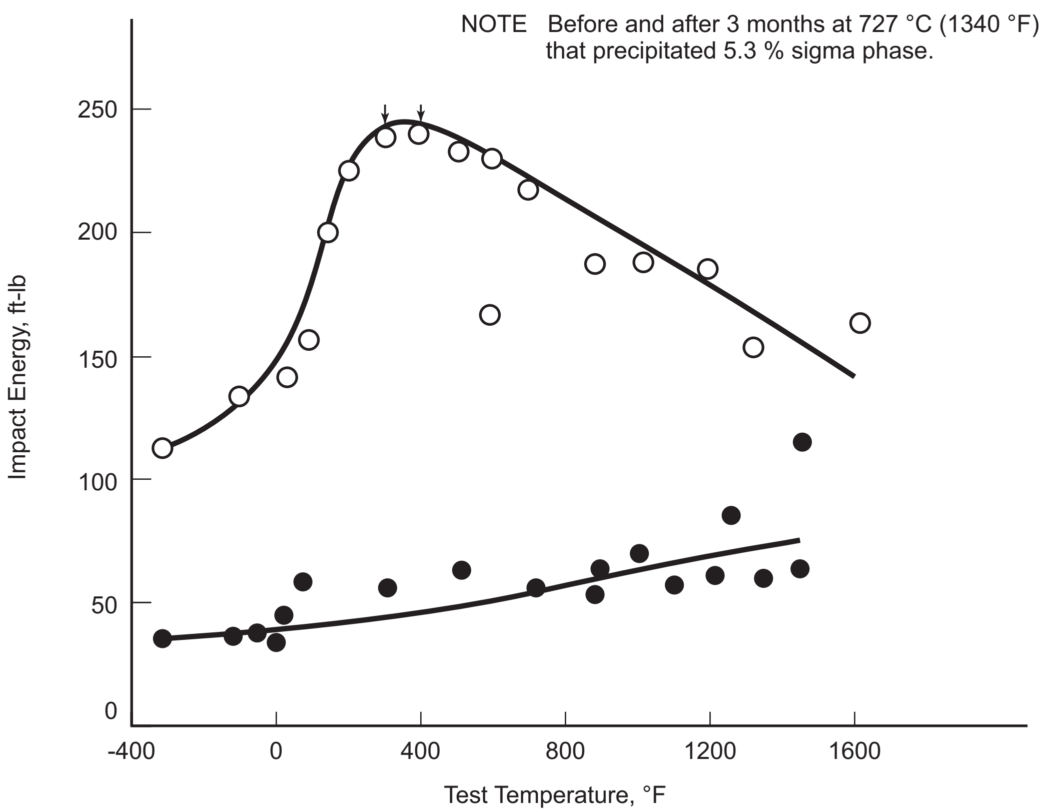

Figure 38—Temperature vs. Charpy V-notch Impact Energy of Type 347 SS Plate

This weld metal was initially developed to avoid in-service HAZ failure in Type 347H stainless steel of >12 mm ($^{1}/_{2}$ in.) thickness. For the same reasons it is also a candidate for Type 321H stainless steel. For high temperature service, it is suitable for joining Type 316H stainless steel since matching weld metal has known sigma formation problems.

Some refiners and contractors prefer the use of a “lean” version of the AWS 16-8-2 grade weld metal. This specialized version has lower alloy content that reduces the potential for sigma formation even further. Table 5 shows the compositions of the standard and lean versions of 16-8-2. Use of this alloy in high sulfur environments should be evaluated in light of its reduced alloy content and lower corrosion resistance than the base metal.

No bismuth-bearing constituents are allowed in these consumables to ensure <0.002 % Bi as required by API 582.

4.2.8 Mitigation of Sigma Phase

While likely impractical for most applications, it is possible to recover some of the lost room-temperature toughness in components with sigma phase. Heating to temperatures above 980 °C (1800 °F) can dissolve sigma and aid the diffusion of Cr and Fe back into the matrix. To restore full ductility it is recommended to solution anneal at 1065 °C to 1177 °C (1950 °F to 2150 °F) for up to four hours (followed by water quench if maximum corrosion resistance is desired). See Table 2 and Table 3 for specific alloy recommendations.

4.2.9 Inspection and Evaluation of Sigma Phase

Most cases of embrittlement are first noted as cracking in either wrought and cast (or welded) components during turnarounds when the material has cooled to below about 200 °C (400 °F). Typically, welds and weld HAZs exhibit cracking first.

Simple bend tests from small samples removed from the edges of cyclones or other locations can give a quick indication of the remaining ductility. However, embrittlement from carburization can also cause a loss of ductility.

Confirmation of sigma embrittlement can be attained by metallographic examination. While laboratory testing can be performed on samples removed from equipment, field metallography and replication can be used to give results from several locations without removing samples (this method is often preferred for severely embrittled material that has not suffered cracking because it avoids having to repair after coupon removal).

4.2.10 Repairs

The lack of ductile fracture resistance at room temperature indicates that care should be taken to minimize stressing sigmatized materials during shutdown, as a brittle fracture could result. This concern should be shared with inspection and maintenance personnel who may need to maneuver around embrittled components.

Prior to beginning repairs, a simple bead on plate test can give an indication of weldability. Using GTAW, weld an autogenous (no filler metal) stringer bead (no weave) on the component to be welded. Grind these welds flush and perform a penetrant test after cooling. If no cracks are found, the material is likely weldable. If cracked, an increase in preheat to 150 °C to 200 °C (300 °F to 400 °F) has been used to improve weldability.

Weldability tests can also be performed by making a butt weld test using a piece of metal from the component to be repaired. The sample can be welded to new stainless steel coupons using the repair weld procedure that will be used in the field.

NOTE Heavily carburized layers should be removed from coupons to be used for the weldability tests. If needed, preheating the surrounding sigmatized material to 150 °C (300 °F) has been shown to be beneficial.

While a crack-free weld is desirable, ideally, the welds should also pass room temperature tensile and bend tests. Such specifications and testing are part of the Welding Procedure Specification/Procedure Qualification Record

(WPS/PQR). However, for non-pressure containing components, such as cyclones, the primary requirement is to produce crack-free repair welds that allow the plant to start up and be placed back in service.

Another method to estimate weldability is to perform Charpy V-notch testing of the base metal. This testing can be performed at reduced and elevated temperatures to quantify the effect of sigma embrittlement.

However, there does not appear to be a clear level of sigma phase content or minimum Charpy toughness value related to weldability. Other factors such as chemistry (including carbon due to carburization), section thickness, type of consumable, and preheat and cooling rate can significantly affect weldability.

Sigma phase can be reversed, if the material is too embrittled to be welded, consider if it is practical to locally de-sigmatize by solution annealing. Solution annealing components that have been in-service involves heating the piece to about 1066 °C to 1095 °C (1950 °F to 2000 °F), and is not typically followed by either a water quench or rapid air cool since water quenching can produce distortion. (Rapid air cooling or water quenching will avoid sensitization, which is typically not an issue for high-temperature service.) For many applications, solution annealing is not practical due to the sizes of the components or due to potential buckling since tensile strength is very low at solution annealing temperatures. Therefore, proper support should be provided to avoid buckling or bowing.

The purpose of solution annealing is to remove embrittling phases, thereby facilitating repair welding. This has been successfully executed on small and uncomplicated pieces such as piping butt welds.

NOTE Material will likely be sensitized during the slower cool, rather than water quenching and sigma will re-form during subsequent service at high temperature.

API 582 recommends controlling austenitic stainless steel welds to a ferrite number of 3 to 10 FN to minimize future sigma phase embrittlement in austenitic stainless steel welds. For Type 347 stainless steel, the weld metal ferrite content should be between 5 to 10 FN, thus increasing its potential for sigma phase formation. This higher ferrite content is recommended since Type 347 stainless steel has low creep ductility and has increased susceptibility to relaxation cracking. It is recommended that the WPS include these requirements and that the PQR include appropriate ferrite content tests on deposited weld metal. However, these ferrite contents do not apply to 16-8-2 weld filler metal. For this filler metal, API 582 gives an allowable ferrite number of 1 to 5 FN.

NOTE Item 5 in Table A.2 of API 582, *Welding Guidelines for the Chemical, Oil, and Gas Industries*, states “E16-8-2 is often specified when the weld deposit will be exposed to high cyclic thermal stresses and creep strains.” Multiple cycles can result in accumulated strains where sigma phase limits the low temperature ductility, resulting in cracking. (E16-8-2 is an austenitic stainless steel filler material with minimal ferrite; this reduces the amount of sigma phase formation during service.)

There is, however, evidence that the 16 % chromium content is insufficient to resist sulfidation damage for a repair application in a Resid FCCU; 18 % chromium was needed.

There are now higher chromium versions of this alloy, such as 17-9-2 and some new versions of Type 308H materials, that reportedly also resist sigma formation during high-temperature service.

Austenitic stainless steels are sometimes used as internal cladding or weld overlays on carbon and low alloy Cr-Mo steels for corrosion resistance. The ferrite content and exposure time to PWHT temperatures should be limited wherever possible.

4.3 Carburization

4.3.1 General

Carburization is the process by which carbon is diffused into a metal at temperatures as low as 500 °C (932 °F), as seen in Figure 39 [43]. Carburization of stainless steels and austenitic Ni-Fe-Cr alloys occurs at high temperatures when in the presence of a carbon rich environment, such as a high gas phase carbon activity (hydrocarbons, coke, gases rich in CO, CO_2, methane, and ethane), and has a low oxygen potential (minimal O_2 or steam). Carbon monoxide, present in hydrogen reformers and FCCU regenerators, can cause carburization, as can layers of coke formed by thermally cracking heavy hydrocarbon molecules in heater tubes. Coke deposits can cause carburization, particularly during steam air decoke cycles where controlled amounts of oxygen are used at temperatures that exceed the normal operation to burn off the coke causing accelerated carburization.

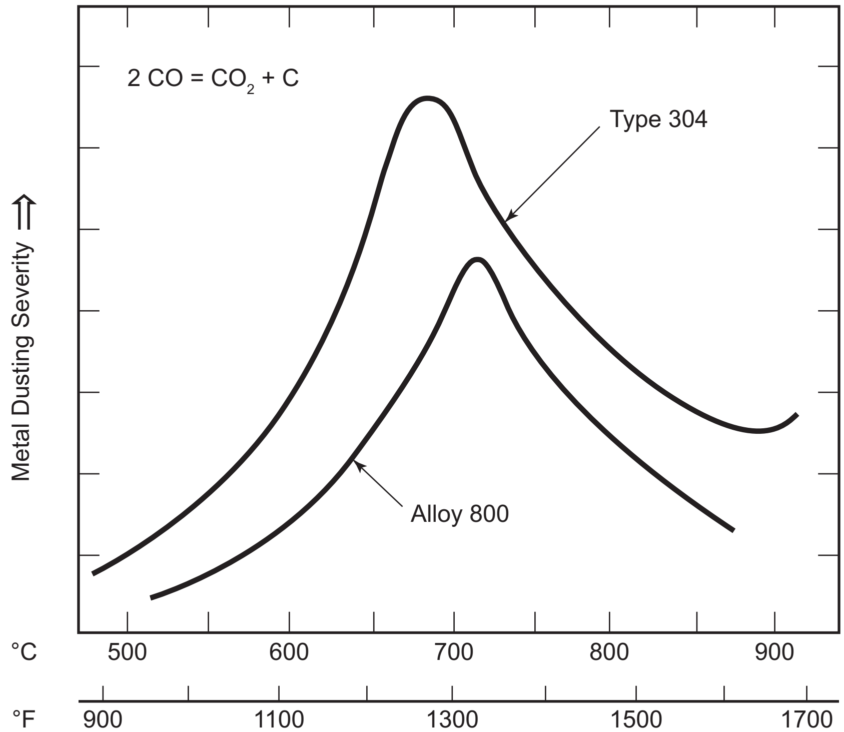

Figure 39—Relative Severity of Carburization in the Form of Metal Dusting for Type 304 Stainless Steel and Alloy 800

Carburization can result in the loss of high-temperature creep ductility, loss of ambient temperature mechanical properties (specifically toughness/ductility), loss of weldability, and corrosion resistance.

In refineries, fired heater tubes (particularly coker heaters and some catalytic reformers) and cyclones in the regenerator sections of FCCUs are the most common type of equipment subject to carburization. Steam methane reformer outlet piping and waste heat boilers that contain carbon monoxide (CO) can also suffer carburization and metal dusting, a catastrophic carburization phenomena that results in pitting and wall loss. Metal dusting damage is associated with relatively low diffusion rates, but with steep carbon gradients. This mechanism is not in the scope of this document and is not covered any further.

Different materials have varying resistance at elevated temperatures. Higher temperatures lead to an increase in carbon ingress diffusion rates, concentration gradients, and depths. Often, a linear increase in temperature can result in an exponential increase in carburization. An industry paper [44] includes a figure depicting curves of relative carburization resistance. Several alloys are plotted, including Type 310 stainless steel and Alloy 800H, at 980 °C (1800 °F) for 96 h in H_2-2 % CH_4, cycling to room temperature daily. Type 310 stainless steel is the top curve, showing the most weight change, from carbon pickup, indicating that this alloy had the lowest carburization resistance.

When comparing carburization resistance, it is important to note how the testing was performed. The type of carburizing atmosphere can make a large difference in the test results. Tests performed using hydrogen and methane are very different from pack carburization tests. Pack carburization will typically cause a weight gain in the sample due to carbon pickup, while hydrogen and methane mixtures could produce metal dusting, with a net loss of surface and weight. Typically, the best results are found when the test is similar to the process environment.

Initially, carbon diffuses rapidly into the alloy surface, but the rate slows down with increasing penetration. It is not unusual in FCC units to see carburized layers of 2 mm to 25 mm ($^{1}/_{16}$ in. to 1 in.) thickness after 12 to 14 years of service. Under severe conditions, significant carburization can occur in weeks/months.

Carburization often promotes sensitization in austenitic materials by providing a continuous source of carbon into the alloy. At elevated temperatures, carbon tends to combine with chromium to form chromium carbides. This is referred to as “sensitization”. The forming of chromium carbides depletes chromium from the surrounding area, thereby promoting a local iron-nickel rich region within the microstructure that has significantly lower intergranular corrosion resistance.

Polythionic acid stress corrosion cracking (PASCC) is an ambient temperature damage mechanism that can develop as a result of sensitization. PASCC was discussed briefly in 3.2.2.3. PASCC occurs when sulfide scales form at high temperature on the surface of the stainless steel and then create polythionic acid when cooled and exposed to moisture. The polythionic acid can cause intergranular SCC on the sensitized stainless steel. Details of this damage mechanism can be found in NACE SP0170 [78].

Sensitization can even occur in stabilized grades, such as Types 321 and 347 stainless steels that use titanium and niobium, respectively, to help prevent carbon present in the alloy from forming chromium carbides in high-temperature service. They cannot prevent sensitization if an environmental source of carbon is present at high temperature supplying more carbon into the material.

Sensitization due to carburization from a carbon rich process environment can overwhelm titanium (in Type 321 stainless steel) and niobium (in Type 347 stainless steel), making these “stabilized” stainless steels susceptible to polythionic acid stress corrosion cracking, when moisture is introduced during shutdowns, but only to the depth of carbon diffusion. Therefore, sensitization depth is dependent on the diffusion rate of carbon into the alloy. (Since PASCC is an ambient temperature damage mechanism, it is not addressed further in this document.)

Through wall sensitization in low carbon or stabilized grades occurs when the metal surface is exposed to a carburizing atmosphere and progresses through the metal according to its carbon diffusion rate at that temperature. In unstabilized and higher carbon “H” grades of stainless steel, sensitization can occur in less than a minute during welding. Through wall sensitization due to carburization generally takes years to occur.

In refinery applications, process-induced carburization is usually detrimental, namely, carburized layers at the surface are brittle, less corrosion resistant and are not weldable.

By tying up the chromium, carburization also reduces oxidation and sulfidation resistance. It adversely affects mechanical strength because of the volume increase associated with the carbon uptake and carbide formation, it imposes additional stresses that contribute to mechanical failure.

Figure 40 [45] shows a cross section through a FCCU regenerator cyclone after macro-etching with Marble’s reagent. A 3 mm (0.125 in.) thick carburized layer was found on the inside diameter (ID) surface. This layer also displayed erosion, while the external surface did not. It is likely that erosion stripped away any protective oxide surface, thus accelerating the carburization diffusion rate.

When present, carburization is more likely to be a concern than sigma formation. Repairs can be a problem due to embrittlement and welding cannot be done until the carburized layer is removed.

Severe carburization can lead to refractory anchor failure due to a loss of ductility or accelerated corrosion, resulting in the falling away of sheets of refractory.

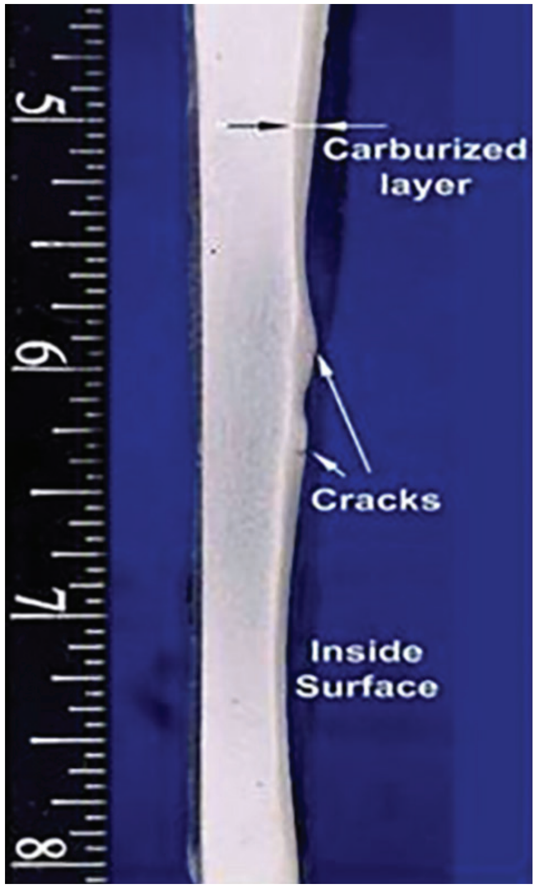

Figure 40—Cross Section of a Type 304H SS Regenerator Cyclone with a 3 mm (0.12 in.) Thick Carburized Layer on the ID Surface

4.3.2 Chemistry

Alloying elements affect the carburization resistance of various alloys. Silicon, niobium, tungsten, vanadium, titanium, and the rare earth elements have been noted as providing increasing resistance to carburization. These elements will preferentially form carbides, keeping the chromium in solid solution so that it can provide corrosion resistance. However, since the alloy composition is fixed, once all of the stabilizing elements are tied up with the added carbon from the process environment, the stainless steel is effectively no longer “stabilized” and is susceptible to sensitization (and PASCC) as well as carburization.

The benefit of silicon on carburization resistance is particularly noteworthy, as there are benefits in terms of reducing weight gain (due to carburization) over the range of 1.5 % to 2.5 % silicon in the bulk for Fe-Ni-Cr alloys of nominally 24 % to 28 % Cr and 20 % Ni. Minor alloying additions of niobium in Ni-Cr-Fe alloys have been shown to reduce carburization rates by up to 25 % over those without niobium. Experience with aluminum and manganese has been varied, although aluminum additions and diffusion coatings have shown particular promise in being able to form a barrier to carbon ingress, thereby increasing resistance to carburization. Studies of alloy ratio of nickel and chromium have shown that alloys based on 50:50 nickel-to-chromium composition have generally better resistance than alloys where this ratio is 0.5 or 0.25. However, the presence of lead, molybdenum, cobalt, zirconium, and boron are considered detrimental to carburization resistance.

4.3.3 Microstructure

Figure 41 [ibid.] shows the microstructure of the FCCU regenerator cyclone cross section previously shown in Figure 40. This image was taken at the transition of the carburized layer (right) to the uncarburized base metal.

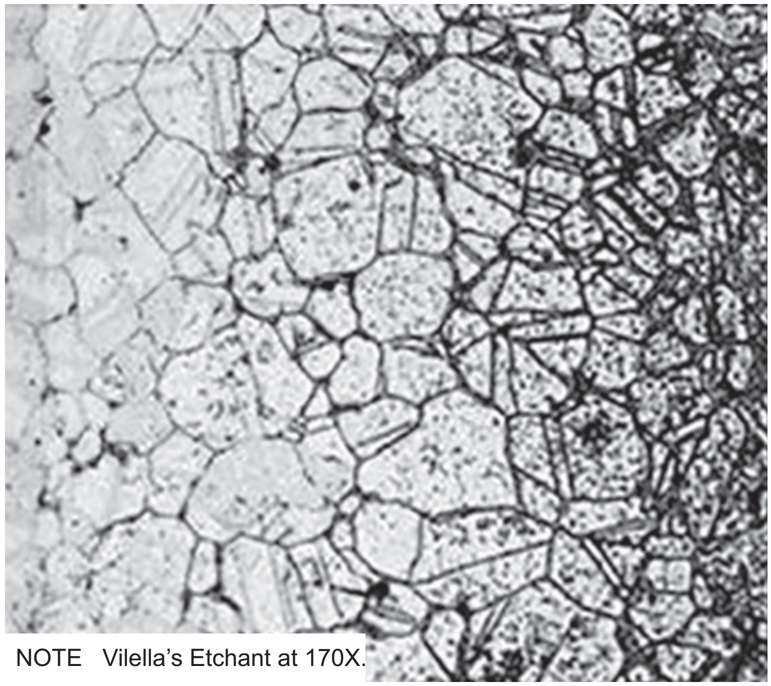

NOTE Vilella's Etchant at 170X.

Figure 41—Microstructure at the Transition from Carburized Layer (Right Side) to the Base Metal of a 304H SS Regenerator Cyclone

An example of carburization in a coker heater tube is shown in Figure 42 [46]. The ID, shown on the left, has a layer that is fully carburized, highlighted by the solid double arrow. A brittle crack that occurred during pigging penetrated through this layer and through some of the partially carburized material (dashed arrow). Carburization has diffused almost halfway through the wall thickness. Sigma phase embrittlement was found in the remaining wall thickness.

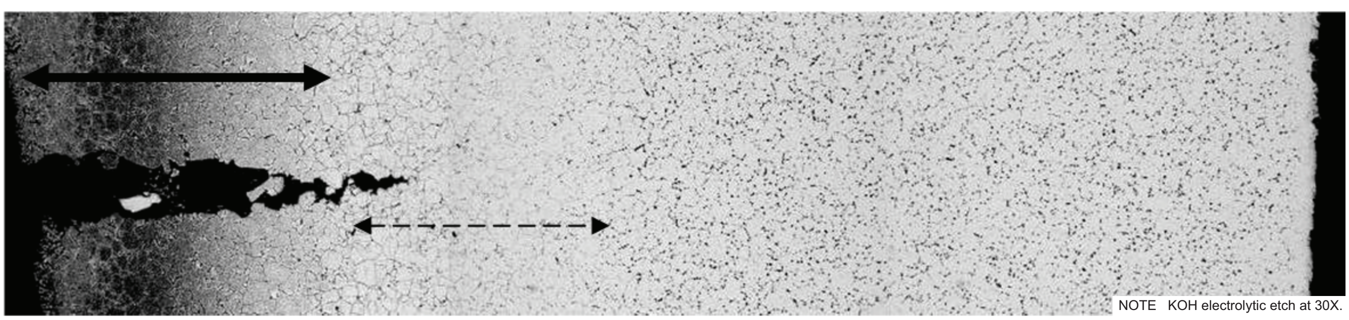

NOTE KOH electrolytic etch at 30X.

Figure 42—Cross Section of a Stainless Steel Coker Heater Tube with a Brittle Crack

Examples of microstructures from five different alloys that were subjected to a gas carburization test are shown in Figure 43 [47]. The most resistant alloy during this test is shown on the left. The microstructures display an increasing amount of carburization from left to right.

As mentioned previously, carburization ties up the chromium in the matrix of austenitic stainless steels, resulting in a reduction of corrosion resistance. This can be seen in Figure 44 [ibid.], and SEM images of the carburized microstructure are shown in Figure 42. The left image shows the microstructure while the other two images are dot maps using energy dispersive spectroscopy to highlight high concentrations of elements.

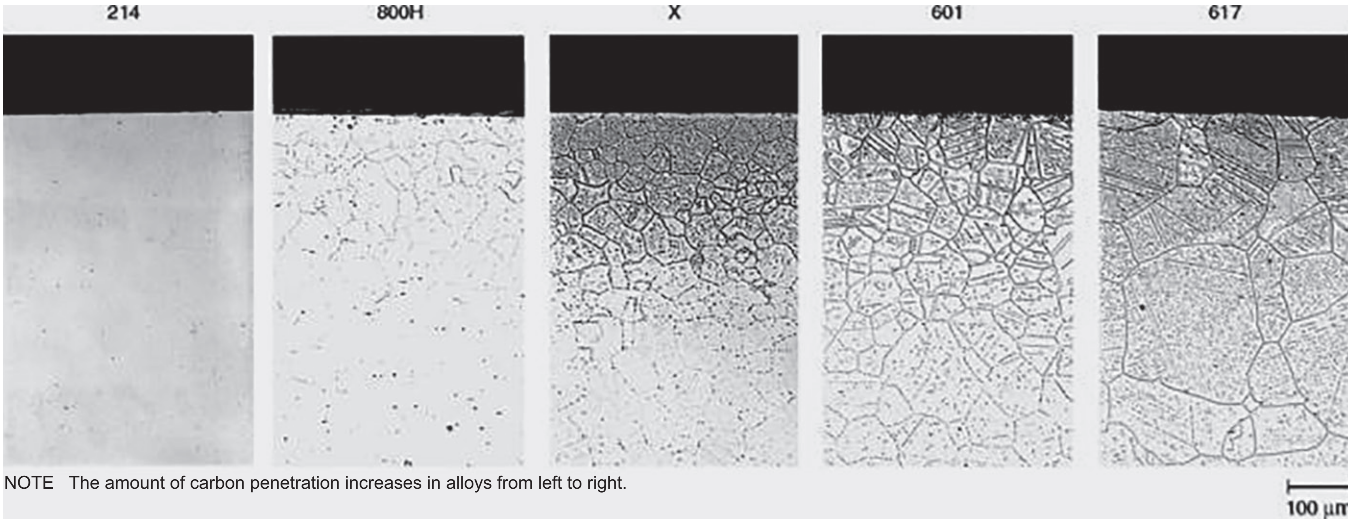

NOTE The amount of carbon penetration increases in alloys from left to right.

Figure 43—Light Micrographs Showing Typical Carburized Structures of Nickel Alloys After Testing at 982 °C (1800 °F) for 55 h in 5 % H_2, 5 % CO, and 5 % CH_4 (Balance Argon)

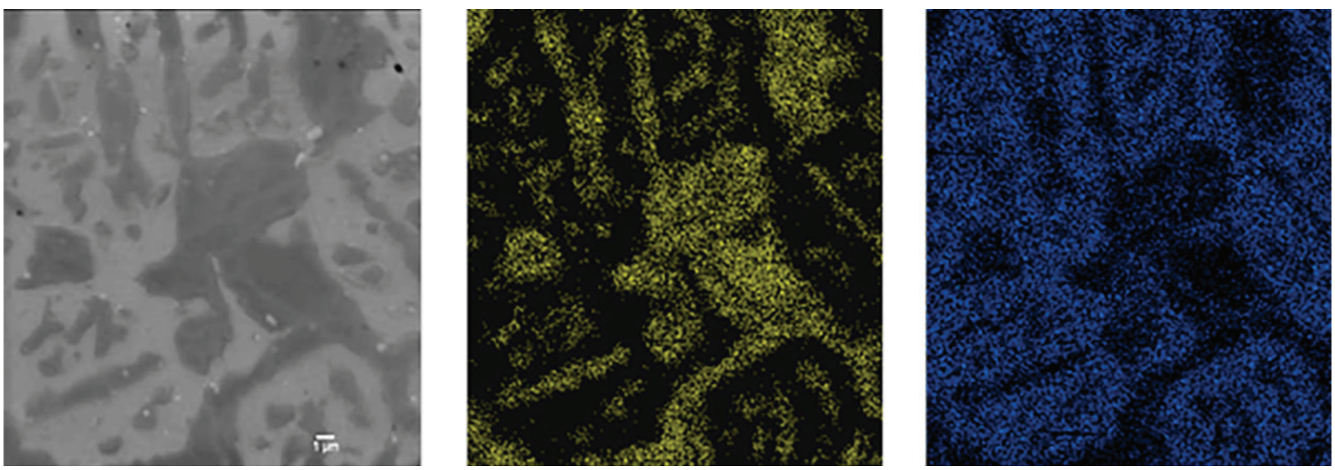

NOTE 1 The ID base metal matrix contained only 5 % Cr.
NOTE 2 At 1000X.

Figure 44—SEM View, Cr Dot Map, and Fe Dot Map of Carburized Zone Near ID of 347 SS Heater Tube

The yellow dot map in the middle shows that the carbides have high concentrations of chromium. The right dot map shows iron and is almost an inverse image of the chromium dot map. The base metal matrix between the carbide particles was analyzed and found to contain only 5 % chromium. Even though the heater tubes were Type 347 stainless steel, high corrosion rates, similar to a 5 % Cr steel, were experienced in these heater tubes.

4.3.4 Mechanical Properties

Carburization can cause an increase in hardness. The depth of carburization can be revealed using microhardness traverses on cross sections. Carburization will also cause a loss in ductility, as seen in tensile testing and creep testing. It generally does not reduce yield strength or creep strength, but can affect the tensile strength since carbon is being added between all of the iron and chromium atoms (interstitially), causing significant strain on the lattice. See Table 8 for the influence of carbon on the mechanical properties of 25Cr-20Ni steel.

Table 7 ibid. gives the results of tensile and bend testing samples from the same coker heater as referenced in Figure 42. The Type 347 stainless steel tubes had more carburization on the fire side, which was compared to the opposite side, which had the least carburization. Results showed a loss of tensile strength, but minimal effects on the yield strength. Bend testing with the ID in compression showed good ductility. However, when the carburized layer was in tension, none of the bends reached 45°, and some cracked after only a 6° bend.

Table 7—Heater Tube Bending Ductile and Tensile Test Results

Amount of Carburization	3.75 in. OD Tube Sample				4.5 in. OD Tube Sample			
	Most	Least	Most	Least	Most	Least	Most	Least
Bending ID	15°	14°	6°	38°	10°	10°	12°	14°
Bending OD	180°	180°	180°	180°	180°	180°	180°	180°
Tensile Strength, ksi	78.5	46.8	80.6	68.1	65.6	47.2	48.4	45.3
Yield Strength, ksi	40.9	40.2	37.5	39.9	43.0	43.3	35.9	41.0
% Elongation	29.2	13.9	38.2	29.9	20.6	9.4	11.6	8.7
NOTE Specimens were extracted from the side of the most severe carburization (ID) and the opposite side (least carburization).								

Table 8—Influence of Carbon Content in 25Cr-20Ni on Mechanical Properties [48]

Carbon Content %	Yield Point MPa	Tensile Strength MPa	Elongation	Area Reduction %	Impact Value J		Sigma Phase %
					As Cast	850 °C/500 h	850 °C/500 h
0.04	242	475	43.0	36.0	103	6	38
0.18	250	480	27.4	28.5	51	6	18
0.31	268	490	17.6	18.4	21	7	8
0.45	268	480	14.2	13.8	8	7	0
0.60	268	480	9.2	8.0	8	7	0
0.90	272	495	3.2	4.5	8	7	0

In a more advanced stage of carburization, there may be a volumetric increase in the affected component. This effect has been reported in a FCCU slide valve; where tolerances were too close to accommodate hexagonal mesh expansion due to carburization.

4.3.5 Prevention/Mitigation

In applications known to be subject to carburization, alloy selection is the primary method of mitigation. Materials with increased carburization resistance vary in cost. Alloy 800H or Type 330 stainless steel can be considered for some types of aggressive carburizing conditions. Alloy 600 and 601 are more carburization resistant, but can suffer metal dusting in some environments.

In refinery applications, some sulfur in the process stream will inhibit carburization. Accordingly, heater tubes and transfer piping handling hot sour processes tend to be more resistant to carburization. However, too much sulfur results in increased corrosion, especially when carburization has occurred.

If possible, reduce the carbon activity of the environment through lower temperatures and higher oxygen/sulfur partial pressures. Fire side carburization on the outer diameter of heater tubes is generally caused by a lack of excess oxygen or incomplete combustion in the fire box.

4.3.6 Inspection and Monitoring [49, 50]

Inspection for carburization in the initial stages of attack is difficult. If the process side surfaces are accessible, hardness testing and field metallography can be used. However, these generally need to be compared to uncarburized material. This can be accomplished by grinding past the suspect depth and retesting.

Destructive sampling and magnetic-based techniques (eddy current) have also been used.

Inspection techniques based on determining increased levels of ferromagnetism (magnetic permeability) are also useful for alloys that are paramagnetic when initially installed (austenitic alloys). However, surface oxides may interfere with the results.

In the advanced stages of carburization where weldability is a concern, a simple magnet test can be used. It has also been found that the color of the grinding sparks gives an indication of carburization. Grinding a carburized layer typically produces an abundance of bright sparks; as the carburized layer disappears, sparking rapidly diminishes. Macro-etching or magnet testing can be done to confirm the removal of the carburized layer.

4.3.7 Repairs

Repair welding cannot be performed without removing the fully carburized material. Since process equipment is rarely carburized entirely through the thickness, determining the depth of carburization is the first step to a successful repair.

Carburization can be detected by using a magnet or by hardness readings. A cross-section of the carburized material can be macro-etched (Marble’s reagent works well with 300 series stainless steels) to determine the depth/extent of carburization.

If a carburized layer is present, it is most often removed by grinding. (If successful grinding is difficult to achieve, air-arc gouging is an option, followed by light grinding.) Use of a magnet is helpful in determining if the carburized layer has been removed; macro-etching can also be used.

Grinding a carburized layer typically produces an abundance of bright sparks; as the carburized layer disappears, sparking rapidly diminishes. The disappearance of sparking indicates that the carburized layer has been removed. Macro-etching or magnet testing can be done to confirm the removal of the carburized layer.

Carburized welds that contain cracks are difficult to repair because the carburization follows the open cracks. Often, the local heat generated by grinding drives cracks deeper due to embrittlement from carburization. Therefore, when repairing an embrittled weld, it is sometimes more efficient to air arc gouge or use a plasma cutting unit to completely remove the weld when repairing deep cracks.

Weld bevels should be dye-penetrant tested to ensure that the prepared surfaces do not contain crack-like indications.

Repair welds for material containing residual carburization typically fail by generating cracks adjacent to and in front of the weld bead. Dye-penetrant testing can also be used after each welding pass to ensure that residual carburization is not causing crack formation. If needed, high temperature dye penetrants can be used to minimize work delays.

4.4 Stress Relaxation Cracking (SRC)

4.4.1 General

Stress relaxation cracking can occur either during fabrication or while in service, as shown in Table 9. It involves cracking of a metal due to stress relaxation during post weld heat treatment (PWHT) or service at elevated temperatures 500 °C to 750 °C; (932 °F to 1380 °F). It is most often observed in welded joints of heavy wall sections. The affected materials include low alloy steels (Cr-Mo) as well as 300 series stainless steel and nickel base alloys such as Alloy 800H/800HT®. The critical factors that increase cracking potential include:

— type of material (chemical composition, impurity elements);

— large grain size;

— high residual stresses from fabrication (cold working, welding);

— heavy section thickness (which controls restraint and stress state);

— notches and stress concentrators;

— weld metal and base metal strength; and

— welding and heat treating conditions.

Table 9—Names for Stress Relaxation Cracking Mechanisms

Fabrication	In Service
Reheat cracking	Stress relaxation cracking
Stress relief cracking	Creep embrittlement cracking
Stress relaxation cracking (SRC)	Stress induced cracking
	Stress assisted grain boundary oxidation (SAGBO) cracking

Table 10 lists the chemical attributes of the 800 series alloys.

Table 10—Chemistry Requirements of the 800 Alloys

UNS Designation	N08800	N08810	N08811
Alloy	800	800H	800HT®
Nickel	30.0 to 35.0	30.0 to 35.0	30.0 to 35.0
Chromium	19.0 to 23.0	19.0 to 23.0	19.0 to 23.0
Iron	39.5 minimum	39.5 minimum	39.5 minimum
Carbon	0.10 maximum	0.05 to 0.10	0.06 to 0.10
Aluminum	0.15 to 0.60	0.15 to 0.60	0.25 to 0.60
Titanium	0.15 to 0.60	0.15 to 0.60	0.25 to 0.60
Al+Ti	—	—	0.85 to 1.20
ASTM Grain Size	—	5 or coarser	5 or coarser

There are a number of factors that influence SRC; however, practical industry experience indicates that Alloy 800HT is probably the most susceptible to SRC, followed by Type 347 stainless steel.

Cracking is due to low creep ductility at high temperature, where ductile strain relief (from applied or residual stresses) cannot occur; instead, cracks develop. Relaxation strains of as little as 0.1 % can cause severe cracking [51].

There appears to be two mechanisms that cause SRC [52], creep cracking that initiates/grows within grains due to the formation of a “precipitation free zone” and grain boundary sliding. The precipitation free zone (PFZ) is the region immediately adjacent to the grain boundaries in a sensitized austenitic alloy. As the sensitization process proceeds, $Cr_{23}C_6$ precipitates form, thereby depleting the adjacent lattice of chromium. The resulting zone is much weaker than the surrounding non-depleted lattice, while the grain interior is unaffected.

The grain interior in stabilized alloys, such as Types 321 and 347 stainless steels, is strengthened by the formation of carbides (NbC in Type 347 and TiC in Type 321 stainless steel). (This aspect is also involved in the grain boundary sliding mechanism, since it makes the grains stronger than the grain boundaries. This tends to force deformation to occur at the grain boundaries.)

The PFZ, being the weakest microstructure in the sensitized alloy, will respond to stresses faster and accumulate strain faster than the stronger, unaffected matrices. When the metal temperature is high enough to initiate the low creep ductility characteristic of SRC, creep cracks begin to form and coalesce.

Grain boundary sliding, which creates grain boundary micro-voids, is the dominant mechanism; presumably because it occurs at a lower level of stress (primarily residual stress in most cases) than does the PFZ mechanism. SRC cracks are almost exclusively intergranular.

Because SRC is a brittle fracture mechanism (i.e. crack propagation is neither preceded nor accompanied by ductile deformation effects such as bulging or necking), sudden in-service cracking and failures can occur.

The temperature range for the most rapid development of SRC is material dependent.

Stress raisers include not only those due to joint design, but can be also generated by welding defects such as undercut, lack of fusion, lack of penetration and solidification cracking.

Alloy composition influences cracking sensitivity. In order from most susceptible to the least susceptible austenitic alloys are [53]: IN 800HT® > Type 347 > Alloy 800H > Type 321 > Type 304 > Type 316 stainless steels. Alloys are more susceptible if they are strengthened by the dispersal of fine intergranular precipitates, such as Types 321 and 347 stainless steels, and are more susceptible than Type 304 stainless steel. Alloy 800HT and Alloys 601 and 617 are also known to be susceptible to strain aging embrittlement.

Bismuth in flux core weld metal flux is added to make the flux easy to remove from finished welds. However, when these welds are exposed to elevated operating temperatures, they have been reported to experience high SRC susceptibility [54]. API 582 limits bismuth to 0.002 % in the weld deposit for operating temperatures above 538 °C (1000 °F).

Bismuth has a detrimental effect on SRC in Type 308 FCAW weld metal. Welding Research Council (WRC) Bulletin 460 shows several cases of FCCU failures. Types 347 and 800HT have high susceptibility, but it is important to mention the Type 308 susceptibility and the bismuth effect, as it has caused several failures. API 582 [79] sets limits for bismuth.

When comparing austenitic stainless steels, in general, Types 304 have less reheat cracking susceptibility than Types 347/321. Table 11 [55] was published in the EWI report “Reheat Cracking and Elevated Temperature Embrittlement of Austenitic Alloys: Literature Review.”

Table 11—Stainless Steel Susceptibility for SRC

Steel	Intergranular Precipitate	Cracking Susceptibility during Heat Treatment
Cr-Ni-Nb (AISI Type 347, Nb stabilized)	NbC	High
CR-Ni-Ti (AISI Type 321, Ti stabilized)	TiC	Medium
CR-Ni (AISI Type 304)	$M_{23}C^6$	Low
CR-Ni-Mo (AISI Type 316, Mo alloyed)	$M_{23}C^6$	Nil

Grain sizes ASTM no. 3.5, and finer, appear to be more resistant to SRC. During fabrication, grain growth can be controlled by solution annealing at lower than traditional temperatures, resulting in grain sizes of ASTM no. 4 and finer. The optimal solution annealing heat treatment soaking temperature is material dependent.[ibid.]

Type 300 series stainless steels and austenitic alloys, in general, are usually supplied by the mill with a solution annealing heat treatment. This heat treatment involves heat soaking the product at about 1093 °C (2000 °F), followed by a rapid quench (the quench is intended to avoid or minimize sensitization). The traditional heat treatment generates a coarse grain size, designed to be no smaller than ASTM no. 7. Typical grain sizes are ASTM no. 5 and coarser. The large grain size is beneficial for creep resistance, but increasing the grain size enhances susceptibility to stress relaxation cracking after cold forming; in addition, coarse grain size can contribute to welding problems.

Cold deformation (in some cases, to less than 2 %) can significantly increase susceptibility to SRC. One source showed that a stabilizing heat treatment of 980 °C (1800 °F), either before or after cold working, is “very effective” in the avoidance of SRC of the welds while in service. This study included a variety of commonly used alloys, including Types 304H and 316H stainless steels and Alloys 800, 800H and 800HT® [56].

4.4.2 Visual Appearance

Liquid penetrant testing is normally used when inspecting for SRC, as shown in Figure 45 [57]. In this weld, the flat to concave bead shape likely contributed to this failure by increasing the weld restraint during solidification.

Cracks are almost always confined to weld metal and heat affected zones. Cracking is most frequently observed in coarse-grained sections of a weld heat affected zone. Cracks show little or no evidence of deformation. In cold deformed areas, cracks can be seen in parent metal. Experience indicates that welds themselves are not the cause of SRC—it is the residual stress fields created by the welds.

4.4.3 Microscopic Appearance

Cracks can be either surface-breaking or embedded, depending on stress and geometry. Crack tips are usually preceded by creep voids (sometimes referred to as creep cavities). Cracks are located on grain boundaries (i.e. they are intergranular) and show little or no evidence of deformation.

Metallic filaments are usually present in the crack. The filament compositions are dependent on parent and weld metal composition.

Metallographic examination of suspected SRC damage should look at the cross sections containing cracks in the as polished condition. Etching can dissolve the filament, as shown in Figure 46 [ibid.], thus altering the microstructure and potentially leading to an incorrect diagnosis.

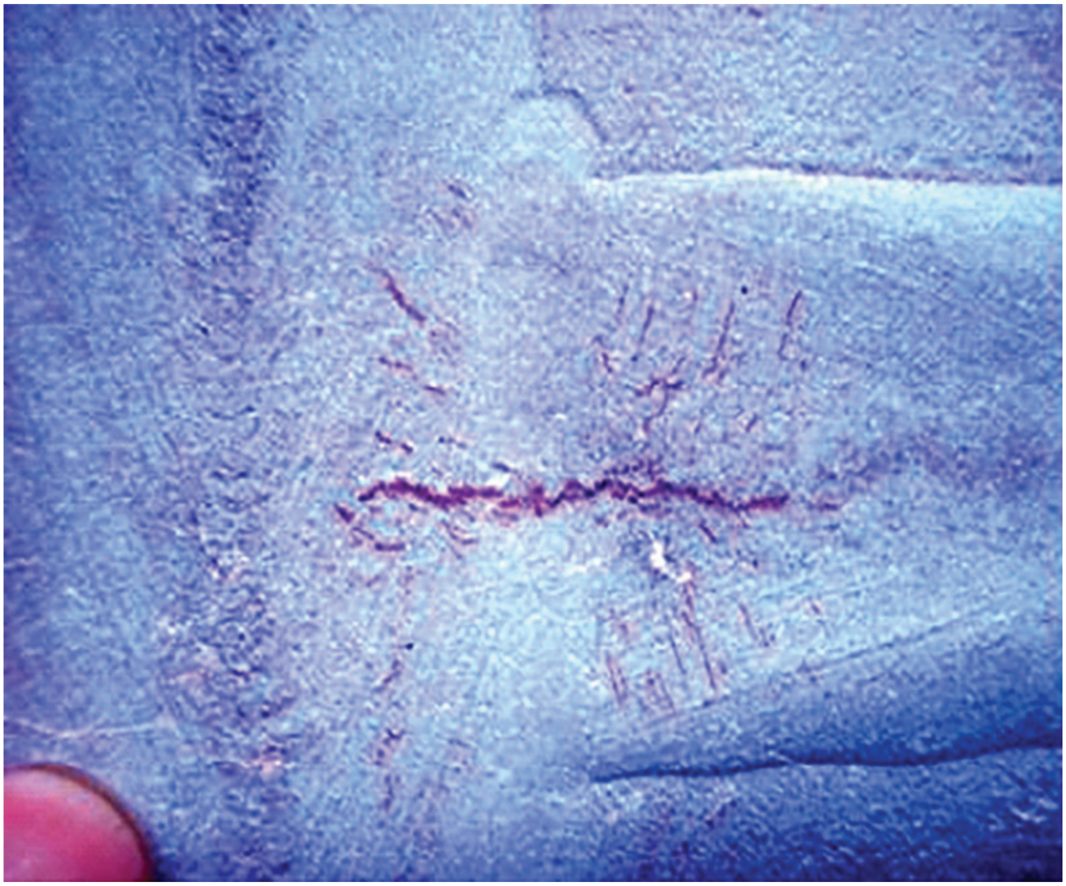

Figure 45—Penetrant Examination Results Showing SRC Cracking

Cracked regions are relatively hard for an austenitic material; the Vickers hardness is usually higher than 200HV. An example is a leak that occurred at a Type 347 stainless steel fillet weld between the pipe and the shoe support after approximately 56 months in service. [58] The tube that failed was 75 mm (3 in.) in diameter, 5.7 mm (0.226 in.) nominal wall thickness, ASTM A312 Grade 347H. The operating conditions cycled in temperature from 454 °C to 621 °C (850 °F to 1150 °F) every 40 to 50 days due to the decoking process of the heater tubes. The process operating pressure was 372 kPa (54 psig). The original welds were made using 347 and ER347 welding electrodes without preheat and without post weld heat treatment.

The analysis identified thermal fatigue as the final propagation failure mechanism. Solidification cracking in the weld fusion zone contributed as initiation sites in some cracks. Other contributing factors for crack initiation were the stress raisers existing at the weld toe due to the filler weld geometry. The presence of carbide precipitation and sigma phase at the grain boundaries and in-service SRC played a role in crack propagation.

This example shows that SRC can occur at wall thicknesses of less than 12 mm ($^1/_2$ in.). Weld joints with high restraint, such as fillet welds and/or with the potential for high stresses, should be considered susceptible to SRC. Where possible, these types of welds should be designed out of the system if operating temperatures and materials combinations are in the susceptibility range. The use of bolted clamp on pipe supports with suspended hangers is preferred.

4.4.4 Mitigation/Prevention

Where stress relaxation cracking has been determined to pose a significant risk, the following measures may be used to minimize cracking potential.

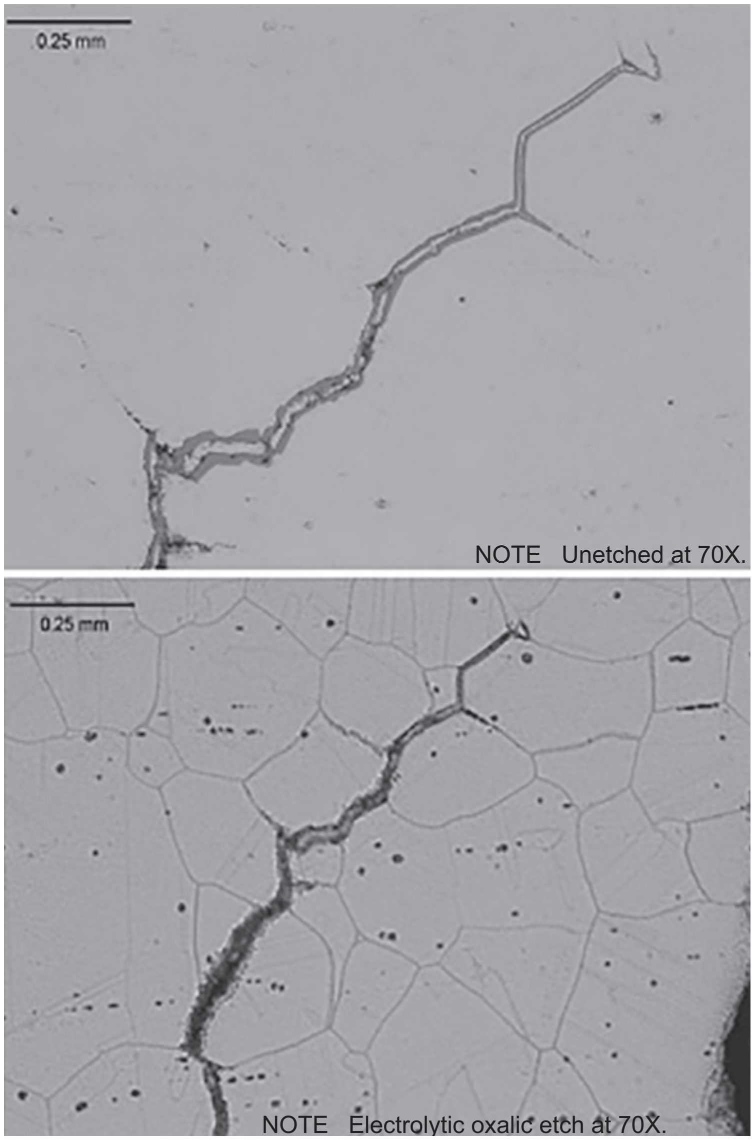

Figure 46—SRC in an Alloy 800H Furnace Tube

— For heavy wall butt weld joints, t > 12 mm ($^{1}/_{2}$ in.), minimize restraint during welding.

— Specify post weld heat treatment: 843 °C to 899 °C (1550 °F to 1650 °F) is the recommended temperature range for stress relief of most 300 series stainless steels. PWHT enables the material to accommodate relaxation strains of more than 2 %, which is often sufficient to accommodate service-induced strains [59]. For Type 347 stainless steel, time at temperature has very little effect compared to temperature on the relaxation of residual stresses [60]. This is typical of austenitic materials.

— In one study, a special post-construction heat treatment (stress relief, followed immediately by solution annealing, followed immediately by stabilizing stress relief at 593 °C (1100 °F), then air cooling) has been shown to minimize or eliminate SRC in Type 347 stainless steel [61]. The laboratory investigation indicated that this multi-step procedure may have some benefit versus the single step (e.g. 843 °C to 899 °C (1550 °F to 1650 °F) post weld heat treatment described above. However, the uses and limitations of the multi-step procedure has not been widely evaluated under field conditions.

— Joint designs should minimize stress concentration.

— Avoid metallurgical notches in welding operations (e.g. lack of penetration, lack of fusion, etc.) since such notches usually give rise to cracking of heat affected zones.

— Control grain size during fabrication and welding procedures because materials with coarse grain size are more susceptible to SRC.

— Low heat-input welding techniques are recommended in order to minimize the risk of welding-induced grain growth. Small diameter filler metal rods, such as 2.5 mm, a maximum interpass temperature of 180 °C (350 °F) and the use of the stringer bead technique (rather than weaving) have been recommended [62].

  Minimizing the risk of SRC in components made of Alloys 800, 800H, and 800HT® has been summarized by Shargay [63]. Limit Al + Ti content to less than 0.7 % in the base material and weld metal. As shown in Table 9, the ranges of Al + Ti content overlap for the 800H and 800HT® alloys. Because of this, material is often "dual-certified" for both alloys. However, to get the lower susceptibility to SRC in the operation range of 540 °C to 700 °C (1000 °F to 1300 °F), the Al + Ti content should be controlled. The material then meets the requirements of Alloy 800H, but not Alloy 800HT®.

— Require stabilization heat treatment of base materials. A stabilization heat treatment at 982 °C (1800 °F) for 3 hours should be performed on Alloy 800H base materials after rolling, forming or other manufacturing steps. This heat treatment is done after the ASTM-required solution annealing and is at a lower temperature. A stabilization heat treatment creates benefits by generating coarse particles within the grains and on the grain boundaries. These carbides form by reacting with age-hardening elements such as Ti, Al, Nb, etc. The result is that at operating temperature, less of these elements are available for the formation of fine carbides within the grains.

— When Alloy 800H is being fabricated, intended for service at 540 °C to 700 °C (1000 °F to 1300 °F), it is recommended that the filler metal chemistry match the major elements of the base metal chemistry such as AWS 5.14 ERNiCr-3 and AWS A5.11 ENiCrFe-2. Above 700 °C (1300 °F), AWS A5.11 ENiCrCoMo-1 and AWS A5.14 ERNiCrCoMo-1 can be used to match the creep strength of the base metal.

— PWHT at a minimum of 900 °C (1650 °F) for 1.5 hours.

— PWHT of Alloy 800H is considered the best prevention against in-service SRC (although it creates the risk of SRC during PWHT). PWHT of Alloys 800H and 800HT® is required by Code for pressure vessels if the service temperature is above 540 °C (1000 °F).

4.4.5 Inspection and Monitoring

UT and PT examination can be used to detect cracks in 300 series stainless steel and nickel base alloys. Embedded cracks can generally only be found through careful UT examination. Due to their short length and that they are tight; radiography is rarely able to detect subsurface cracking.

4.5 Creep

4.5.1 General

Creep is the time-dependent deformation or flow of materials under relatively constant stress at elevated temperatures. Creep strain occurring at stresses less than the metal's yield strength results from grain boundary sliding and/or creep void nucleation and growth, both mechanisms requiring temperatures hot enough to promote vacancy diffusion.

The temperature above which creep can occur depends upon the material. The rule of thumb is that the temperature required for creep is half of the metal's melting point, measured on an absolute scale. The resistance of steels to creep is increased by the addition of alloying elements such as molybdenum, chromium, and nickel.

4.5.2 Design Considerations

Metals and alloys have a "creep threshold" temperature, below which creep is a trivial mechanism. Above the threshold temperature, creep damage will occur at a rate which depends on the strength of the material, the imposed stress and the temperature. For a constant temperature and stress, the magnitude of creep depends upon the length of time in which the material was creeping.

Metals and alloys also have a temperature threshold above which the accumulation of creep damage is rapid. Table 12 was developed from information obtained from API 530 [64].

Table 12—Creep Threshold Temperatures [64, 65]

Material	Creep Onset (Note 1, Note 2)	Creep Threshold (Note 3)	Rapid Creep Threshold (Note 4)
304/304H SS	510 °C (950 °F)	580 °C (1075 °F)	815 °C (1500 °F)
316/316H SS	538 °C (1000 °F)	610 °C (1125 °F)	815 °C (1500 °F)
321/321H SS	538 °C (1000 °F)	550 °C/565 °C (1020 °F/1050 °F)	815 °C (1500 °F)
347/347H SS	538 °C (1000 °F)	595 °C (1100 °F)	815 °C (1500 °F)
Alloy 800H/800HT®	565 °C (1050 °F)	650 °C (1200 °F)	980 °C (1800 °F)

NOTE 1 From Table 4.1 in API 579-1/ASME FFS-1 2007, *Fitness for Service* [65].

NOTE 2 Large variations in creep onset temperatures vary with stress.

NOTE 3 Creep thresholds: 100,000 hour line crosses elastic allowable stress.

NOTE 4 From Table 5, in API 530, *Calculation of Heater-Tube Thickness in Petroleum Refineries*., 7th Edition [64].

NOTE The ASME *Boiler and Pressure Vessel Code* [80] gives allowable stresses for several types of stainless steel Including:

— Alloy 800H plate per ASME SB-409, UNS N08810,

— 304H plate per ASME SA-240, UNS S30409,

— 316H plate per ASME SA-240, UNS S31609,

— 321H plate per ASME SA-240, UNS S32109,

— 347H plate per ASME SA-240, UNS S34709.

There are two common creep design criteria [66]. The design stress is chosen to avoid: 1) rupture in less than 100,000 hours, or 2) to permit the accumulation of no more than 1 % creep strain in 100,000 hours. The latter criterion has a potential problem. In operation, conditions may exist for a short or long period of time which places the component at higher-than-design stress and/or temperature levels. Such conditions may promote creep beyond the design criterion and have the potential of leading to premature failure.

Creep rate follows an Arrhenius-rate function with respect to temperature and follows the power-law as a function of stress. Short-term increases in either temperature or applied loads can significantly reduce life. For example, doubling the maximum allowable heater tube stress can reduce creep life by a factor of 40.

Creep can be controlled or eliminated by proper choice of materials for high-temperature applications and by operating the equipment at or below design conditions at all times. Control of creep is an integral part of the design of high-temperature equipment and piping. Various design codes, such as ASME Section VIII and B31.3, incorporate consideration of creep in establishing the maximum allowable stress at any given design temperature. API 530, *Calculation of Heater Tube Thickness in Petroleum Refineries*, provides recommended procedures for utilizing the Larson-Miller Parameter for the design of heater tubes in creep service. Numerous design curves are provided for many common heater tube materials. In addition, design curves are provided by vendors for numerous proprietary alloys (most of which are used in non-refinery applications).

An example of a series of stress rupture curves based on rupture in 100,000 hours is shown in Figure 47 [67] and corresponding creep rate curves are shown in Figure 48.[ibid.]

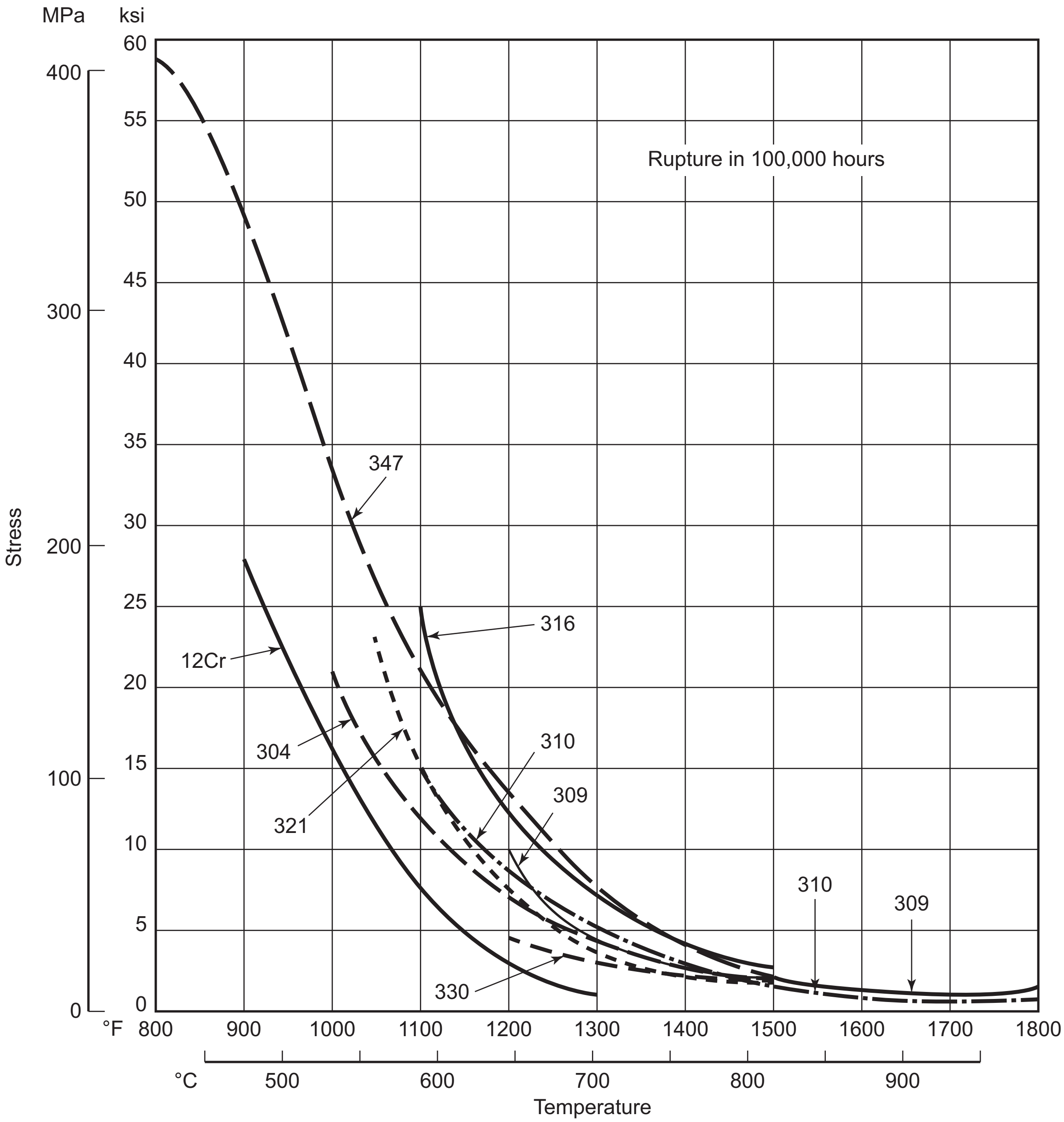

Figure 47—Stress Rupture Curves for Several Annealed Stainless Steels (Extrapolated Data)

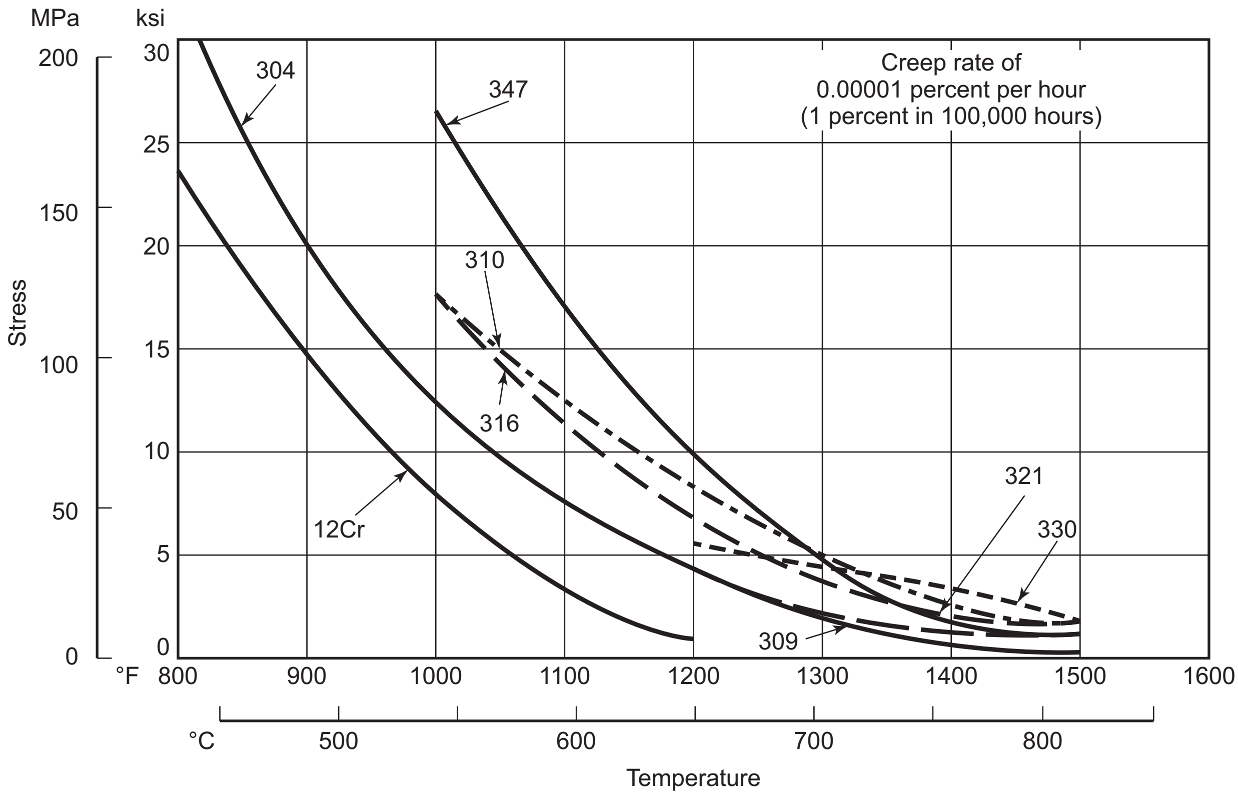

Figure 48—Creep Rate Curves for Several Annealed Stainless Steels

The presence of geometrical discontinuities or weld defects that could act as localized stress concentrators should be avoided in the design and fabrication of equipment in creep service.

Assuming the design and material selection have been properly executed for a component operating in creep service, the most effective prevention is routine monitoring and control of the metal temperatures to keep them below the design metal temperature limits. It is important that operational limits be carefully identified so that individual components do not exceed their design temperature limit unknowingly. This can be difficult for heater tubes where internal fouling can cause significant variations in metal temperatures. It is for this reason that skin thermocouple readings should not be relied on alone, but should be supplemented by visual checks of the heater during operation and periodic infrared thermal imaging studies, especially when internal fouling is an issue.

4.5.3 Damage Characteristics

Creep is a multi-stage process that leads to the development of voids along grain boundaries which grow and then interconnect to form microfissures and, ultimately, macroscopic cracks.

When a material is subjected to a constant stress at an elevated temperature, the resulting strain occurs initially at a decelerating rate due to strain hardening, called first-stage or primary creep—as shown in Figure 49 [68].

Subsequently, the creep rate becomes essentially constant for a period of time during which microscopic voids are formed (second-stage creep). During this stage, strain hardening competes with grain boundary sliding and void/ fissure formation mechanisms. Finally, the creep rate accelerates as the voids interconnect to form cracks (third-stage creep) and, if the process is not interrupted, rupture occurs (the rupture event, when the cause is creep, is called “stress rupture” or “creep rupture”). The three stages of creep are shown on an idealized constant-load creep curve depicting an idealized constant-stress creep curve as a function of time.

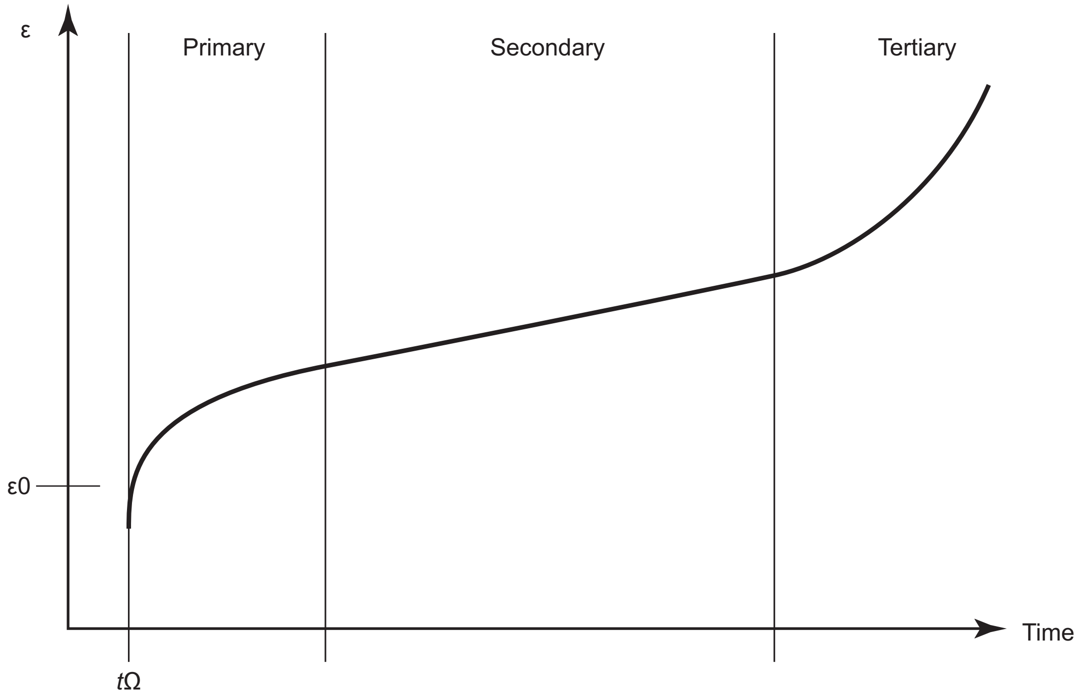

Figure 49—Three Stages of Creep Damage

For most, if not all, stainless steels and Fe-Cr-Ni alloys, creep strength may be enhanced as a result of the sigma phase formation, carbide precipitation, or carburization, primarily due to precipitation strengthening. However, while creep strength may be enhanced, creep ductility will be reduced, resulting in premature cracking at stress concentrators. Such behavior makes it difficult to accurately predict creep life.

Geometric discontinuities, or weld defects (i.e. stress concentrators), can promote abnormally low creep ductility and increased creep cracking susceptibility of these steels when they operate in the temperature range of 454 °C to 565 °C (850 °F to 1050 °F). Also, there is some evidence that long-term elevated temperature exposure may promote reductions in creep ductility.

In refineries, creep rupture failures are typically encountered in fired equipment (e.g. heaters, boilers, steam superheat coils, steam-methane reformers).

Due to the grain boundary sliding and void/fissure mechanisms, creep failures typically exhibit a thick lipped fracture. Necking, which is observed in lower temperature tensile overloading and in short-term overheating failures, is not observed.

Metals (such as austenitic stainless steels and nickel-based alloys) with close-packed structures (most have face-centered cubic unit cells) have significantly better creep resistance when compared to most ferritic and martensitic engineering alloys.

The Electric Power Research Institute (EPRI) has developed a creep classification scheme [69] to assist in evaluating the seriousness of creep damage. For reference purposes, this classification contains five different stages of creep, ranging from Class 1 to Class 5. Class 1 involves no damage; Class 5 involves the formation of macro cracking. The classification diagrams appear in the referenced publication.

4.5.4 Inspection and Mitigation

Equipment in creep service should be inspected, especially as the design creep life is approached or exceeded, to determine the degree of creep deformation or other evidence of creep damage that may have been experienced. For equipment operating in the creep range, it is impractical to attempt to assign a generalized rejection criterion based on a specific creep deformation percentage. However, factors which may be employed to help in arriving at acceptance/rejection decisions in specific cases include: type of material, service conditions, process environment, operating history and inspection history.

NOTE The 1 % creep deformation value frequently referred to is normally a design criterion only and not a measure of creep void formation or other damage. Therefore, while creep design curves can be used to estimate when to begin inspecting for creep, they are not intended to dictate equipment retirement.

When vessels are inspected for creep damage, close attention should be paid to locations that are most likely to suffer damage, such as areas around vessel wall penetrations, including nozzles or manways and external attachments, such as supports. These areas are particularly susceptible to creep damage because the local stress levels may be considerably higher than the stress used for design purposes. Furthermore, the presence of welds may promote creep. Dye penetrant inspection can often detect cracks resulting from creep damage, and confirmed by the use of in-situ metallographic replica (also referred to as field metallography and replication) techniques.

Creep failure will not always be accompanied by a significant degree of deformation. For certain materials and geometries, creep failure may take place in a brittle mode. The creep ductility of these materials, particularly in weld zones, decreases after prolonged operation at high temperature. Cracks can initiate at stress raisers such as complex nozzle attachments.

An attempt to correlate creep damage level to an inspection or mitigation action was conducted by Neubauer and Wedel [70]. Figure 50 shows Neubauer's approach which assigns a corrective action based on the damage parameter.

It is possible to estimate the remaining useful life of a component that has been operating in the creep range by using the Larson-Miller parameter approach or the Omega method [71], as given in API 579-1/ASME FFS-1, *Fitness for Service*. The life fraction that has been consumed so far can be estimated based on past operating conditions. An estimate can then be made as to the remaining useful life based on projected future operating conditions. An analysis of this type should be treated as only an approximation because of the numerous assumptions employed, significant variations in creep strength properties of materials and uncertainties regarding actual metal temperatures and stress levels during operation.

For heaters designed to operate in the creep range, routine visual inspection plays the key role in responding to overheating episodes that may suddenly accelerate the accumulation of creep damage.

The heater tubes should be visually inspected periodically. If visual inspection detects an anomaly, the inspection should promptly be repeated, using infrared thermal imaging. If the anomaly is confirmed, the responsible engineering department should be immediately advised.

Heater tubes in services in which internal deposits can form have the potential of developing hot spots. This can happen even if the tube metal temperatures are usually low enough so that coking is not expected; flame instabilities are usually the root cause in this event. Detection of a hot spot should prompt an appropriate response to confirm the hot spot and to initiate corrective measures as necessary.

Creep strength may not necessarily deteriorate as a result of the sigma phase formation, carbide precipitation or carburization. On the contrary, it may even gain further creep strength due to the presence of these strengthening particles. However, while creep strength is not reduced, creep ductility is often reduced.

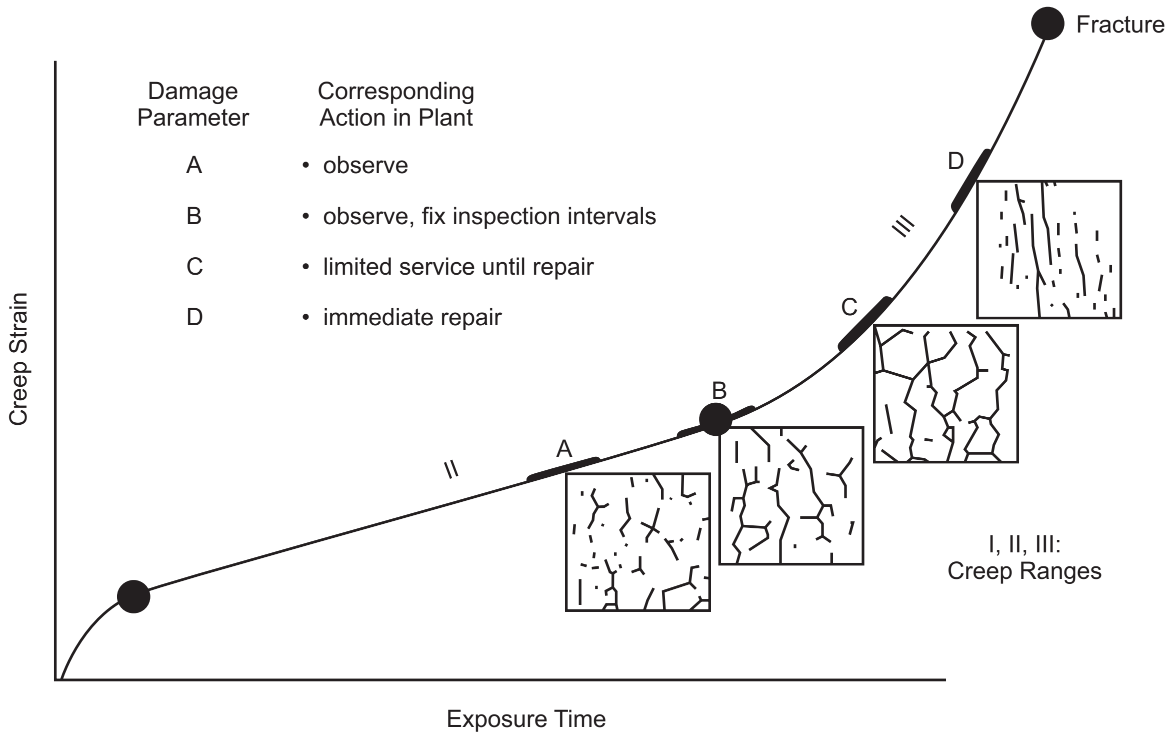

Figure 50—Neubauer's Classification of Creep Damage from Observation of Replicas [70]

Heater tube diameter measurements can be taken by strapping, a term that describes the process of measuring the circumference of the component. Special tape measures are available, referred to as "PI" tapes that are marked to give diameter measurements by wrapping the tape once around the pipe. This will give an average measurement. Local bulging can be detected by using a caliper. There are also nondestructive examination (NDE) methods of internal (ID) measurements using laser-based tools inside a smart pig, but the tube diameter must be known.

Field metallography and replication can be used to identify the microstructure that displays the hottest exposure. The microstructure can be examined for evidence of creep voids or cracking. The degree of agglomeration of carbide networks at grain boundaries can be used as evidence of total heat input. Creep damage may not initiate at the outer diameter of the tube. In this case, replication is not a reliable method of inspection and should be used in combination with another non-destructive testing (NDT) technique. Removal of a sample for metallographic analysis would be the best option to assess damage.

A short pipe segment can be removed and used for Omega or stress rupture testing as shown in Figure 51. This figure shows two solid/dotted lines that represent the heater tube being tested. The tangential samples shown at the top of this figure is the preferred method of testing since this allows the testing to be made in the same direction as the hoop stresses in the heater tube. If desired, these results can be compared to a sample oriented in the axial direction (see the bottom coupon in Figure 51), which generally only experiences half of the hoop stress.

4.5.5 Repairs

Creep damage in austenitic alloys is often accompanied by other types of high-temperature damage mechanisms such as carburization or sigma phase embrittlement. Such damage is more difficult to repair. If other damage mechanisms have occurred, the required repair procedures are usually dominated by concerns other than creep damage.

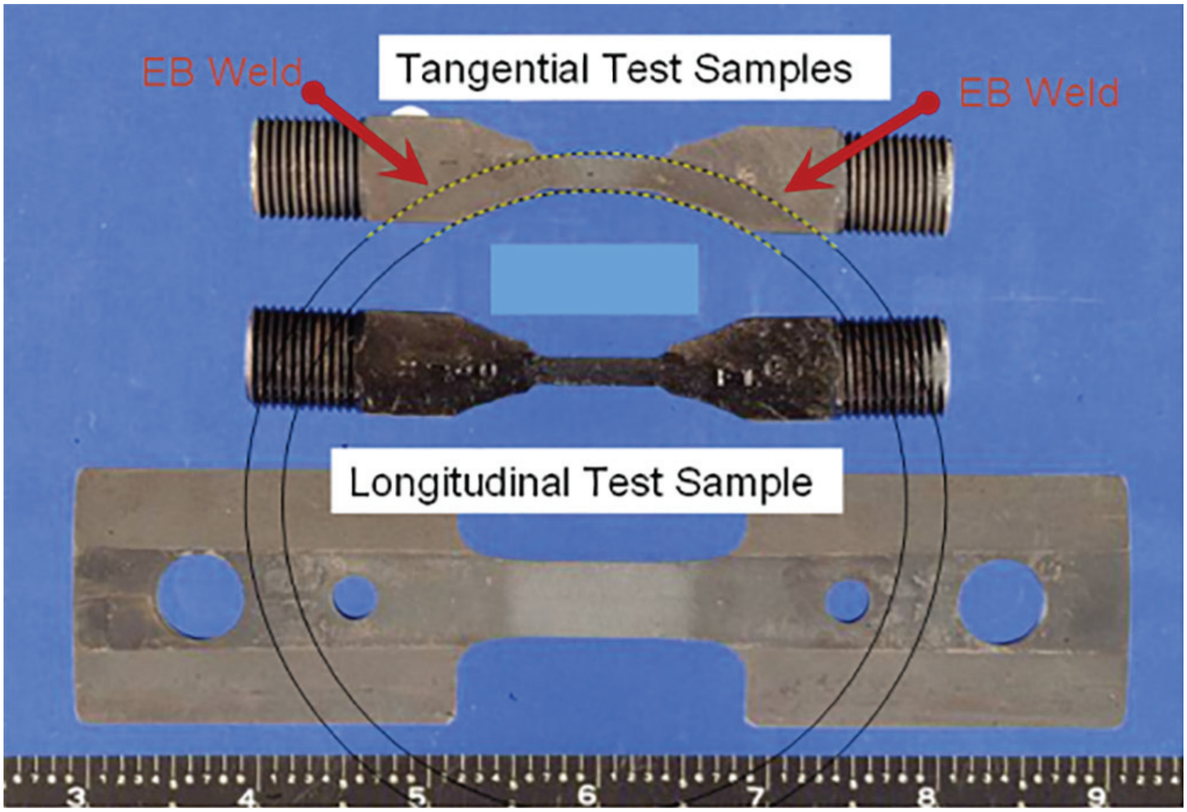

NOTE The two circles represent the pipe/tube cross section of the top sample to show orientation.

Figure 51—Two Types of Creep Test Samples, Tangential and Longitudinal

Experience indicates that wrought material containing no more than isolated creep voids in the HAZ can be successfully repair welded. Nearby isolated voids are removed by fusion from the weld metal pool. More advanced stages of creep damage are usually out of the reach of the weld metal pool.

Worse damage, e.g. EPRI Class 3, 4, and 5 damage (oriented cavities, micro-cracks, and macro-cracks), usually results in cracked repair welds or repair welds containing unacceptable porosity.

Creep-damaged materials can be dye-penetrant tested to help define the extent of material that should be removed prior to repair welding. Linear porosity and/or crack-like defects should be removed by grinding (or gouging followed by light grinding).

Isolated voids (often referred to as “pinholes”) are usually acceptable in weld bevels.

Dye-penetrant testing can be used after the root bead is welded and after each weld layer to ensure that undetected creep damage is not causing the formation of cracks. The use of high-temperature dye penetrants can help minimize inspection time.

4.6 Thermal Fatigue

4.6.1 General

Thermal fatigue occurs as a result of fluctuating thermal stresses usually caused by through-thickness cyclic temperature gradients associated with rapid heating and cooling cycles. The larger the temperature gradient, the higher the stress generated within the material. Thermal fatigue causes a typical mud cracking appearance, evidence that the stainless steel tube suffered thermal fatigue.

Thermal gradients are affected by:

— rate of temperature change—higher stresses will form during rapid changes;

— heat transfer coefficient of the process fluid—for example, liquids transfer heat much faster than vapors; and

— thermal conductivity of the metal—the higher thermal conductivity of ferritic alloy steels results in a lower temperature gradient between the surface and the interior, as compared to austenitic stainless steel.

Time to failure is a function of the magnitude of the stress (sometimes referred to as the “stress amplitude”) and the number of cycles to failure decreases with increasing stress. Increasing rates of thermal cycles also decreases the time to failure. Thermal fatigue cracking may occur anywhere in a metallic component where cyclic thermal expansion is constrained.

Frequent start-up and shut-down of elevated temperature equipment increases the susceptibility to thermal fatigue. Generally, if the temperature swing exceeds about 167 °C (300 °F), the risk of cracking should be considered [72].

Thermal expansion of a piping circuit that is fixed at either end can cause high stresses if sufficient flexibility is not included in the design. Piping expansion loops are used for this purpose.

Notches (such as an undercut at the toe of a weld) and sharp corners (such as the intersection of a nozzle with a vessel shell that has not been blend ground) and other stress concentrations (such as excessive weld cap and abrupt thickness transitions) may serve as initiation sites.

Additional factors include:

— material strength—high cycle fatigue strength increases with increasing tensile strength. In contrast, low cycle fatigue strength is often affected more by ductility, thus lower strength materials can have a longer low cycle fatigue life at a given stress;

— microstructure—finer grains are usually more resistant to the propagation of fatigue cracks, but the effect is often not significant;

— localized points of restraint and stress concentration.

Joints composed of two materials having different coefficients of thermal expansion (e.g. dissimilar weld joints) are especially vulnerable to thermal fatigue cracking due to triaxial stresses that are formed, even when temperatures are uniform.

There are no set rates of change to avoid thermal fatigue. However, for heavy-wall reactors, heat-up and cool-down rates are often limited to 30 °C to 55 °C/hr (50 °F to 100 °F/hr) to minimize the thermal gradients. Dynamic thermal and stress analysis using finite element methods can be used to modify startup and shutdown procedures to optimize a balance between thermal fatigue cracking potential, while minimizing the time to start-up or shut-down critical equipment items.

Ferritic steels are generally considered to be more resistant to thermal fatigue than austenitic steels. This has been confirmed in several instances in which parts made of ferritic steels have withstood service conditions under which austenitic steel parts have failed. One such instance involved two flanged 18Cr-12Ni austenitic stainless steel valves that were bolted to 5Cr-½Mo ferritic steel piping in a petroleum plant. The valves were alternately exposed to atmospheric temperature and to an elevated temperature between 595 °C and 620 °C (1100 °F and 1150 °F). Each valve was subjected to 1.5 thermal cycles per day, that is, three cycles every 2 days; about 8 hours elapsed between the start of the heating portion of the cycle and the start of the cooling portion, and conversely. After 10 days of operation, cracks were found radiating from the bore into the flange of one valve; the other valve failed shortly thereafter. The mating 5Cr-½Mo ferritic steel piping gave excellent service, as did replacement valves made of 9Cr-1Mo ferritic steel.

The superiority of ferritic alloy steel over several wrought austenitic stainless steels in applications involving thermal cycling is a result of differences in thermal conductivity and coefficient of thermal expansion between the two types of steel. In addition, because of the lower coefficient of expansion of ferritic steel, a given temperature gradient produces less expansion, and thus less thermal stress, in ferritic alloy steel than in wrought austenitic stainless steel. The combination of these two factors can result in appreciably less thermal stress and longer life for ferritic steel under a given set of cyclic thermal conditions.

Thermal fatigue may result in either low-cycle or high-cycle failure. Low-cycle thermal fatigue is usually associated with ductile cracking due to large plastic strains and is most often caused by large changes in temperature or large differences in thermal expansion between two structural members. If a change in temperature is especially severe and if it occurs rapidly (for example, a cold liquid against a warmer metal where the difference in temperature is >56 °C (100 °F), it is called thermal shock. Cracks due to thermal shock generally initiate in ten thermal cycles or less—sometimes in only one thermal cycle when the material is sufficiently brittle or restraint is very localized. Generally, fatigue is considered low cycle if there are fewer than 10,000 cycles. These fracture surfaces are characterized by rough uneven fractures due to ductile cracking in steps.

High-cycle thermal fatigue frequently results from intermittent quenching of a hot surface by a lower temperature liquid. In such instances, the wetted surface contracts rapidly, whereas the metal below the surface does not. This produces large tensile stresses at the wetted surface. As the water absorbs heat and evaporates, the temperature of the metal surface drops dramatically. After all the liquid is vaporized, the surface returns to its previous value and surface stresses are relaxed. After a sufficient number of thermal cycles, a crazed pattern of cracks appears on the surface. Eventually, one or more of the surface thermal fatigue cracks may propagate completely through the section by fatigue. High cycle fatigue is usually associated with more than 100,000 cycles. These fractures are generally smooth and sometimes display beach marks and other arrest lines indicating a slow progression of cracking over time.

Affected units and equipment includes:

— steam purges or lances directed at hot stainless steel equipment can experience slugs of condensate that rapidly cool a localized area—steam traps can be used to divert condensate;

— water injection systems into FCCU or Resid FCCU regenerator plenums;

— rain water deluges on high temperature furnace inlet/outlet piping due to insufficient weather protection, particularly at suspended pipe support locations.

4.6.2 Visual and Microscopic Appearance

Cracks start at a surface and are almost always initiated by a stress concentration, if present. While embedded surfaces can be the source of a fatigue crack, the initiating surface is usually a free surface.

The fracture surface is normal to the direction of the principal thermal tensile stress, even though the part may be acted upon by bending, torsional, or hydrostatic loads.

Fatigue cracks have a broad range of appearances; they can be single, in bands, networks, planar or curved, branched or unbranched, single or multiple origin, either through-thickness or partial penetration and axial, circumferential, or some combination of the two. When thermal fatigue cracks start at the toe of a weld, they tend to propagate lengthwise along the toe of the weld.

While visible beach marks may be present on fracture surfaces, the surface oxidation caused by high-temperature exposure often obscures this feature. Because of oxidation and/or exposure to hot process fluids, thermal fatigue cracks are often filled with corrosion products (such as from oxidation or sulfidation) or coke.

4.6.3 Prevention

Equipment subject to significant thermal cycling should be designed and fabricated to avoid or minimize stress concentration sites. Design details, such as blend grinding of weld caps and smooth thickness transitions on accessible surfaces, are recommended. Designs should also minimize localized points of restraint. Gussets and stiffeners should be avoided. However, if needed, they should be tapered to make smooth transitions at their ends. Designs should also incorporate sufficient flexibility to accommodate differential expansion.

Thermal fatigue can also be minimized by controlling heating and cooling rates during startup and shutdown operations.

4.6.4 Inspection and Monitoring

Visual examination and PT are effective methods of inspection when suspect surfaces are accessible since cracking is usually surface connected.

External shear wave ultrasonic inspection can be used for non-intrusive inspection for internal cracking at and downstream of quench nozzle tie-ins.

Heavy wall reactor internal attachment welds can be inspected using angle beam ultrasonic techniques.

4.6.5 Repairs

Thermal fatigue damage in austenitic alloys is usually accompanied by other types of high-temperature damage mechanisms such as carburization or sigma phase embrittlement. Such damage is more difficult to repair. If multiple mechanisms are present, repair procedures are usually dominated by concerns other than thermal fatigue damage. (Accordingly, consult the repair sections covering embrittling mechanisms, if applicable.)

Fatigue cracks can be singular cracks, sets of roughly parallel cracks or web-like networks sometimes called “mud cracking”. In wrought austenitic materials, they can usually be repaired simply by grinding to sound metal, cleaning and then repair welded by a low heat input process such as GTAW.

For major repairs, the following is recommended.

— Candidate materials can be dye-penetrant tested to help define the extent of fatigue-damaged material that should be removed prior to repair welding.

— Fatigue-damaged material (i.e. material showing crack-like indications as a result of dye-penetrant testing) should be removed by grinding (or gouging followed by light grinding). The final weld bevel should be checked by dye penetrant testing to ensure that there is no residual cracking.

— After welding, blend-grind the weld profile to develop a smooth contour. Fill in any undercut or blend out to minimize stress concentration effects.

4.7 Solidification Cracking

4.7.1 General

Solidification cracking is often called "center line cracking", "hot cracking", or "liquation cracking", and typically occurs during the solidification phase of the weld. The most classic cause of this type of cracking is the presence of a phase that solidifies at a temperature lower than the surrounding material. This phase will often segregate and has virtually no strength since it is still in liquid form. This is also referred to as "liquation cracking". Welds that are highly restrained are more susceptible. There are three factors that contribute to solidification cracks in clean base metals: alloy composition, welding parameters and restraint.

"Hot short cracking" is a form of liquation cracking (typically due to a low melting contaminant such as sulfur). It is not necessary to have a contaminant to cause liquation cracking.

Weld filler metal for applications involving the high temperatures covered by this report should have controlled ferrite content (minimal ferrite content improves ductility and is needed to avoid solidification cracking). Use a filler metal that will produce ferrite content in the weld deposit with a ferrite number (FN) in the range 3 to 10. Too low a ferrite content is frequently the single most important variable that leads to solidification cracks; in general, the ferrite content (i.e. FN) needs to be above 3 (this does not apply to 16-8-2 welds, for this material, API 582 gives an allowable ferrite number of 1 to 5 FN). Avoid weld deposits with FN >10, as this might promote sigma phase during PWHT or due to high temperature in-service conditions.

If solidification cracking persists during weld repairs, butter the bevels to reduce the root gap and hence minimize solidification shrinkage stresses.

The following statements summarize information from WRC-421 on the effect of solidification cracks on mechanical properties.

— Tensile properties are unaffected when cracking is present in less than 5 % of the cross section, or less than 25 fissures per square inch.

— Fracture toughness, measured in COD testing at –196 °C (–321 °F), was not affected by the presence of microfissures, indicating that they are inconsequential in weldments subjected to impact loading.

— Fully austenitic Type 316 weld metal with microfissuring comprising 3.5 % of the cross sectional area gave substantially higher absorbed energy in impact tests at –196 °C (–321 °F) than fissure free welds with 5 % ferrite.

— Weldments with weld metal microfissures most commonly fail at the weld toe, with cracking occurring through the base metal. If these are not removed by careful grinding and blending, microfissures will initiate fatigue failures through the weld metal.

— Creep rupture properties may be adversely affected by crack initiation at microfissures, suggesting that optimum creep resistance is obtained in Type 316 weld metals with ferrite at about 5 %.

— Defect sizes below 0.4 mm (0.016 in.) have no significant effect on fatigue life at elevated temperatures.

— Microfissures may initiate corrosive attack in some environments, especially by acting as initiating sites for stress corrosion cracking, and by inducing crevice and crevice corrosion.

4.7.2 Appearance

With solidification cracking in austenitic alloys, the dendrite nodules have an egg crate appearance that is very distinctive of cracking that formed during the solidification process. Cracking is intergranular/interdendritic.

4.7.3 Austenitic Stainless Steels

Avoiding or minimizing weld solidification in austenitic stainless steels is accomplished by controlling the composition of base and filler metal. For most austenitic stainless steel weld metals not subjected to sigma forming temperatures, the composition should be controlled to achieve a FN of 3 to 20. The most effective way to avoid cracking in these weld metals is to reduce impurity content and/or minimize the weld restraint. Fully austenitic weld metals can be quite resistant to weld cracking under conditions of low to moderate restraint. Convex shape and filled/blended craters are also helpful in preventing solidification cracking. Ferrite above FN 10 may compromise mechanical properties if the weldment is to be stress relieved or the structure is put in service at either cryogenic temperatures or elevated temperatures.

4.7.4 Nickel-based Alloys

In the case of Ni-based alloys, weld metal solidification cracking can often be avoided by proper selection of the welding consumable. The control of impurities to low levels is always advisable, since phosphorus, sulfur, boron, lead and silver are known to increase cracking susceptibility. It is also advisable to limit elements that form low melting eutectic constituents, such as niobium, titanium, and silicon.

4.7.5 Ferrite Content

The ferrite content may be determined magnetically, in addition to a metallurgical estimation. The scale used is not absolute; there will probably be differences in the results of measurements obtained from different laboratories (e.g. variations between 3.5 % and 8.0 % in a specimen with approximately 5 % ferrite). Ferrite measurements for welds should be based as much as possible upon measurements of FN, using instruments calibrated following AWS 4.2.

The ferrite number may be equated with the percentage of ferrite up to approximately 10 FN. According to the Welding Research Council (WRC), it is not possible at present to determine the absolute ferrite content in austenitic-ferritic weld metal deposits. Variations resulting from differences in the welding and measuring conditions are to be anticipated, even in specimens with pure weld metal deposit. The usual standardization assumes a 2-sigma variation which means a variation of ±2.2 FN for 8 FN.

Greater variations are to be anticipated if the welding procedure permits higher absorption of nitrogen from the ambient air. High nitrogen absorption may lead to a weld metal with 8 FN falling to 0 FN in the ferrite content. Absorption of 0.10 % nitrogen typically reduces the ferrite content by 8 FN.

Use a calibrated ferritescope to confirm the FN in the weld deposit. Some filler metal suppliers include the FN or ferrite content in the material test report (MTR). In weld metal deposits, dilution with the base metal leads to further ferrite reductions since base metals with the same composition usually have lower ferrite contents than the pure weld metal. In addition to measurement, it is also possible to calculate the ferrite content from the chemical composition of the pure weld metal.

Various structural diagrams may be referred to for this purpose. The most common are the WRC-92 diagram, the Schaeffler diagram and the DeLong diagram. There may be very great variations between the results of the individual diagrams, as they were prepared on the basis of series examinations for different groups of materials.

The Schaeffler diagram is the oldest of the diagrams referred to, and until now, has been widely used for calculation of the ferrite content. It has a broad scope of application, but does not allow for the highly austenizing effect of nitrogen. The DeLong diagram, shown in Figure 52 [73], is a modification of the Schaeffler diagram, which shows the ferrite content in ferrite numbers up to about 18 FN. The diagram allows for the nitrogen content in the calculation and exhibits better concurrence between measurement and calculation than does the Schaeffler diagram. It overlaps approximately with the WRC-92 diagram (shown in Figure 53 [74]) in its applicability.

The WRC-92 diagram provides a prediction of the ferrite content in many applications. It is the most recent of the diagrams mentioned and exhibits better correlation between the measured and the calculated ferrite contents than does the DeLong diagram. However, the WRC-92 diagram does not take into account the silicon and manganese content, and should not be used for weld metals with silicon and manganese contents greater than 8 wt%. The WRC-92 diagram should also not be used for weld metals with nitrogen contents greater than 0.2 wt% [75, 76, 77].

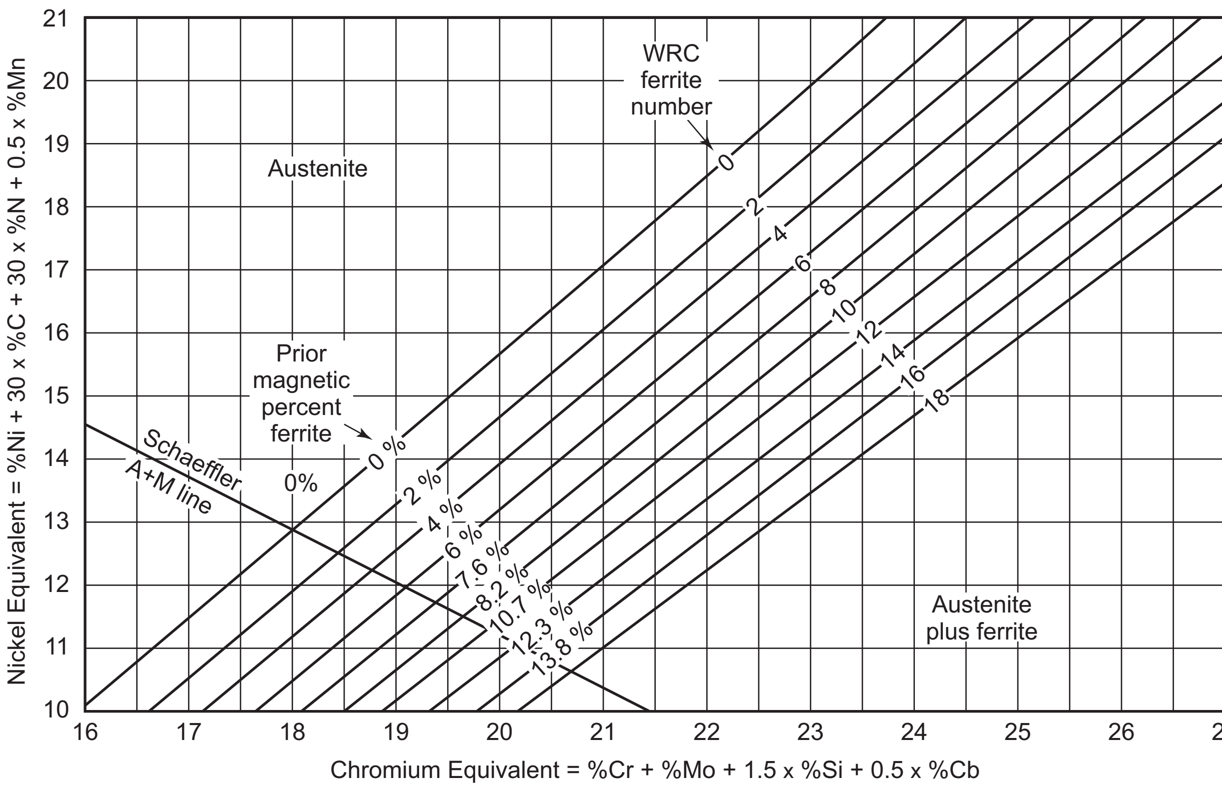

Figure 52—DeLong Diagram for Estimating Ferrite Content in Austenitic Stainless Steels

If the nitrogen content is not known for determining the nickel equivalent, then it is possible to assume a content of 0.06 % for TIG welding and manual electrode welding and a content of 0.08 % for gas-shielded welding with solid wire electrodes. Using the WRC-92 diagram, it is possible to predict the ferrite number within a range of ±3 FN in approximately 90 % of the measurements, assuming an accurate chemical composition.

4.7.6 Weld Repairs of Austenitic Stainless Steels With Low Ductility/Toughness Due to Embrittlement Mechanisms

The following are recommendations for weld repairs of austenitic stainless steels with low ductility/toughness due to embrittlement mechanisms, such as in-service sigma embrittlement.

Cleanliness is important to all welding procedures. Avoid using marking crayons, etc., which can promote cracks. Also avoid using tools and grinding materials that may have been used elsewhere and can transfer contamination.

Clean the weld joint surface to avoid any sulfur and other weld deposit contamination. Also try to select a filler metal with S+P <0.02 wt% or as low as available.

Impurities can often come from service environments. For this reason, extra care is needed when repair welding equipment that has been in service. Metal surfaces contaminated by sulfur or sulfur compounds can cause a condition called "hot short" cracking during the solidification of weld metal. If the process contained sulfur or sulfur

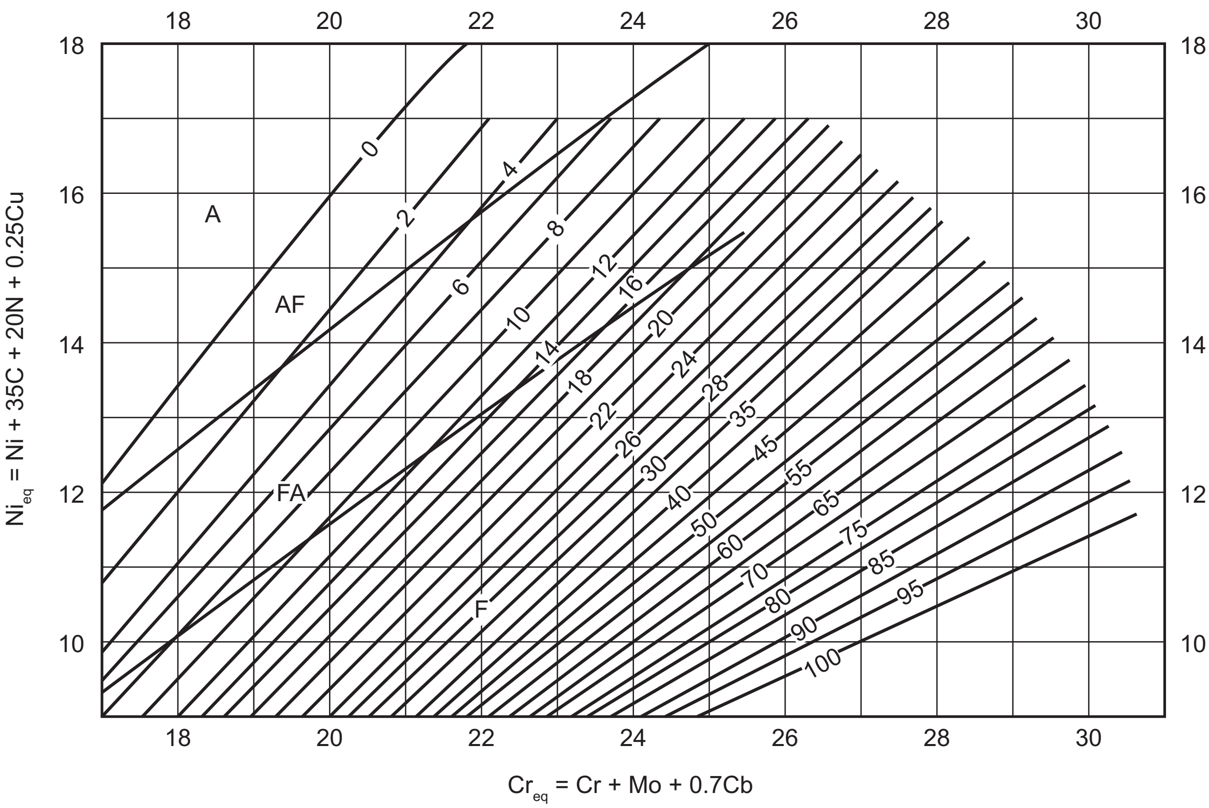

Figure 53—WRC Diagram Including Solidification Mode Boundaries

compounds, such as H_2S or organic sulfides, grind back the internal and external surfaces 25 mm to 50 mm (1 in. to 2 in.) to remove carbon, sulfur and other contaminants and corrosion products. Avoid using tools and grinding materials that may have been used elsewhere and can transfer contamination.

Use of a filler metal with a ferrite content that produces a weld deposit with FN 3 to 8 leads to a primary ferrite solidification mode, which decreases the likelihood of solidification cracking. Calibrated ferritescopes can be used to confirm ferrite number in the weld deposit.

WRC-92 can be used to predict ferrite content based on the chemistries of the filler metal and base metal. Some filler metal suppliers include the FN or ferrite content in the MTR. Very low ferrite content frequently is the single most important variable leading to solidification cracks; the ferrite content needs to be above FN 3. Avoid weld deposits with a FN >8, as they might promote the formation of excessive amounts of sigma phase in service.

Use low heat input welding processes; these reduce the solidification time, and therefore, minimize the temperature window where solidification cracking occurs. High heat inputs resulting in large weld beads, or excessive travel speeds that promote teardrop shaped weld pools, are most problematic with respect to cracking. Maintain a short arc length. Use stringer beads not wider than 1.5 times the electrode diameter. Use a staggered progression (skip welding) when possible.

Avoid concave bead shape and under-filled craters at weld stops, as they promote solidification cracking. Avoid crater cracks by filling the crater at termination of welding and washing back across previously deposited weld metal. If crater cracks occur, they should be removed by grinding before proceeding further. Aluminum oxide wheels are preferred by some users over the silicon carbide variety.

Maximum interpass temperature should be limited to 175 °C (350 °F).

In case cracking persists during weld repairs, “butter” the bevels (apply a layer of weld metal on top of the existing bevel using stringer beads and then grind smooth) to provide new material to attach to, reduce the root gap and hence minimize solidification shrinkage stresses. Buttering the bevel faces applies a weld layer with minimal stress pulling against the base metal so that cracking is unlikely. This new material is then more forgiving and less likely to crack during welding.

Highly embrittled materials can be solution annealed for a distance of at least one pipe diameter before welding to restore ductility during welding. Post weld heat treatment should also be performed to reduce localized stresses that can cause SRC.

Bibliography

[1] API Recommended Practice 571, *Damage Mechanisms Affecting Fixed Equipment in the Refining Industry*, Second Ed., April, 2011.

[2] Image courtesy of Phillips 66 Company.

[3] Tom Farraro, Refin Cor 92F5.2-08 NACE International, Houston, 1992.

[4] Bashir, H. and Hesselberth, A., "Humber Refractory Anchor Failure", ConocoPhillips to API CRE-SCCM Presentation, June 2008.

[5] Images courtesy of Phillips 66 Company.

[6] Tom Farraro, Refin Cor 98F5.3-09 NACE International, Houston, 1998.

[7] Ron Stalker, Refin Cor 98F5.3-011 NACE International, Houston, 1998.

[8] Andy Gysbers, Refin Cor 98F5.3-014 NACE International, Houston, 1998.

[9] Sigma Phase Embrittlement of Stainless Steel in FCC Service, J. Hau and A. Seijas, Paper No. 06578, NACE Corrosion 2006 [1].

[10] Weld Cracking in a 72-inch (1829-mm) Stainless Steel FCU Duct, Wilks, G.W., Paper No. 01522, NACE International, Houston, 2001.

[11] Two Newer Damage Mechanisms Affecting Hydrogen Units. Shargay, Cathy. Powerpoint Presentation, API Round Table, May 2006.

[12] Alloy 800HT Failure Cases Chevron H_2 Manufacturing Furnace Steam Superheat Coils, D. Cooke, Presentation, May 2006.

[13] Cayard, Mike. "H_2 Reformer Effluent vs. 400# Steam Superheater Inlet Cone Failure, Lessons Learned." Powerpoint Presentation, NACE, January 2, 2010.

[14] http://www.uop.com/reforming-ccr-platforming/.

[15] Haynes International Inc. website, Haynes 625 Alloy Information, http://www.haynesintl.com/Haynes625Alloy/625HaynesAlloyPF.htm.

[16] Image courtesy of Lloyd's Register.

[17] http://www.ambigen.org/files/image/h-plants.gif

[18] Technical Basis for Improved Reliability of 347H Stainless Steel Heavy Wall Piping in Hydrogen Service, M. Farhion, A. Birke, J. Brown, J. Hassell, Paper No. 03647, NACE Corrosion 2003.

[19] Thick wall Stainless Steel Piping in Hydroprocessing Units—Heat Treatment Issues, Cathy Shargay and Anil Singh, NACE 02478, 2002.

---

1 NACE International (formerly the National Association of Corrosion Engineers), 1440 South Creek Drive, Houston, Texas 77084-4906, www.nace.org.

[20] Cracking in Welds of Heavy-Wall Stainless Steel and Nickel Alloy Piping During Fabrication. Tomoaki Kiso, Kunio Ishii, and Ichiro Seshimo. ASME Pressure Vessel and Piping Conference 2009.

[21] The Effect of Welding Parameters on Penetration in GTA Welds, A. A. Shirali and K.C. Mills, *Welding Journal*, Welding Research Supplement, June 1993.

[22] *Practical Guidelines for the Fabrication of High Performance Austenitic Stainless Steels*, International Molybdenum Association [2], ISBN 978-1-907470-10-3, 2010.

[23] Data compiled by Michael Cayard, Flint Hills Resources.

[24] ASME [3] Sec II, Part D, Non Mandatory Appendix A-208.

[25] Precipitation in Creep Resistant Austenitic Stainless Steels, Chapter 1, p. 14, Ph.D. thesis by Thomas Sourmail, University of Cambridge, 2002.

[26] *Metals Handbook*, Vol. 8, Metallography, Structures and Phase Diagrams. ASM [4], 1973.

[27] *Thermal Aging Embrittlement of Austenitic Stainless Steel Welds and Castings*, Gargi Choudhuri, K.R.Gurumurthy, and B.K.Shah.

[28] *Prediction of sigma type phase occurrence from compositions in austenitic superalloys*, L. Woodyatt, C. Sims, and H Beattie, Trans. AIME, 1966, 236, 519.

[29] *Behavior of Superheater Alloys in High Temperature, High Pressure Steam*, edited by George E. Lien, ASME, 1968.

[30] Rolled Alloys Investigation 27-84, by Gene R. Rundell, Temperance, Michigan, August, 1984.

[31] *Heat Resistant Alloys*, James Kelly (Director of Technology), Rolled Alloys Inc., November 2003.

[32] Precipitation in Creep Resistant Austenitic Stainless Steels, Chapter 2, p. 41, Ph.D. thesis by Thomas Sourmail, University of Cambridge, 2002.

[33] Precipitation in Creep Resistant Austenitic Stainless Steels, T. Sourmail, *Materials Science and Technology*, January 2001, Vol. 17.

[34] Sigma Phase Embrittlement of Stainless Steel in FCC Service, J. Hau and A. Seijas, Paper No. 06578, NACE Corrosion 2006.

[35] Buchheim, G. M., C. Becht, K. M. Nikbin, V. Dimopolos, G. A. Webster, and D. J. Smith. “Influence of Aging on High-Temperature Creep Crack Growth in Type 304H Stainless Steel.” Nonlinear Fracture Mechanics, ASTM STP 995 (1988): 153-172.

[36] Sigma Phase Embrittlement of Stainless Steel in FCC Service, J. Hau and A. Seijas, Paper No. 06578, NACE Corrosion 2006.

[37] Figure developed by API.

[2] International Molybdenum Association, 454-458 Chiswick High Road, London, W4 5TT, United Kingdom, http://www.imoa.info/index.php

[3] ASME International, 2 Park Avenue, New York, New York 10016-5990, www.asme.org.

[4] ASM International, 9636 Kinsman Road, Materials Park, Ohio 44073, www.asminternational.org.

[38] Sigma Phase Embrittlement of Stainless Steel in FCC Service, J. Hau and A. Seijas, Paper No. 06578, NACE Corrosion 2006.

[39] Materials Experience in Methanol Reforming Units, by K. L. Baumert and J. J. Hoffman, Paper No. 494, NACE Corrosion 97.

[40] Embrittlement of Type 347 Stainless Steel Weldments by Sigma Phase, E.L. Creamer, L Rozalsky and R.W Leonard, *Welding Journal*, June 1969, Research Supplement, p 239-s–244-s.

[41] Private communication from Mr. William Webb to Tim Munsterman, June 2011.

[42] Catastrophic Oxidation of High-Temperature Alloys, E.C. Green, ORNL Report TM-51, 1961.

[43] Materials Engineering Workshop—Proceedings, Nickel Institute Publication 11001, 2nd edition, 1994, p.25 (available as download www.nickelinstitute.org).

[44] Proposed Standard Carburization Test Method, G.Y. Lai et al., Paper 03473, Corrosion 2003, NACE International, 2003.

[45] Image courtesy of Lloyd's Register.

[46] Sigma Phase Embrittlement of Stainless Steel in FCC Service, J. Hau and A. Seijas, Paper No. 06578, NACE Corrosion 2006.

[47] *Carburization—A High Temperature Corrosion Phenomenon*, H.J. Grabke, Publication 52, MTI [5], 1998.

[48] Materials Engineering Workshop—Proceedings, Nickel Institute, Publication 11001, 2nd edition, 1994, p.26 (available as download www.nickelinstitute.org).

[49] *ASM Metals Handbook, Corrosion*, Volume 13, ASM International.

[50] Carburization, Part 1: State-of-the-Art Review; Part 2: Best Practices for Testing Alloys, Dr. Hans J. Grabke, MTI Publication No. 52.

[51] Control of Relaxation Cracking in Austenitic High Temperature Components, Hans van Wortel, Paper No. 07423, NACE Corrosion 2007.

[52] An Investigation of Reheat Cracking in the Weld Heat Affected Zone of Type 347 Stainless Steel, a PhD dissertation submitted by Mr. Phung-on Isaratat to the Graduate School of The Ohio State University, 2007.

[53] Stress Relaxation Cracking of Welded Joints in Thick Sections of a TP347 Stabilized Grade of Stainless Steel, Christian E. van der Westhuizen, Paper No. 08454, NACE Corrosion 2008.

[54] Reheat Cracking of FCAW 308 Weld Metal at Elevated Temperature, Yasuhiro Hara and Eiich Yamamoto, API 64th Fall Meeting, New Orleans, 1999.

[55] Reheat cracking and elevated temperature embrittlement of austenitic alloys: Literature Review, EWI Summary Report SR0401, H. Zhang, S. Shi, J. Ramirez, and J.C. Lippold, January 2004.

[56] Capstone Engineering Services, Inc.

[57] Image courtesy of Lloyd's Register.

[5] Materials Technology Institute, 1215 Fern Ridge Parkway, Suite 206, St. Louis, MO 63141.

[58] Private communication from Mr. Jorge Penso to Mr. Tim Munsterman, May, 2010.

[59] *Behavior of Superheater Alloys in High Temperature, High Pressure Steam*, edited by George E. Lien, ASME, 1968.

[60] *Practical Guidelines for the Fabrication of High Performance Austenitic Stainless Steels*, International Molybdenum Association, 2010.

[61] Optimized Heat Treatment of 347 Type Stainless Steel Alloys for Elevated Temperature Service to Minimize Cracking, B. Messer, V. Oprea and T. Phillips, Paper No. 04640, NACE Corrosion 2004.

[62] Stress Relaxation Cracking of Welded Joints in Thick Sections of a TP347 Stabilized Grade of Stainless Steel, Christian E. van der Westhuizen, Paper No. 08454, NACE Corrosion 2008.

[63] Private communication from Ms. Cathy Shargay to Mr. Tim Munsterman, May, 2010.

[64] API Standard 530, *Calculation of Heater-Tube Thickness in Petroleum Refineries*, Seventh Ed., April, 2015.

[65] API Standard 579-1/ASME FFS-1 2007, *Fitness for Service*, Table 4.1.

[66] Private communication from Mr. Richard Coldwell to Mr. Tim Munsterman, May, 2010.

[67] Report on the Elevated-Temperature Properties of Stainless Steels, Simmons and Van Echo, *ASTM Data Series Publication* DS-5-S1.

[68] Wikimedia Commons, 3stagecreep.svg, strafpeloton2, October 2009.

[69] EPRI *Manual for Investigation and Correction of Boiler Tube Failures*, EPRI CS-3945, April 1985.

[70] Rest Life Estimation of Creeping Components by Means of Replicas, Neubauer, B.; and Wedel, U., *Advances in Life Prediction Methods*, ASME, p. 307–314, 1983.

[71] Development of the MPC Omega Method for Life Assessment in the Creep range, Prager, M. Press. V*ess. Techn*, 117, 1995 p. 95.

[72] *Refinery Injection and Process Mix Points*. NACE International Publication 34101.

[73] Long, C. J., and DeLong, W. T. 1973, The ferrite content of austenitic stainless steel weld metal, *Welding Journal*, 52 (7). 281-s to 297-s.

[74] D.J. Kotecki and T.A. Siewert, 1992, WRC-1992 Constitution Diagram for Stainless Steel Weld Metals: A Modification of the WRC-1988 Diagram, *Welding Journal*, 71 (5), 171s–178s.

[75] WRC-421, Welding Type 347 Stainless Steel—An Interpretative Report, R. David Thomas, Jr. and Robert W. Messener, Jr., May 1997.

[76] *Welding Metallurgy and Weldability of Stainless Steels*, John C. Lippold and Damian J. Kotecki, Wiley-Interscience, 1st edition, April 7, 2005.

[77] *Welding Metallurgy and Weldability of Nickel-Base Alloys*. John Dupont, John Lippold and Samuel Kiser. Wiley. 2009.

energy API®

AMERICAN PETROLEUM INSTITUTE

1220 L Street, NW
Washington, DC 20005-4070
USA

202-682-8000

Additional copies are available online at www.api.org/pubs

Phone Orders:	1-800-854-7179	(Toll-free in the U.S. and Canada)
	303-397-7956	(Local and International)
Fax Orders:	303-397-2740	

Information about API publications, programs and services is available on the web at www.api.org.

Product No. C942B01